Photocatalytic hydrogen production through photoreforming of organics using copper – based photocatalyst under visible light radiation

Thesis by
Marica Muscetta

Degree of Doctor of Philosophy
in
INDUSTRIAL PRODUCT AND PROCESS ENGINEERING
(XXXIV)

University of Naples "Federico II"
School of Polytechnic and Basic Sciences
Department of Chemical Engineering, Materials and Industrial Production (DICMAPI)

2018 - 2021

Photocatalytic hydrogen production through photoreforming of organics using copper – based photocatalyst under visible light radiation

by

Marica Muscetta

Tutor:

Prof. Roberto Andreozzi

Scientific Committee:

Prof. Roberto Andreozzi

Prof. Raffaele Marotta

Dott. Ing. Ilaria Di Somma

Course coordinator:

Prof. Andrea D'Anna

Abstract

Nowadays, 80% of global energy consumption is dependent on fossil fuels, leading different problems such as the decreasing of energy sources and the environmental problems (global warming, greenhouse effect, production of harmful gases, ozone layer depletion and acid rain). Hydrogen represents a potential alternative energy carrier due to its stability and zero emission of greenhouse gases, and many researches are directed toward the utilization of metal oxides semiconductors (such as TiO_2 and ZnO) as photocatalysts to convert solar energy into hydrogen; in particular TiO_2, due to its high chemical stability and photocatalytic activity in the UV range is the most widely used material; despite the great number of positive characteristics, TiO_2 presents different problems such as high electron – hole recombination rate and poor absorption under the visible light, due to its wide band gap (about 3.2 eV). To overcome these drawbacks, several studies reported the utilization of TiO_2 in association with other semiconductors such as ZnO and Cu_2O; in particular much attention has attracted Cu_2O: this is a non-toxic and abundant material, with a narrow band gap (about 2.1 eV); as p – type semiconductor, if combined with a n – type semiconductor, it is able to form a heterojunction photocatalyst, extending the light absorption in the visible range and reducing of electron-hole recombination rate. Several techniques have been used for Cu_2O/TiO_2 composite preparation and numerous disadvantages are still associated to each of them. In the present research, based on the outcomes of an extended literature analysis, a ball milling method to dryness has been chosen as alternative technique to prepare the photocatalysts, due to its simplicity and industrial applicability. The effect of milling time, rotation rate and Cu_2O percentage on the photocatalytic hydrogen generation have been evaluated, obtaining the best performances (H_2 generation about 60 µmol/h) with a milling time of 1 minute and a rotation rate of 200 rpm, when 1%wt of Cu_2O is used in the composite in presence of methanol as scavenger. Moreover, the effect of the sacrificial agent used is evaluated adopting in the tests other species, and recognizing glycerol as the best candidate to produce hydrogen among the tested organics. Furthermore, the photocatalytic activity of the best prepared photocatalyst was *evaluated at varying the pH and the temperature of the suspension, methanol concentration and catalyst load. In particular, a great positive effect was recorded at increasing the temperature of the system, showing a hydrogen productivity about 4.5 – fold higher than that obtained at the lowest temperature. Moreover, being the aim of the present work devoted to the development of a visible light active photocatalytic system, the possibility of using it by exploiting the solar light was evaluated, obtaining a hydrogen production about 5 – fold higher than that collected under simulated solar conditions. Finally, the development of a suitable mathematical model able to predict the hydrogen production in presence of the selected catalyst was also attempted.*

Keywords: Hydrogen production, visible – light active photocatalyst, p – n heterojunction, sacrificial photocatalysis, photocatalyst preparation.

Table of contents

List of Symbols 9

List of Figures 11

List of Tables 16

1. Background 17

1.1. Energy production and renewable sources. Photocatalytic hydrogen production. 17

1.2. Photocatalytic processes aimed to hydrogen production 19

1.3. Photocatalysts. Advantages and disadvantages 22

2. State of art 25

2.1. Enhancement of the photocatalytic activity of semiconductors 25

2.2. Cu_2O as semiconductor and p-n type heterojunction with titania 28

2.3. Preparation of Cu_2O/TiO_2 composite materials 30

2.3.1. Reducing agents 30

2.3.2. Electrochemical deposition 33

2.3.3. Impregnation/calcination 34

2.4. Characterization techniques for Cu_2O/TiO_2 composite materials.......................... 36

2.4.1. X-Ray Diffraction spectroscopy.. 37

2.4.2. X-Ray photoelectron spectroscopy... 38

2.4.3. Raman spectroscopy 39

2.4.4. High – resolution transmission electron microscopy..................................... 40

2.4.5. Diffuse reflectance UV–Visible spectroscopy 42

2.4.6. Photoluminescence Spectroscopy.. 42

2.5. Mechanisms of hydrogen evolution reaction 44

2.6. pH influence 48

2.7. Effect of sacrificial agent 49

2.8. Hydrogen generation efficiency 50

2.8.1. Photoelectrochemical cells... 50

2.8.2. Photocatalytic reactors... 51

2.9. Ball milling as alternative preparation method 61

3. Aim of the thesis 65
4. Materials and methods 66
4.1. Materials 66
4.2. Photocatalysts preparation 66
4.3. Experimental set-up 66
4.4. Experimental procedures 68
4.5. Recovery of the photocatalysts 68
4.6. Analytical methods 69
4.7. Catalyst characterization 69
5. Results I. Cu_2O/TiO_2 composites prepared by facile mechanochemical synthesis for visible light driven hydrogen production 71
5.1. Introduction 71
5.2. Results and discussion 72
5.2.1. Preliminary results 72
5.2.1.1. Effect of mixing 72
5.2.1.2. Effect of sacrificial agent 73
5.2.2. Factorial design approach 74
5.2.3. Physico – chemical characterization 79
5.2.4. Photocatalytic tests 94
5.2.4.1. Effect of Cu_2O percentage 94
5.2.4.2. Effect of milling time and rotation rate 95
5.2.4.3. Effect of calcination 97
5.3. Summary 99
6. Results II. Investigations on the best performing photocatalyst 100
6.1. Introduction 100
6.2. Results and discussion 101
6.2.1. Effect of catalyst load 101
6.2.2. Effect of organic concentration 102
6.2.3. Effect of temperature 103

6.2.4. Effect of pH ... 104

6.2.5. Quantum yield and light-to-chemical energy efficiency calculation ... 106

6.2.6. Photocatalyst recycling ... 107

6.2.7. Photocatalytic activity under solar conditions ... 113

6.3. Summary ... 116

7. Results III. Kinetic modeling of H_2 production over Cu_2O/TiO_2 catalyst through photoreforming of methanol ... 117

7.1. Introduction ... 117

7.2. Kinetic model ... 117

7.3. Results and discussion ... 122

7.4. Summary ... 125

Conclusions ... 126

Appendix ... 128

References ... 130

List of Symbols

Symbols	Units	Meaning
Cat	[mol]	Reacting photocatalyst
h^+	[mol]	Photogenerated hole
e^-	[mol]	Photogenerated electron
k_r	$[M^{-1}\cdot s^{-1}]$	Electron-hole recombination rate constant
k_{h^+}	$[M^{-1}\cdot s^{-1}]$	Kinetic constant associate to the oxidation of the organic
θ	[mol]	Moles of the active sites of the photocatalyst
Org_{ads}	[mol]	Organic species adsorbed on the catalyst surface
K_{ads}	$[M^{-1}]$	Adsorption equilibrium constant
$Org^{\bullet}_{ads}$	[mol]	Radical of the organic species adsorbed on the catalyst surface
P	[mol]	Generic indication of oxidation by-products
CB	[eV]	Conduction band of semiconductor
VB	[eV]	Valence band of semiconductor
E_g	[eV]	Band gap of the photocatalyst
NHE	[eV]	Normal Hydrogen Electrode: potential of a platinum electrode in 1 M acid solution
HER	[–]	Hydrogen evolution reaction
MTA	[–]	Mesoporous TiO_2 nanoparticles
MC – CAR	[–]	Multiple-cycle chemical adsorption plus reduction method
TNA	[–]	TiO_2 nanotube arrays
TNTs	[–]	TiO_2 nanotubes
F(R)	[a.u.]	Kubelka – Munk function
$(F(R)\ hv)^{1/2}$	[a.u.]	Tauc – plot
λ	[nm]	Wavelength
LSPR	[–]	Localized surface plasmon resonance
J_{sc}	$[mA\cdot s^{-1}]$	Short – circuit photocurrent density
η_F	[–]	Faradaic efficiency for H_2 production
P_i	$[mW\cdot cm^{-2}]$	Incident irradiation power density
AM 1.5 G	[–]	Standard solar irradiation
STH	[–]	Solar to hydrogen conversion efficiency
RHE	[–]	Reversible hydrogen electrode
$\|J\|$	$[mA\cdot cm^{-2}]$	Photocurrent under AM 1.5 G irradiation
V_{RHE}	[V]	Applied potential versus RHE
$V(H^+/H_2)$	[V]	Nernst potential for hydrogen evolution
P_s	$[mW\cdot cm^{-2}]$	Incident solar irradiance

AQE	[–]	Apparent Quantum Efficiency
r_{H_2}	[μmol/h]	Hydrogen production rate
I	[W·cm^{-2}]	The specific irradiance of the light source
S	cm^2	Irradiated area
T	[°C]	Temperature
P	[atm]	Pressure
C_{cat}	[ppm]	Catalyst load
V	[L]	Volume of the suspension
Y	[μmol/h]	Polynomial response of the factorial design
a_0	[μmol/h]	Average response
a_i	[–]	Principal effect of the factors
a_{ij}	[–]	Interaction effects between the two factors
a_{ijk}	[–]	Interaction effects between the three factors
α	[–]	Significance level
R-squared	[–]	Coefficient of determination
C_t	[M]	Total concentration of active sites on the catalyst surface
q	[g/L]	Catalyst load
CH_3OH	[M]	Methanol
CH_3OH_{ads}	[M]	Adsorbed methanol
N	[mol/g]	Total moles of active sites per unit mass of catalyst
$k^{'}$	[μmol/h]	Apparent kinetic constant of substrate oxidation
Cu_2O/TiO_2	[mol]	Composite photocatalyst
$Cu_2O/TiO_2(h^+)$	[mol]	Photogenerated hole
$Cu_2O/TiO_2(e^-)$	[mol]	Photogenerated electron
Q	[cal]	Heat
θ_{TiO_2}	[mol]	Moles of the active sites of the photocatalyst
G_{vis}	[μmol/h]	Reaction rate of the photochemical step
ϕ_{vis}	[mol·ein^{-1}]	Quantum yield in the visible range
L	[cm]	Optical pathway
I_i^0	[E·s^{-1}]	Specific powers of the lamp
ε_{vis}	[M^{-1}·cm^{-1}]	Extinction coefficient of the composite material in the visible range
$[\theta]_{tot}$	[M]	Moles of total sites of the photocatalyst
N_{TiO_2}	[mol/g]	Total moles of active sites per unit mass of TiO_2
φ	[-]	Objective function
$Y_{k,j,i}$	[μmol/h]	Calculated data
$C_{k,j,i}$	[μmol/h]	Experimental data

List of Figures

Figure 1. Energy band diagram of Cu_2O and TiO_2 before and after contact [118]... 29

Figure 2. XRD signals of Cu^0 (a), Cu_2O (b), and CuO (c). 37

Figure 3. XPS spectra of $Cu^0/Cu_2O/$ Cu^0/TiO_2, Cu^0/TiO_2, Cu_2O/TiO_2, and CuO/TiO_2 adapted by Zhen et al.[121]: (1) CuO/TiO_2; (2) Cu/TiO_2; (3) $Cu^0/Cu_2O/$ Cu^0/TiO_2; (4) Cu_2O/TiO_2. 39

Figure 4. Raman spectra of CuO and Cu_2O. 40

Figure 5. HRTEM of Cu_2O in Cu_2O/TiO_2 composite [150]. 41

Figure 6. (a) Typical DRUV absorption spectra in presence of bare TiO_2, bare Cu_2O and Cu_2O-TiO_2 composite, and (b) plots of $(F(R)h\nu)^{1/2}$ versus photon energy hv for Cu_2O and Cu_2O-TiO_2 composite [64].. 42

Figure 7. Schematic illustration for the hydrogen evolution reaction (HER) process over Cu based TiO_2 composite photocatalysts: oxidation of organic species (or water) by positive holes in the valence band and proton reduction by photogenerated electrons in the conduction band. 44

Figure 8. Schematic reaction mechanism of HER process over $Au/Cu_2O/TiO_2/WS_2$ photocathode proposed by Li et al. [9]. 46

Figure 9. HER process over $Cu^0/Cu_2O/TiO_2/WS_2$ composite photocatalysts under visible light irradiation. 47

Figure 10. Schematic representation of the mechanical mixing of powder materials in a ball miller.. 62

Figure 11. (a) Schematic illustration of the annular batch reactor. (b) Experimental set-up for the experiments conducted under artificial UV and/or Visible light source. (c) Experimental set-up for the experiments conducted under the solar source..... 67

Figure 12. Comparison of hydrogen production with different mixed commercial semiconductors. Experimental conditions: [Methanol]=2.5 M; V=0.30 L; C_{Cat}= 1000 ppm; T=35 °C; P=1 atm; pH≈8.5; Cu_2O percentage in TiO_2: (■) 0 % Cu_2O; (Δ) 1% Cu_2O; (○) 2% Cu_2O; (◆) 98% Cu_2O; (▲) 100% Cu_2O; (All samples were prepared by manual mixing). 72

Figure 13. Effect of sacrificial agents (alcohols) on hydrogen production. Experimental conditions: [Organic]=2.5 M; V=0.30 L; T=35 °C; P=1 atm; pH≈ 6.0-8.5; Ccat (ppm)= 1000 ppm; Cu_2O percentage in TiO_2 = 1% wt; Milling time= 10 min; rotation rate= 500 rpm. Organic: No (Water splitting) (□); Methanol (▲); Ethanol (○); Glycerol (●); 1,2-Ethandiol (■). 73

Figure 14. Normal probability plot of the residuals for hydrogen generation.......... 77

Figure 15. Pareto chart for standardized effects for hydrogen production, considering as response hydrogen production rate. Significance level α=0.05. Factors: A – Cu_2O percentage; B – Milling time; C –Rotation rate. 77

Figure 16. Main effects plot for Cu_2O percentage, milling time and rotation rate of the miller considering the hydrogen production rate as response. 78

Figure 17. Interaction effects plot for the three factors, considering the hydrogen production rate as response. 79

Figure 18. XRD patterns of several 1% and 2% Cu_2O – TiO_2 composite materials tested. 81

Figure 19. XRD patterns of several 5% and 10% Cu_2O – TiO_2 composite materials tested, before and after the reaction. 82

Figure 20. XRD patterns of the bare TiO_2 and Cu_2O samples. 82

Figure 21. Diffusive reflectance spectra of several A%Cu_2O-B-C samples, with: (A) Cu_2O percentage, (B) milling time, (C) rotation rate. The bare TiO_2 and Cu_2O are indicated as: Cu_2O (and TiO_2) for the commercial samples and Cu_2O-B (and TiO_2-B) with B=milling time and rotation rate = 500 rpm. 84

Figure 22. XPS spectra of Cu_2O powders: green line (commercial grade), blue line (sample prepared through ball milling: milling time=10 min; rotation rate=500 rpm). 85

Figure 23. XPS spectra of 1% Cu_2O – TiO_2 composite material (prepared through ball milling: milling time=1 min; rotation rate=500 rpm): (red line) Fresh sample, (blue line) reacted sample. 86

Figure 24. SEM analysis of bare Cu_2O and TiO_2. TiO_2 – 10: sample prepared through ball milling (Milling time = 10 min; rotation rate = 500 rpm); Cu_2O – 10: sample prepared through ball milling (Milling time = 10 min; rotation rate = 500 rpm). 87

Figure 25. SEM analysis of several A%Cu_2O-B-C samples, with: (A) Cu_2O percentage, (B) milling time, (C) rotation rate. 88

Figure 26. TEM micrographs of the bare TiO_2 (P25) and Cu_2O. 89

Figure 27. TEM micrographs of some A%Cu_2O-B-C samples, with: (A) Cu_2O percentage, (B) milling time, (C) rotation rate. 90

Figure 28. TEM micrographs of some (a) 10%Cu_2O-TiO_2 and (b) 1%Cu_2O-TiO_2 samples prepared through ball milling (1 min, 200 rpm), after the reaction. 92

Figure 29. PL spectra of some Cu_2O – TiO_2 composites, (A) at different rotation rates and (B) at different milling times. 93

Figure 30. Effect of commercial Cu_2O percentage in TiO_2 on hydrogen production. Experimental conditions: [Methanol]=2.5 M; V=0.30 L; Cat= 1000 ppm; T=35 °C; P=1 atm; pH≈8.5; milling time= 1 min; speed rate = 500 rpm. Comparison between experimental data (full symbols) and calculated data (empty symbols). 95

Figure 31. Hydrogen production after 5 hours of reaction at varying the operative variables during the preparation of the photocatalyst. Experimental conditions: [Methanol]=2.5 M; V=0.30 L; T=35 °C; P=1atm; pH≈8.5; C_{cat}(ppm) = 1000 ppm; Cu_2O percentage in TiO_2 = 1% wt. Milling rotation rate (rpm): (empty bars) 100; (light grey bars) 200; (grey bars) 500. Comparison with a simple manual mixed composite material (Full black bar). Data predicted through the regression model, at varying milling rotation rate (rpm): (○) 100; (●) 200; (●) 500. 96

Figure 32. Comparison between the hydrogen production after 5 hours of irradiation in presence of the best photocatalyst analysed calcined under nitrogen atmosphere or used as prepared. Experimental conditions: [Methanol]=2.5 M; V=0.30 L; T=35 °C; P=1 atm; pH≈8.5; Cu_2O percentage in TiO_2 = 1% wt.; Milling time: 1 min; Rotation rate (rpm): 200 rpm. Calcination temperature: 500°C; Calcination time: 2 hrs. 97

Figure 33. XRD patterns of the 1% Cu_2O – TiO_2 composite materials prepared through ball milling (1 min, 200 rpm) not calcined (black line) and calcined (red line). 98

Figure 34. Hydrogen production rate at varying the catalyst load. Experimental conditions: [Methanol]=2.5 M; V=0.30 L; T=35 °C; P=1 atm; pH≈8.5; Cu_2O percentage in TiO_2 = 1% wt.; milling time: 1 min; rotation rate (rpm): 200 rpm. 101

Figure 35. Hydrogen production rate at varying the organic concentration (methanol). Experimental conditions: [Catalyst]=700 ppm; V=0.30 L; T=35 °C; P=1 atm; pH≈8.5; Cu_2O percentage in TiO_2 = 1% wt.; milling time: 1 min; rotation rate (rpm): 200 rpm. 102

Figure 36. Hydrogen production rate at varying the temperature of the system. Experimental conditions: [Catalyst]=1000 ppm; V=0.30 L; P=1 atm; pH≈8.5; [Organic] = 2.5 M; Cu_2O percentage in TiO_2 = 1% wt.; milling time: 1 min; rotation rate (rpm): 200 rpm; visible range. (■) Methanol; (□) Glycerol. 104

Figure 37. Hydrogen production rate at varying the pH of the suspension. Experimental conditions: [Catalyst]=1000 ppm; V=0.30 L; P=1 atm; T=35°C; [Organic] = 2.5 M; Cu_2O percentage in TiO_2 = 1% wt.; milling time: 1 min; rotation rate (rpm): 200 rpm; visible range. 105

Figure 38. (a) Produced hydrogen amount and (b) mean hydrogen production rate during a single run (●) and 3-runs by using the recovered material: (○) first cycle; (Δ) second cycle; (□) third cycle. Experimental conditions: [Methanol]=2.5 M; V=0.30 L; T=35 °C; P=1 atm; pH≈8.5; Cu_2O percentage in TiO_2 = 1% wt.; Milling time: 1 min; Rotation rate (rpm): 200 rpm. 109

Figure 39. (a) FTIR spectra of 1%Cu_2O-TiO_2 photocatalyst prepared through ball milling (1 min, 500 rpm), before and after the reaction; (b) FTIR spectra of 2%Cu_2O-TiO_2 photocatalyst prepared through ball milling (30 min, 500 rpm), before and after the reaction. 112

Figure 40. Hydrogen production rate during experimental runs conducted under solar radiation. Experimental conditions: [Catalyst]=1000 ppm; V=0.30 L; P=1 atm; pH≈8.5; [MeOH] = 2.5 M; Cu_2O percentage in TiO_2 = 1% wt.; Milling time: 1 min; Rotation rate (rpm): 200 rpm. 113

Figure 41. Comparison between experimental results (□) and data obtained through the mathematic model (■). The experimental conditions for each photocatalytic run are reported in Table 9. 124
Figure 42. EDX spectra on the (1%wt) Cu_2O-TiO_2 composite material before and after the reaction. 128
Figure 43. EDX spectra on the (10%wt) Cu_2O-TiO_2 composite material before and after the reaction. 129

List of Tables

Table 1. Literature review of recent studies on Cu_2O/TiO_2 composite materials..... 53

Table 2. Coded and un-coded values and levels of the factors................................ 75

Table 3. Design table for the chosen factors and statistical factorial design. The coefficient of determination (R-squared) is equal to 99.88%. 76

Table 4. Detailed information about the materials on which XRD, diffusive reflectance, XPS, SEM, TEM, FT-IR and PL characterizations were performed. The calculated bandgaps and crystallite sizes are also reported. 80

Table 5. Ratio of Cu to O calculated on the fresh and the recovered samples......... 91

Table 6. Mean hydrogen production rate, apparent quantum efficiency, and light to chemical energy efficiency obtained using a manually mixed catalyst (Cu_2O% in TiO_2= 1% wt.) and the milled catalyst (best conditions: Cu_2O% in TiO_2= 1% wt.; Milling time = 1 min; rotation rate = 200 rpm) under visible (λ>400 nm) and UV-A + Visible light conditions. 106

Table 7. Mean hydrogen production rate and light to chemical energy efficiency (in the UV and total solar range) obtained using the milled catalyst (best conditions: Cu_2O% in TiO_2= 1% wt.; Milling time = 1 min; rotation rate = 200 rpm) under solar conditions. 115

Table 8. Values obtained for the unknown kinetic constants. Reference values adopted in the current investigation reported by Clarizia et al. [236]................... 123

Table 9. Experimental conditions used in the mathematical model. For all runs: pH=8.50; T=35°C; Cu_2O percentage = 1%wt; milling time = 1 min; rotation rate = 200 rpm.. 122

1. Background

1.1. Energy production and renewable sources. Photocatalytic hydrogen production

Nowadays, 80% of global energy consumption is dependent on fossil fuels [1], leading two different problems: firstly, the fossil energies such as petroleum or natural gas are decreasing strongly [2]; secondly, use of the fossil fuels due to the industrial revolution and their incomplete combustion, lead several environmental problems: global warming, greenhouse effect, production of harmful gases as well as ozone layer depletion and acid rain [2,3]. To overcome these drawbacks, it is necessary to develop suitable processes aimed to produce energy from renewable sources [4,5], such as solar energy, a clean and inexhaustible source, receiving much attention in the last 20 years [6–8].

In terms of energy carrier, hydrogen is, most of all, the potential alternative fuel due to its stability and zero emission of greenhouse gases [9]. Hydrogen is the simplest and lightest element in the periodic table, as well as the most abundant on the Earth's surface. Indeed, it is present in water and in organic compounds; the occurrence in water has attracted the attention of the major scientists, as a possible way to produce energy economically. In terms of physical properties, the gravimetric heating value is higher [10], while the volumetric heating value is lower than the other fuels (flammable limits in air 5.0% v/v and 75.0% v/v [11]), leading several problems related with the transport and the storage [12].

Despite the properties of flammability and explosivity and the high production costs [13], a growing interest in hydrogen utilization is recorded in recent years [12]. As concerns the application indeed, hydrogen can be used for electricity production by the utilization of fuel cells [14–16] in the power plants and in automotive industry [17].

Nowadays, several processes for hydrogen production are reported [13,18], from fossil fuels (steam reforming of natural gas, partial oxidation, hydrocarbon pyrolysis)[19] as well as from renewable sources (biomass, photocatalytic processes, water splitting etc.) [20–22]; in recent years, however, solar route for hydrogen production has stimulated the interest of more than few authors [23,24], several studies being carried out photoelectrolysis [25–27], photocatalytic water splitting [28,29] and on photoreforming of organics [30–32], the latter derived from renewable sources or wastewater containing them [33,34]. The possibility to use the organic pollutants contained in the wastewater is very attractive and widely reported in literature, due to the possibility to associate the hydrogen production and the water treatment as well as the low cost of the feedstock if compared to the produced hydrogen [33,35–37].

In the following pages a general overview of the photocatalytic processes related to hydrogen production are presented, highlighting the principles and the current applications.

1.2. Photocatalytic processes aimed to hydrogen production

The term photocatalysis is generally used to describe a process in which a material, called "photocatalyst" is excited by a properly radiation, resulting in chemical reactions involving the substances present in the system [38]. The International Union of Pure and Applied Chemistry (IUPAC) has decided that the term photocatalysis is reserved for the reactions carried out in the presence of a semiconductor and light [39]. Despite in the first years of the 20th century several Authors began to take an interest to the phenomena related to the exploitation of the solar energy [40], the birth of the photocatalysis was attributed to Fujishima and Honda, that, in 1972 conducted the photolysis of water using a semiconductor electrode based on titanium dioxide TiO_2 [41]. Since then, several studies were conducted on photocatalytic processes, placing the attention on the environmental and energetic fields. Moreover, several researchers focused on the study of the photocatalytic mechanism to understand the fundamentals of the process.

From a theoretical point of view, the photocatalytic process begins when the photocatalyst is irradiated through a UV or visible radiation (depending on the band gap energy of the semiconductor), generating electron-hole pairs (r.1)

$$\mathrm{Cat} \xrightarrow{\text{radiation}} h^{+} + e^{-} \qquad \text{r. 1}$$

However, electron-hole pairs may rapidly recombine through radiative or non-radiative processes, producing heat and light, due to the presence of defects in the structures and the natural tendency of the charges to return at a lower energy level (r.2).

$$h^{+} + e^{-} \overset{k_r}{\rightarrow} \text{Heat + light} \qquad \text{r. 2}$$

Reaction (r.1) depends on the rate of photon absorption by the photocatalyst, whereas reaction (r.2) depends on the electron/hole recombination rate constant.

Therefore, photocatalytic hydrogen production may take place by adopting two different approaches: *(i)* the photocatalytic water splitting as well as *(ii)* the photocatalytic reforming of organics.

In the first case, water decomposition gives rise to the formation of hydrogen and oxygen gases as reported in the r. 3 and r. 4.

$$H_2O + 2h^+ \xrightarrow{k_{h^+}} {}^1/_2\, O_2 + 2H^+ \qquad \text{r. 3}$$

$$2H^+ + 2e^- \xrightarrow{\text{Fast}} H_2 \qquad \text{r. 4}$$

However, the high electron-hole recombination rate reduces the effectiveness for the H_2 generation in the case photocatalytic water splitting when pure water is used [42]. As a result, photocatalytic hydrogen production is typically studied in the presence of sacrificial species, such as methanol, ethanol, and glycerol, which react with positive holes to enhance charges separation.

In the case of photoreforming of organics, the organic compounds in the system, depending on the pH of the suspension, may be adsorbed on the catalyst surface (r.5), thus forming complexes (monodentate, bidentate etc.).

$$Org + \theta \overset{K_{ads}}{\longleftrightarrow} Org_{ads} \qquad \text{r. 5}$$

Then, the adsorbed species may react with positive holes, producing hydrogen gas and by-products (r. 6 – r. 7):

$$Org_{ads} + 2h^+ \xrightarrow{k_{h^+}} Org^{\bullet}_{ads} + h^+ \xrightarrow{\text{Fast}} P + 2H^+ \qquad \text{r. 6}$$

$$2H^+ + 2e^- \xrightarrow{\text{Fast}} H_2 \qquad \text{r. 7}$$

As previously discussed, the semiconductor bandgap represents a key parameter for a selected photocatalyst, due to the straight relation with the wavelength of activation of the material. Generally, a semiconductor with a bandgap higher than 3.0 eV only absorbs UV radiation, which represents only about 5% of the solar spectrum [43]. However, along with the band gap, the potential of the valence and conduction bands strongly influences the photocatalytic hydrogen production; in fact, the conduction band should be more negative than the reduction potential of H^+ to H_2 (0 V vs. NHE at pH = 0) to effectively produce hydrogen gas, while the valence-band edge should be more positive than the oxidation potential of water ($E_{O2/H2O}$ = 1.23 V vs. NHE at pH = 0) in case of the water splitting, or of the organic compound, in case of the sacrificial photocatalysis, to effectively oxidize the selected species [44].

Considering what reported above, the choice of the photocatalyst represents the critical point for the photocatalytic hydrogen production, which limited, at present, the industrialization of the process.

Based on this general overview on the topic, in the next section a more detailed description of the most used photocatalysts is proposed, highlighting the advantages and the key challenges.

1.3. Photocatalysts. Advantages and disadvantages

Generally, heterogeneous photocatalysis is proposed for hydrogen production. Compared with homogeneous photocatalysts, heterogeneous photocatalysts have several advantages, such as the good thermal stability as well as the simpler and cheaper separation and reutilization with respect to other methodologies [45]. A particular class of solids, i.e., semiconductors, are widely used as photocatalyst, due to the band gap value of the order of 1 eV [44]. As previously discussed, to efficiently convert solar energy the photocatalyst should possess suitable band gap to satisfy *(i)* an efficient light absorption and *(ii)* suitable CB and VB levels for redox reactions and *(iii)* highly efficient separation and transfer of photogenerated charges. At the moment, there are always inherent deficiencies in the semiconductors, and it is very difficult to find a single component that can address all these requirements.

As concerns the UV active photocatalytic materials, a wide range of semiconductors have been developed, typically classified in four different groups, as reported by Chen et al. [43]: *(i)* d^0 metal oxide photocatalysts, such as TiO_2, $Na_2Ti_3O_7$, VO_2, RuO_2 and Ta_2O_5; *(ii)* d^{10} metal oxide photocatalysts, from which Ga_2O_3 is the most widely studied [46,47]; *(iii)* f^0 metal oxide photocatalysts, such as CeO_2 powder, and *(iv)* nanoxide photocatalysts.

At present, TiO_2 represents one of the most investigated photocatalysts due to its high chemical stability, photocorrosion resistance, non-toxicity, easy availability, and high photocatalytic activity under UV range [41,48]. Anatase and rutile have gained particular attention in the photocatalytic field, representing the most used phases of TiO_2. Despite of the great number of positive characteristics, titanium dioxide presents different problems such as high electron-hole recombination rate and, as above mentioned, poor absorption in the visible light range, due to its wide band gap (about 3.2 eV) [49,50]. Several authors proposed some strategies to improve the activity of TiO_2, in particular to reduce its bandgap and increase its conductivity [51]. The addition of metals as co-catalyst and the association with other semiconductors are only few examples of the proposed methods to modify the photocatalyst.

Along with TiO_2, also zinc oxide represents a popular metal oxide, due to its utilization in a wide range of application, such as UV light emitters, catalysis, electronics and piezoelectric devices, chemical sensors, pharmaceutical uses, antimicrobial agents, photoanode materials for dye-sensitized solar cells; moreover, ZnO semiconductor is nowadays considered as a suitable and promising alternative for TiO_2 photocatalyst [52], due to despite the similar photocatalytic activity with TiO_2, the production cost of ZnO is up to 75% lower than that of TiO_2 [53]. It is an extensively examined photocatalyst, resulting a low cost, non-toxic and environmentally friendly material, with high redox potential and electrochemical stability, good isoelectric point (pH = 9.0–9.5), and attractive electro-optical features [54,55]; In recent years, a large attempt has been dedicated on the synthesis and characterization of ZnO, due to the morphological versatility [56] and the above-mentioned characteristics. It represents a wide band gap semiconductor (3.37 eV – 3.7 eV [57–59]), in which valence band is separated by various sub – levels at different energies due to native or intrinsic defects in the structure [60]; moreover, it is generally a n – type semiconductor, with a large excitation binding energy (60 meV) and a large and deep violet/borderline ultraviolet (UV) absorption at room temperature [53].

As part of the visible active photocatalytic materials, CdS results an interesting semiconductor for hydrogen production, due to its narrow band gap of about 2.42 eV, which allow the activation under visible light radiation. However, its small band gap leads to a higher electron-holes recombination rate, thus making necessary the association with other materials as well as the modification of the structure of the semiconductor [61,62].

Moreover, Cu_2O represents another alternative photocatalytic material for hydrogen production, due to its narrow band gap (about 2 eV [63,64]) is favourable for the activation under visible light radiation, its abundance (as metal) on Earth and its cost-effectiveness [65,66]; cuprous oxide is a p-type semiconductor, and its negative potential of the conduction band potentially allows the production of hydrogen. However, several disadvantages are associated to copper (I) oxide, such as the poor photostability and the high electron-hole recombination rate. Also for this photocatalyst, the association with other semiconductors, or more in general with other materials have been proposed by several authors as possible solutions to improve its photocatalytic performance [67–72].

2. State of art

2.1. Enhancement of the photocatalytic activity of semiconductors

As previously discussed, many metal oxides semiconductors (such as TiO_2, ZnO and CdS) have been proposed as photocatalysts to convert solar energy into hydrogen [73]. Among them TiO_2 – due to its high chemical stability, photocorrosion resistance, non-toxicity, great availability, and significant absorption of solar radiation – is the most widely used photocatalyst since the first report by Fujishima and Honda [41,48,74]. Despite of the great number of positive characteristics, titanium dioxide presents different problems such as high electron – hole recombination rate (3.0×10^{10} M^{-1} s^{-1}[75]) and poor absorption in the visible light range, due to its wide band gap (about 3.2 eV) [49]. In order to overcome these disadvantages, many researchers have directed their efforts to improve the efficiency of bare TiO_2 through the combination of the semiconductor with other materials capable to extend the light absorption to the visible range and to reduce the recombination rate [76,77]; on the other hand, many studies present in the literature are focused on the utilization of different semiconductors able to replace TiO_2 [25,78,79].

With reference to the first approach, noble metals (Ag, Pt, Au, Pd) have been found to be excellent co – catalysts for hydrogen production [80,81], despite of the fact that they have high costs; impregnation, co-precipitation or photodeposition methods are only some examples of the preparation methods proposed for metal – doped photocatalyst by several authors [82,83].

Generally, noble metals have gained great attention due to their physicochemical characteristics, which effectively enhance the photocatalytic activity; in particular, the deposition of metals with a large work function, such as Ag, Au as well as Pt and Pd can reduce the recombination rate because of the formation of Schottky barriers at the metal/TiO_2 interface: being the work function of the metal higher than that of the titanium dioxide there is the formation of an electrons flow from TiO_2 to the metal to align the Fermi energy levels (EF), with a shift of the Fermi levels of the metal to the conduction band of TiO_2 [84]. The metal, with a more negative energy levels, leads to a thermodynamic favourable proton ion reduction and favours the proton reduction also from a kinetic point of view. Hence, metal nanoparticles *(a)* act as antennas, producing a higher light absorption and *(b)* promote the transfer of free excited electrons into the conduction band of the semiconductor [85].

Despite the improvement in the photocatalytic activity of the metal doped photocatalysts, these kind of materials does not demonstrate a significant activation under visible light radiation. Hence, to extend the light adsorption to wavelength higher than 400 nm, a different approach was proposed by different authors; in particular, the association of two (or more) different semiconductors (semiconductor – semiconductor heterojunction) was discussed in several articles [86–91]. Generally, two different categories of semiconductor-semiconductor photocatalytic materials are reported: p – n semiconductor heterojunction and non – p – n heterojunction systems. Focusing the attention on the first case, when two semiconductors (a p – type semiconductor with a n – type semiconductor) are in contact, the diffusion of electrons and holes leads to the formation of a space-charge region at the interfaces. When irradiated, the photogenerated electrons are transferred from the CB of one photocatalyst (generally the p – type) to the CB of the other photocatalyst forming the heterojunction (generally the n – type), while the holes can migrate between the valence bands of the semiconductors, depending on the relative redox potentials; the phenomenon leads to a more efficient charge separation and a lower electron-holes recombination rate.

Three types of heterojunctions are reported by Moniz et al. [92]: Type I: two semiconductors whereby the CB of component B is higher than that of A. The VB of B is lower than that of A, therefore holes and electrons will transfer and accumulate on component A. Type II: the photoexcited electrons migrate from B to A, due to the more negative CB position of B, while holes can move in the opposite direction from the more positive VB of A to B, leading to all-round efficient charge separation and enhanced photocatalytic activity. Type III: as for Type II, except for the higher driving force for charge transfer, due to the more marked difference in VB and CB positions.

The extension of the photocatalytic activity at the visible light range was detected by different authors through the association of a selected semiconductor, such as TiO_2, with another one with a narrow band gap [64,86–89,93,94]; the obtained composite may be able to absorb the visible light radiation by the latter, thus giving rise to the above discussed diffusion of electrons and holes. With reference to this approach, the association of two semiconductors, TiO_2 and Cu_2O, will be discussed in the next section, focusing the attention on the most reported preparation methods, on characterization technique as well as on the obtained results in terms of hydrogen generation.

2.2. Cu_2O as semiconductor and p-n type heterojunction with titania

Composites prepared coupling TiO_2 and Cu_2O are an example of p – n type heterojunction that have been proposed as photocatalysts for organic reforming.

It is interesting to remember that Cu_2O-based materials are employed for a wide range of applications, such as sensing, desulfurization, disinfection, organic synthesis, photodegradation, photovoltaics, and photocatalysis [70,72,95–106]. Recent literature findings indicate a growing interest towards Cu_2O as cocatalyst on titanium dioxide for photocatalytic hydrogen evolution [71,107,108] with performances comparable with Ag and Au [109–111].

Cu_2O is a typical p – type semiconductor exhibiting a narrow band gap of 2.2 eV, whereas TiO_2 is an extensively investigated n – type semiconductor. Their combination may result in a p – n heterojunction, which can (*i*) absorb radiation within the solar spectrum [112–114] and (*ii*) increase the photogenerated charge carrier separation, leading to photocatalytic efficiencies up to about 100 – fold higher than that obtained in the presence of the bare TiO_2 [92,115,116].

Within the crystalline structure of n – type TiO_2 and p – type Cu_2O most charge carriers are negative electrons and positive holes, respectively. As soon as the p – n heterojunction is formed at the TiO_2/Cu_2O interface, the difference in Fermi levels drives the charge carrier flow until an equilibrium state in which the Fermi level is constant at any point in the system is reached, as schematically shown in Figure 1 [117,118]. As a result of interfacial charge flow, an electric field from TiO_2 to Cu_2O and band bending are formed due to resulting local zones of Cu_2O and TiO_2 carrying excess negative and positive charges, respectively. Finally, the arising p – n heterojunction promotes the photocatalytic hydrogen generation process by enhancing electron flow from Cu_2O to TiO_2.

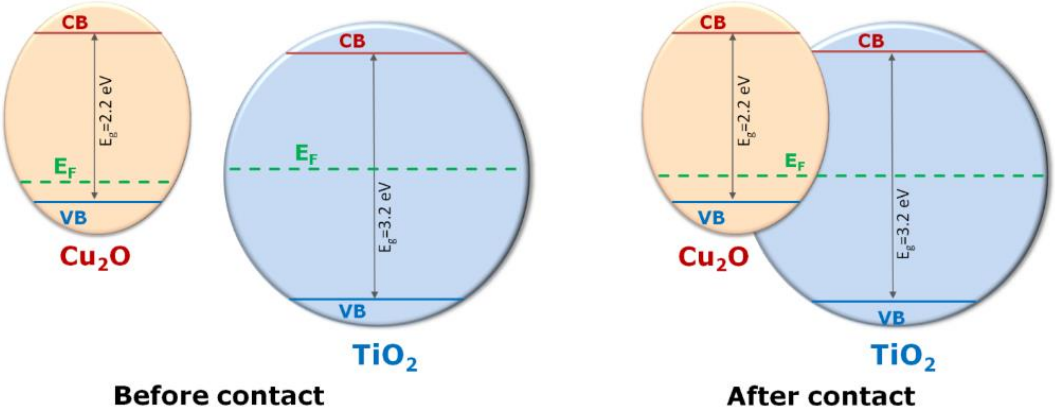

Figure 1. Energy band diagram of Cu_2O and TiO_2 before and after contact [118].

2.3. Preparation of Cu_2O/TiO_2 composite materials

From literature indications, the preparation methods of Cu_2O/TiO_2 composite photocatalysts primarily differ depending upon TiO_2 type used. Based on this consideration, a first classification is herein made by considering the TiO_2 type. In particular, the papers analyzed in the present investigation can be classified in two different classes: a first class using TiO_2 in its commercial mixed phase (i.e., P25 – TiO_2), and a second one employing home – prepared titanium dioxide. In the latter case, the different preparation method will be not discussed in the present work. As concerns Cu_2O, Cu^{2+} is the commercially available form of copper species with highest chemical stability, hence most of the Cu_2O/TiO_2 preparation procedures found in the literature survey involve the use of a cupric salt, such as cupric nitrate, perchlorate, or sulphate. Cupric species, generally dissolved in aqueous solution, are selectively reduced in the presence of titanium oxide, so that cuprous ion can be promptly incorporated on the surface or in the crystalline structure of TiO_2, using different reduction methods as well as reducing agents.

Several reduction methods are reported in the next paragraphs. Moreover, as reported in Table 1, others distinguishing factors found in the preparation of Cu_2O/TiO_2 photocatalysts are the deposition method of active species (e.g., impregnation/calcination, photodeposition, electrochemical deposition, etc.) and the employment of selected cocatalysts (e.g., WS_2, Au, Pt, etc.). Some examples of distinguishing factors in the preparation of Cu_2O – TiO_2 composite materials are briefly given hereunder.

2.3.1. Reducing agents

Several authors employed glucose as reducing agents in the preparation procedure of Cu_2O/TiO_2 photocatalysts for hydrogen evolution [64,114,119,120]. Segovia – Guzman [64] et al. prepared Cu_2O/TiO_2 samples by impregnation followed by a microwave – assisted method employing glucose as reducing and stabilizing agent at two levels of concentration. To this aim, a fixed amount of P25 – TiO_2 was added to deionized water at room temperature together with an aliquot of glucose,

$CuCl_2$, and NaOH solutions. The suspension was then magnetically stirred at room temperature for and heated at 120 °C microwave system to obtain a hydrothermal effect. After centrifugation, the precipitates were washed and dried at 70 °C. The formation of cuprous oxide was clearly demonstrated by XRD and XPS spectra. After using such catalyst for H_2 generation through glycerol photoreforming under UV-visible irradiation through a metal halide lamp, the chemical stability of the recycled photocatalyst was confirmed by XPS results, which excluded the occurrence of Cu_2O transformation after the photocatalytic process. Tamiolakis et al. [119] prepared Cu – loaded mesoporous TiO_2 nanoparticles (MTA) with different Cu_2O content by chemical reduction deposition method. Typically, a fixed amount of MTA was dispersed in a copper (II) nitrate ethanol solution, which was subsequently stirred at 40 °C. Reduction of copper (II) on MTA surface was performed by suspending the Cu^0/TiO_2 composites into an aqueous solution containing glucose and NaOH. The resulting mixture was then stirred for at 60 °C, filtered, and the deriving solid was dried at 60°C. HR – TEM images and XRD spectra clearly showed the presence of Cu_2O nanocrystals on the MTA surface. A rigorous comparison among the photocatalytic performances of the systems above described is not possible due to the different operating conditions employed (i.e., sacrificial organic agent, irradiation type, co-catalyst, etc). However, by simply comparing the values of hydrogen production rate per unit mass of photocatalyst, the best result between Cu_2O/TiO_2 composites prepared via glucose – based reduction method was recorded by Cheng et al.[120]. The Authors employed Cu_2O – decorated mesoporous TiO_2 beads (Cu_2O/MTBs) for methanol photoreforming by means of 400 W high – pressure mercury lamp without any UV cut – off filter and collected a maximum value of hydrogen production rate per unit mass of photocatalyst equal to 223 mmol/h·g. Cu_2O/MTBs samples showed significantly higher (4.4 – 5 – fold) evolution rates than P25-TiO_2.

Zhen et al. [121] prepared Cu_2O/TiO_2 catalysts using selective reduction by hydroxylamine under alkaline conditions. More in detail, fixed amount of $CuCl_2$ and sodium dodecyl sulfate were added to deionized water containing P25 – TiO_2. After adding NaOH to the aqueous mixture, a light blue suspension containing a $Cu(OH)_2$

precipitate was observed. Finally, $NH_2OH{\cdot}HCl$ was quickly added into the suspension. After stirring, the mixed solution was kept at 30 °C for the growth of the Cu_2O crystals. The resulting orange solid was collected by centrifugation, followed by washing and drying in a 50 °C vacuum oven. Various samples with different loading amounts of Cu_2O on TiO_2 were prepared according to the same procedure and successively added to an aqueous mixture containing Eosin – Y and triethanolamine (TEOA). The mixed solution was then irradiated with visible light to prepare $Cu^0/Cu_2O/Cu^0/TiO_2$ composite photocatalysts through *in situ* photoreduction. The presence of Cu_2O was confirmed by XPS spectra, XRD spectra, and HR – TEM images. The Authors obtained a photoefficiency value expressed as Apparent Quantum Efficiency of about 45% at 520 nm, corresponding to a value of hydrogen production rate per unit mass of photocatalyst equal to 3.94 mmol/h·g. Such highest value of hydrogen production rate per unit mass of photocatalyst reached almost 196 times that recorded over bare P25-TiO_2 and 3 times that of a reference Cu^0/TiO_2 sample.

Zhu et al.[122] reported the formation of Cu_2O/TiO_2 nanotube-array heterogeneous structures by coating Cu_2O nanoparticles onto titanium dioxide via multiple-cycle chemical adsorption plus reduction method (MC – CAR). At first, TiO_2 NTAs were immersed into an aqueous solution containing $CuSO_4$ and glucose to ensure adequate absorption. TiO_2 NTAs were then soaked with deionized water to remove excessive $CuSO_4$.

Subsequently, the coated TiO_2 NTAs substrates, with Cu^{2+} monolayer, were dipped into a different aqueous mixture containing N_2H_4 and NaOH, in which Cu^{2+} was reduced to Cu_2O monolayer. The reduction process was again followed by soaking with deionized water. All such procedures were performed at 40 °C in a thermostatic bath. The resulting Cu_2O/TiO_2 composite materials were then dried at 100 °C in nitrogen atmosphere. The presence of Cu_2O clearly resulted from XRD spectra.

For photoelectrocatalytic hydrogen evolution experiment, Cu_2O/TiO_2 NTAs was used as the photoanode in a Na_2SO_4-ethylene glycol electrolyte solution. The photoanode was subjected to continuous irradiation under illumination intensity of 100 mW/cm^2 by a solar simulator coupled to an AM 1.5G filter. The highest photoefficiency value collected was equal to 6.2 mmol/h·cm^2, which was 2.5 times that of TiO_2 NTAs (pure anatase phase).

Le et al. [123] obtained Cu_2O/TiO_2 nanorod arrays (TNA) through a growth method based on cyclic impregnation. Two samples of TNA film on fluorine doped tin oxide glass substrates were immersed into four distinct solutions (i.e., 0.1 M $CuSO_4$ and 0.1 M $Na_2S_2O_3$ mixture, highly purified water, 0.1 M NaOH and highly purified water) for 5 seconds sequentially. The immersing process was repeated for 10 or 30 cycled times, respectively. At the end of this sequence, the two samples were dried at the atmosphere. Cu 2p XPS spectra before and after HER upon a Xe lamp irradiation with UV cut off filter demonstrated the presence of Cu_2O on the catalyst surface.

As regards the best photocatalytic activity for hydrogen evolution found by using this method, a maximum photoefficiency value of about $4.8 \cdot 10^{-4}$ mmol/h·cm^2 was recorded by adopting glycerol as sacrificial organic species and a 300 W Xenon Lamp endowed with a UV – cut off filter (λ>400 nm). Such maximum photoefficiency for hydrogen evolution was about 4 – fold higher than that of pure TNAs (rutile phase).

2.3.2. Electrochemical deposition

As shown in Table 1, Column I, electrochemical deposition method was adopted by plenty of authors in the literature survey to prepare Cu_2O/TiO_2 composites for photocatalytic hydrogen evolution [9,124,125], most of whom employed Cu_2O/TiO_2 as an effective and low-cost photocathode material in photoelectrochemical cells.

Zhang et al. [125] employed a three-electrode system to fabricate a film made of TiO_2 nanotube arrays, which was used as working electrode. A Pt mesh and an Ag/AgCl electrode were employed as auxiliary and reference electrodes, respectively. A suitable electrolyte was prepared by dissolving a fixed amount of $CuSO_4$ in a lactic acid solution, whose pH was adjusted by adding proper quantities of NaOH. Electrodeposition charges of 500 mC were applied on the stirred electrolyte during the deposition process. Different types of Cu_2O/TNA samples were synthesized by varying the deposition potential applied vs Ag/AgCl. The obtained samples were then dried at 50°C in vacuum. SEM images, as well as XRD spectra, revealed the presence of octahedral Cu_2O particles on the TNA surface. The best photocatalytic performances were obtained by using methanol as sacrificial agent and a light source (Xenon lamp) with a UV cut-off filter. In such conditions, 8.9 $mmol/h \cdot cm^2$ of hydrogen were produced, indicating a remarkable activity of the electrode employed. Such maximum photocatalytic hydrogen evolution rate recorded over Cu_2O/TNA photocatalyst was about 42 times higher than pure TNA (mixed anatase-rutile phase).

2.3.3. Impregnation/calcination

Amongst most adopted Cu_2O/TiO_2 preparation techniques, wet impregnation followed by calcinations should be mentioned. Impregnation was used in several studies from the literature survey to merge TiO_2 (i.e., commercial or home prepared) and Cu_2O nanoparticles, always followed by calcination under various temperature and atmosphere conditions and for different treatment times [126–131].

Liu et al. [129] prepared Cu_2O/TiO_2 photocatalysts employing TiO_2 with different phase structures as well as P25 as supports via an incipient wetness impregnation/calcinations method. More in detail, a fixed amount of TiO_2 (i.e., commercial P25 or anatase, rutile, and mixed phases of anatase/rutile/brookite prepared via hydrothermal method) was impregnated with appropriate quantity of $Cu(NO_3)_2$ in aqueous solution at room temperature, and was then dried at 100°C. The resulting powder was successively calcined at 400°C in air. XPS spectra, as well as HR-TEM images and H_2-TPR profiles revealed the presence of cuprous oxide on the surface of the titania supports with various crystalline phase composition.

Dubey et al. [131] employed a wet chemical treatment to obtain Cu_2O/TiO_2 nanostructures by using crystallized aligned TiO_2 nanotubes (TNTs) and a solution containing $Cu(NO_3)_2$ and NaOH. For a typical preparation procedure, fixed amounts of $Cu(NO_3)_2$ and crystalline aligned TNTs were suspended and stirred in aqueous solution. NaOH was then added drop wise to such suspension at varying molarities. These samples were successively washed with alcohol and dried through an air stream, and then heated at 200°C. Cu_2O formation was confirmed by XRD spectra, SEM images, and HR – TEM analyses. As concerns the photocatalytic performances of the as prepared Cu_2O/TiO_2 composites, a maximum value of hydrogen production equal to 79.8 mmol/h·g was achieved by Praveen Kumar et al. [130] by adopting ethylene glycol as sacrificial organic agent under direct solar light irradiation with an average light intensity of $1.15 \cdot 10^5$ lx. The Cu_2O/TiO_2 photocatalyst prepared by Praveen Kumar et al. [130] exhibited enhancements of 33 and 18 – fold in hydrogen production rate as compared to commercial P25 – TiO_2 nanoparticles (TNP) and calcined TNTs, respectively.

In conclusion of this paragraph, it can be stated that, irrespective of the preparation method, Cu_2O/TiO_2 composite photocatalysts prepared as above reported are all capable of ensuring hydrogen production rates higher than bare P25-TiO_2 and sometimes under visible light irradiation only. In particular, the highest increase in reactivity was firstly observed for a Cu_2O/TiO_2 photocatalysts prepared through via reduction of cupric species by means of hydroxylamine. Significant results may be also obtained by the adoption of an electrochemical deposition method.

2.4. Characterization techniques for Cu_2O/TiO_2 composite materials

The main techniques adopted to characterize Cu_2O/TiO_2 composite materials are described hereafter. Two distinct classes of characterization are reported for such materials:

1) Characterization techniques devoted to the unique identification of the oxidation state of copper, which is deposited on the photocatalyst surface and responsible for the co-catalytic activity. X – ray diffraction spectroscopy (XRD), X – ray photoelectron spectroscopy (XPS), Raman Spectroscopy, and High – resolution transmission electron microscopy (HR – TEM) belong in this category.
2) Characterization techniques aimed at evaluating the capability of such photocatalysts to (*i*) absorb irradiated light, with special attention to visible-light-responsive materials, and (*ii*) reduce the likelihood of charge carrier recombination. Diffuse Reflectance UV (DRUV) Spectroscopies and Photoluminescence (PL) belong in this category.

2.4.1. X-Ray Diffraction spectroscopy

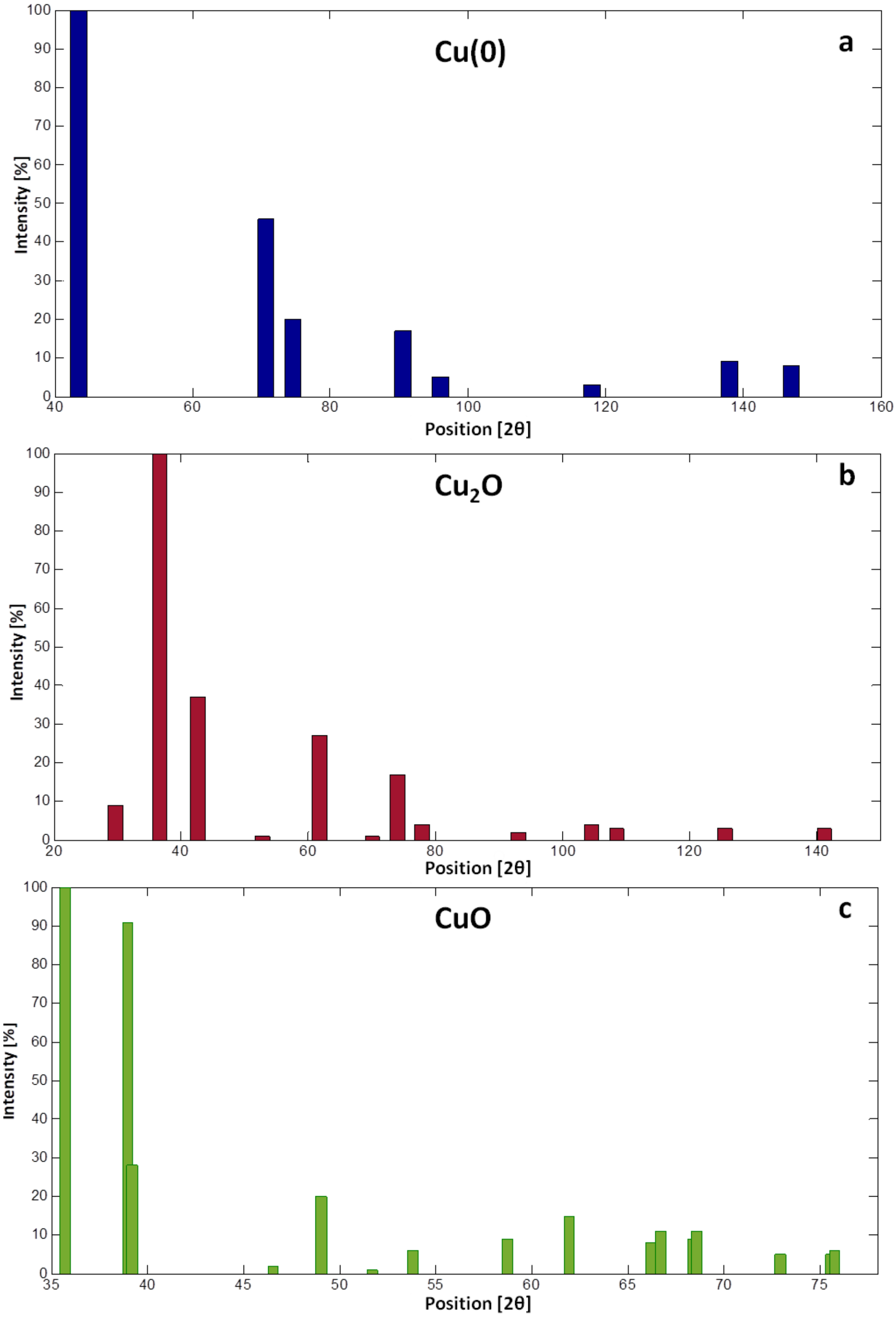

Figure 2. XRD signals of Cu^0 (a), Cu_2O (b), and CuO (c).

X-Ray Diffraction (XRD) spectra signals can be used to univocally identify copper oxidation state on the photocatalyst surface through the knowledge of the spectra of the single oxidation state. To this aim, as shown in Figure 2, XRD data recorded using an analytical method previously reported [132] indicate that:

i) the spectrum of Cu^0 presents the peaks corresponding to an angle 2θ [°] of 43.23, 50.51, 74.30 with d-spacing values [Å] of 2.09, 1.81, 1.28, respectively. These peaks are expected for a cubic form of metallic copper[133];

ii) the spectrum of Cu_2O is characterized by the presence of some peaks 2θ values [°] equal to 29.74, 36.65, 42.57, 52.80, 61.76, 70.06, 74.05, 77.89, 93.11, 104.60, 108.52, 125.56, and 141.22, with d-spacing values [Å] of 3.02, 2.4, 2.13, 1.74, 1.51, 1.35, 1.29, 1.23, 1.07, 0.98, 0.95, 0.87, and 0.82, respectively.

iii) for cupric oxide nanoparticles (CuO), the peaks found in the XRD spectrum at 2θ values [°] of 35.44, 35.49, 38.72, 48.65, with d-spacing values [Å] of 0.253, 0.252, 0.232, and 0.187, respectively, well agree with JCPDS data (JCPDS cards n. 65-2309).

2.4.2. X-Ray photoelectron spectroscopy

The following remarks, matched with the spectra in Figure 3 reported by Zhen et al. [134], may help to clearly identify the oxidation state of copper species on the photocatalyst surface by means of XPS. In CuO/TiO_2 The peaks at nearly 933.6 and 953.6 eV univocally indicate the presence of copper (II) [121]. The double-peak between 940 eV and 945 eV is reported to be a copper (II) satellite peak [121,135] but in the same position also Cu^{1+} showed a low satellite peak. On the other hand, the typical copper (I) peaks of Cu_2O in Cu_2O/TiO_2 are individuated at 932.2 and 952.0 eV.

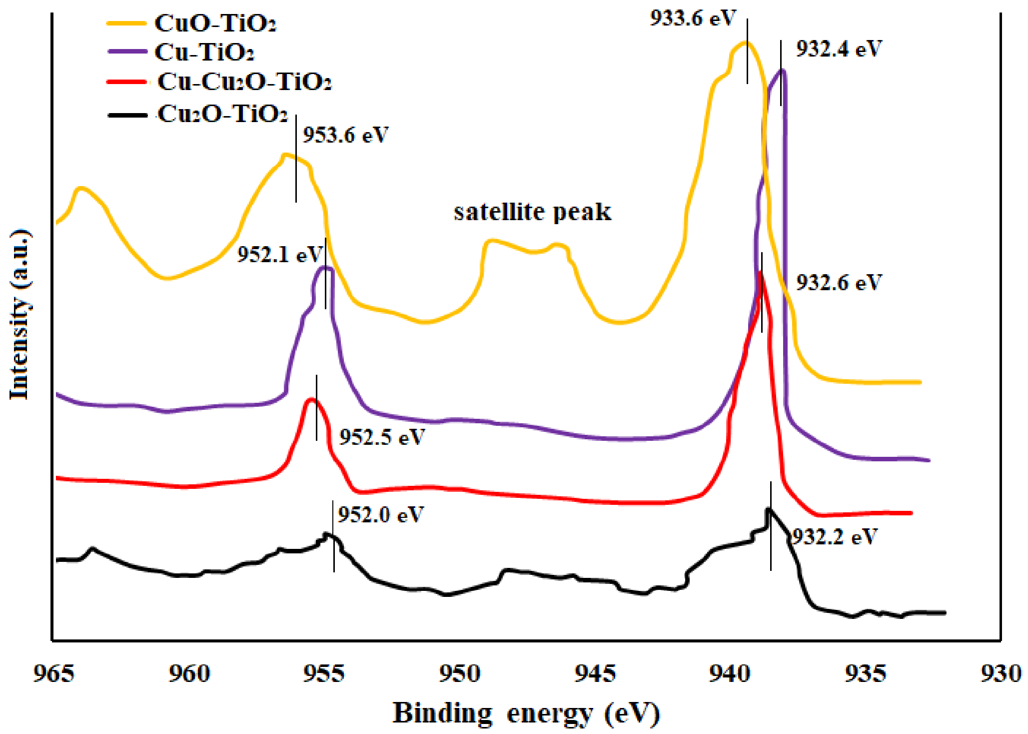

Figure 3. XPS spectra of $Cu^0/Cu_2O/ Cu^0/TiO_2$, Cu^0/TiO_2, Cu_2O/TiO_2, and CuO/TiO_2 adapted by Zhen et al.[121]: (1) CuO/TiO_2; (2) Cu/TiO_2; (3) $Cu^0/Cu_2O/ Cu^0/TiO_2$; (4) Cu_2O/TiO_2.

On the basis of the consideration reported above, an application of this technique was presented by Jung[136]: they indicated that most part of copper in air-calcined Cu^0/TiO_2 based photocatalysts is present in the form of copper (II) with a peak at 934.1 eV, whereas a reduced presence of Cu^{1+} and Cu^0 is generally recorded (the presence of Cu^{2+} can be due to the oxidation of copper (I) in air). On the other hand, when such photocatalytic materials are reduced under hydrogen atmosphere, an increase in intensity of the peaks related to Cu^{1+} and Cu^0 and a decrease in intensity of both Cu at 934.1 eV and satellite peaks are observed.

It is generally accepted that the similarity between the binding energies of copper (I) and copper (0) does not allow to unequivocally differentiate these two species and further spectroscopic indications are required (e.g., XRD, Raman, etc).

2.4.3. Raman spectroscopy

Limited literature information is available on Raman spectroscopy of Cu oxides [119,137–140]. Conflicting indications about the correlation between copper species and related peaks in Raman spectra are reported. Therefore, selected peaks providing a clear distinction between cupric and cuprous oxides were considered. More in details, the typical most intense Raman peaks corresponding to 216, 520, and 640 cm^{-1} are reported [141–143] for Cu_2O, whereas a peak at around 280 cm^{-1} is commonly attributed to the presence of CuO [141,142,144–147]. Some of the most intense peaks capable to unambiguously identify cupric and cuprous oxides obtained according to an analytical procedure previously reported [132] are shown in Figure 4.

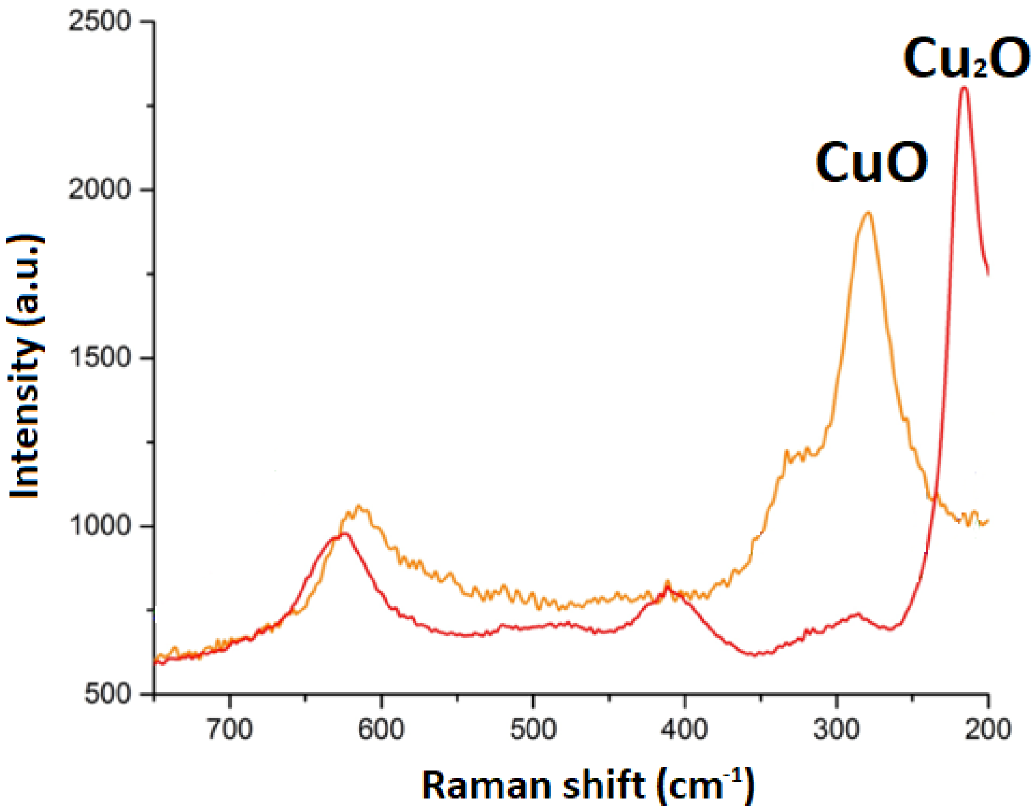

Figure 4. Raman spectra of CuO and Cu_2O.

2.4.4. High – resolution transmission electron microscopy

Several authors used high – resolution transmission electron microscopy (HR – TEM) analyses for structural and morphological characterization of Cu/TiO_2 composite materials, obtaining different results using commercial or home prepared TiO_2 as well as a different preparation method. HR – TEM images also allow to undoubtedly identify the Cu valence state in Cu-based TiO_2 photocatalysts for hydrogen evolution. In this regard, plane spacing values of nearly 0.25 and 0.28 nm corresponding to the d spacing of Cu_2O (111) have been reported [113,121,148,149] in Cu_2O/TiO_2 nanocomposites, as shown in Figure 5.

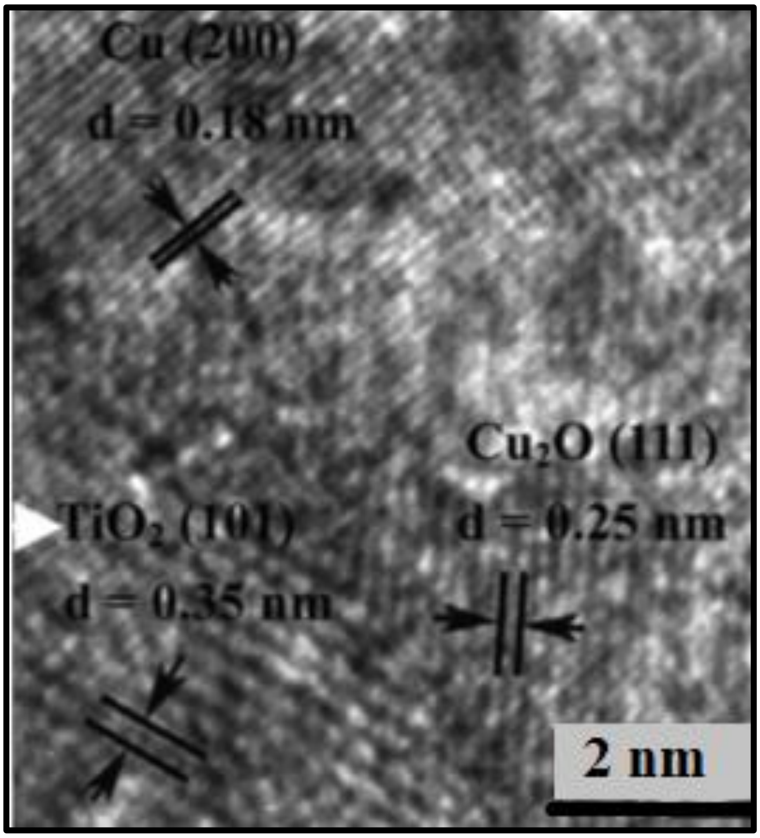

Figure 5. HRTEM of Cu_2O in Cu_2O/TiO_2 composite [150].

The presence of Cu_2O nanoparticles in Cu_2O/TiO_2 composites can be also clearly distinguished in TEM images by their peculiar structure, which is reported to have cubic shape [151]. On the other hand, as previously reported [149], the presence of CuO in Cu-based TiO_2 nanocomposites could be distinguished through the existence of particles with rhombic shape in HR-TEM images. In general, the attribution of specific planes and their corresponding lattice spacings in HR-TEM images could give relevant information about the crystallinity grade and the morphology of Cu_2O/TiO_2 composites.

2.4.5. Diffuse reflectance UV–Visible spectroscopy

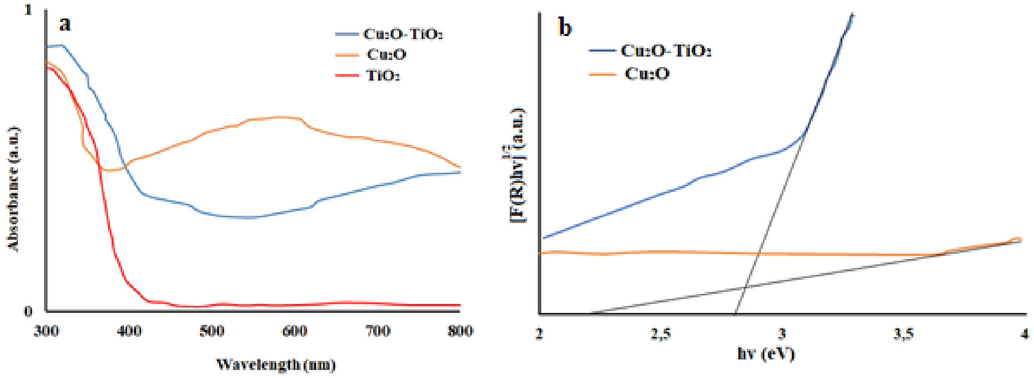

Figure 6. (a) Typical DRUV absorption spectra in presence of bare TiO_2, bare Cu_2O and Cu_2O-TiO_2 composite, and (b) plots of $(F(R)hv)^{1/2}$ versus photon energy hv for Cu_2O and Cu_2O-TiO_2 composite [64].

Figure 6 (a) shows the typical UV – vis absorption spectra for pure Cu_2O and Cu_2O/TiO_2 composites, obtained according to an analytical method previously reported[132]. As concerns cuprous oxide, it exhibits a broad absorption band in the visible range from about 430 nm. The intensity recorded in UV – visible spectra maybe also indicated by the Kubelka – Munk function F(R). Figure 6 (b) shows the energy gap value estimated through the linearization of Tauc plot of $(F(R)\ hv)^{1/2}$ versus photon energy (*hv*). The energy gap value resulting for Cu_2O (i.e., ≈2.2 eV) is consistent with other literature data[152]. Several authors [1,64,78,121,127] employed such diagnostic technique to evaluate the absorption property as well as the photocatalytic activity of Cu_2O/TiO_2 composite materials. As shown in Figure 6 (a), they reported an increase in visible light absorption with respect to bare TiO_2 above 430 nm due to the presence of Cu_2O (as previously reported). In addition, a reduction in energy gap value (see Figure 6 (b)) over Cu_2O/TiO_2 composite photocatalysts for hydrogen evolution was recorded.

2.4.6. Photoluminescence Spectroscopy

In photocatalysis, investigation on absorption/emission properties is essential to understand electronic interaction between composite materials and charge transfer mechanism for photocatalytic reactions. To gain a fully understanding on the electronic effect of copper species embedded as co – catalysts, photoluminescence studies on Cu_2O – TiO_2 materials have been performed by several authors in the literature review [64,78,121,126,128,153]. PL spectra of Cu_2O – TiO_2 photocatalysts revealed a decrease in photoluminescence intensity in with respect to bare TiO_2 [64,128], thus indicating that cuprous oxide lowers the recombination likelihood of photogenerated charge carriers. Indeed, the best photocatalytic performances in terms of hydrogen generation were commonly recorded over Cu_2O – TiO_2 samples showing the lowest PL intensity, as lower electron – hole recombination results in decreased light emission intensity, thus increasing photocatalytic efficiency [154].

2.5. Mechanisms of hydrogen evolution reaction

A reaction mechanism for p – n heterojunction based Cu_2O/TiO_2 materials attributes to cuprous oxide the role of energy antenna, due to its capability to absorb energy in the visible light spectral range. After charge carriers' generation, it is reported that electrons in the conduction band (CB) of Cu_2O, due to the difference in potential of the CB bands (i.e. −1.5 V versus NHE for Cu_2O and −0.5 V versus NHE for TiO_2 [155]) are transferred firstly to TiO_2, and subsequently to proton ions which are reduced. At the same time, as shown in Figure 7, photogenerated holes are consumed by the sacrificial organic species which oxidizes [129].

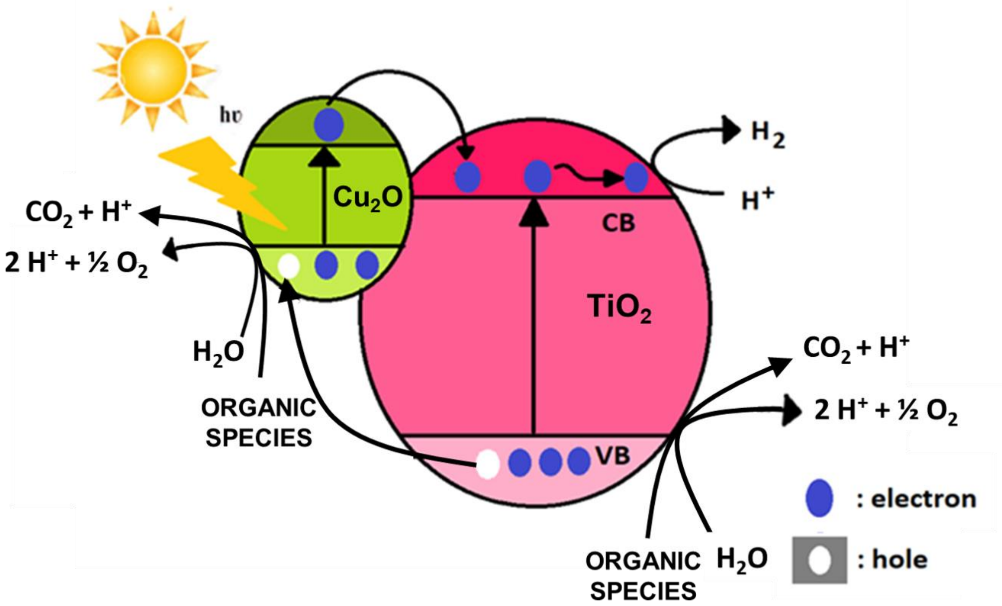

Figure 7. Schematic illustration for the hydrogen evolution reaction (HER) process over Cu based TiO_2 composite photocatalysts: oxidation of organic species (or water) by positive holes in the valence band and proton reduction by photogenerated electrons in the conduction band.

The possibility for Cu^{1+} of being reduced to Cu^0 species, according to reaction r. 8, was also considered by some authors as a possible explanation for a decrease in H_2 evolution photoefficiency [28,52]:

$$Cu^{1+} + e^- \rightarrow Cu^0 \qquad \text{r. 8}$$

On the other hand, a prompt reoxidation of copper (0), by holes as expressed by reaction r. 9, was proposed by studies reporting that the presence of copper (I) remains unchanged on photocatalyst surface during hydrogen evolution reaction (HER) [113,114].

$Cu^0 + h^+ \rightarrow Cu^{1+}$ r. 9

However, it is noteworthy that such aspects are analyzed only in some of the studies considered in the present review, so that no conclusion can be actually drawn on the fate of Cu^{1+} on the TiO_2 surface upon irradiation.

The effects of selected co-catalysts, such as WS_2 [9], Pt [156], Bi_2O_3 [1] and Ga_2O_3 [102,157] on the performances of Cu_2O/TiO_2 materials for HER were also investigated, as reported in Table 1, Column V. It is reported that they essentially help enhance photogenerated charge carrier separation, thus reducing their likelihood of recombination.

As reported by Li et al. [9] for instance, the role of WS_2 nanosheets in an $Au/Cu_2O/TiO_2/WS_2$ composite photocathode for hydrogen evolution is that of accepting electrons for water reduction rapidly, thus promoting the separation process of the electron–hole pairs for a higher photocurrent. As shown in Figure 8, under visible light irradiation ($\lambda \geq 420$ nm), electrons of Cu_2O are excited and easily transferred first to the CB of TiO_2, and then to the WS_2 layer, as the CB of TiO_2 and the Fermi level of WS_2 are more positive than the CB of Cu_2O. Subsequently, protons from the electrolyte promptly react with electrons, thus releasing hydrogen on the WS_2 surface. On the other hand, it is considered that the Au layer in the Cu_2O-based photocathode only decrease the electrochemical impedance of the Cu_2O photocathode.

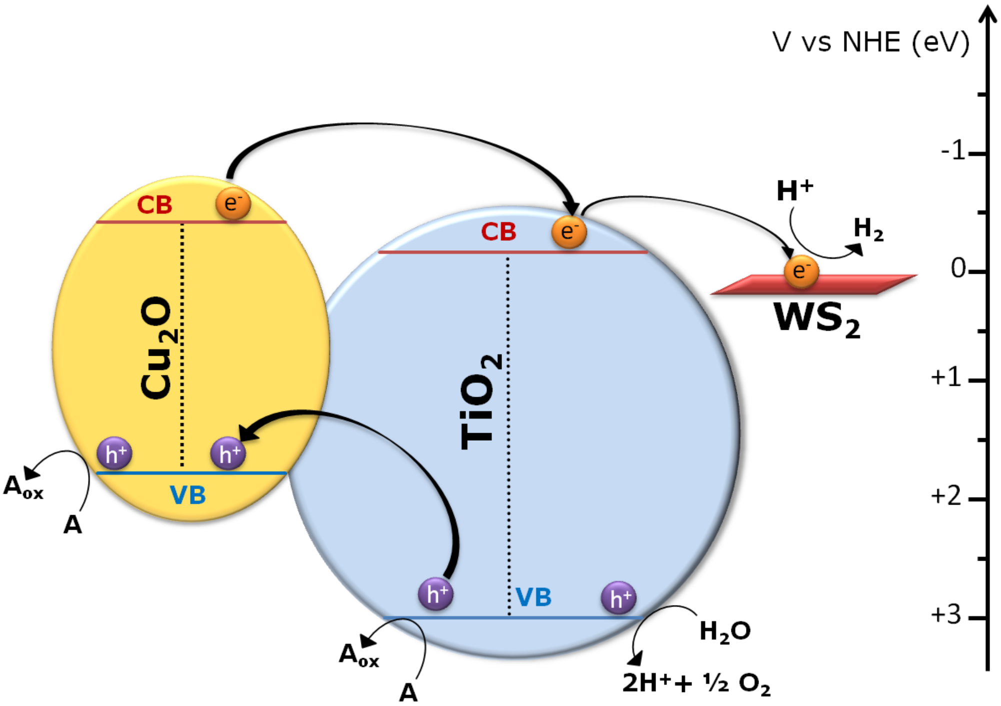

Figure 8. Schematic reaction mechanism of HER process over Au/Cu_2O/TiO_2/WS_2 photocathode proposed by Li et al. [9].

Metal copper is also reported to act as a cocatalyst in Cu^0/Cu_2O/TiO_2 composites [119,130,158–160]. The double effect of (*i*) promoting charge carriers' separation and (*ii*) improving visible light absorption and photoactivity due to the localized surface plasmon resonance (LSPR) of Cu nanoparticles is related to the presence of Cu^0 [119]. The mechanism of hydrogen evolution over Cu^0/Cu_2O/TiO_2 has been schematically illustrated in Figure 9.

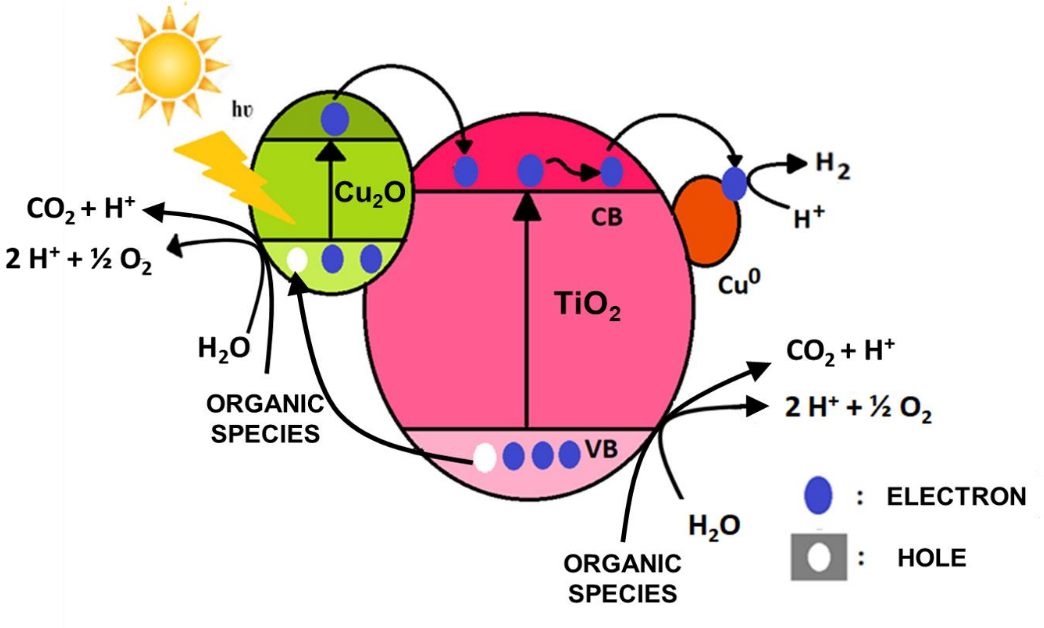

Figure 9. HER process over $Cu^0/Cu_2O/TiO_2/WS_2$ composite photocatalysts under visible light irradiation.

As regards the effect of TiO_2 type on the reaction mechanism over Cu_2O/TiO_2 photocatalysts, it is significant to note that the use of home – prepared mesoporous TiO_2 is related to a remarkable enhancement in photoefficiency for hydrogen evolution [119,161]. Such positive effect has been mainly attributed to a reduced recombination of photogenerated charge carriers and an increase in the interfacial electron transport within the Cu_2O/TiO_2 heterojunction, thus resulting in enhanced photocatalytic hydrogen generation [119,161].

2.6. pH influence

Some of the Authors reported in a previous paper [162] that pH considerably affects photocatalytic hydrogen generation over copper – modified TiO_2 catalysts.
It is widely acknowledged that moderate alkaline conditions may result into a favorable environment for generating hydrogen, probably due to higher photocatalyst stability and absence of cupric ion release in the reacting solution. While not all studies considered pH as a key factor in HER, some results reported in the literature survey support the crucial role of pH in photocatalytic H_2 evolution over Cu_2O/TiO_2 composites.
Indeed, Zhen et al.[158] reported that the results collected during photocatalytic hydrogen generation over a ternary catalyst (i.e., $Cu^0/Cu_2O/TiO_2$) indicate an intense activity at pH values around 9.0. On the other hand, a decline in photoefficiency for higher and lower pH values with a standstill in H_2 generation for values smaller than 5.0 and greater than 13.0 was recorded. Under acidic conditions, such experimental findings were related to Cu_2O instability and sacrificial agent (i.e., triethanolamine) protonation. Instead, under alkaline conditions, extremely low proton concentration may considerably slow down hydrogen generation rate.

2.7. Effect of sacrificial agent

Despite the main purpose of the photocatalytic processes aimed to hydrogen production is water photosplitting [29], only few studies considered in this review reported the photocatalytic hydrogen production in the absence of organic species. In this respect, in the presence of Cu_2O/TiO_2 composite materials the effect of the sacrificial agent was evaluated. As reported in Table 1 Column VI, methanol [119,120,127,128,138,153,163–171] and glycerol [1,64,123,125,126,131,136,160,172,173] are the most widely used organics for photocatalytic hydrogen production.

Li et al. [167] reported the results in terms of hydrogen generation in the presence of several sacrificial agents, thus showing an enhancement in photocatalytic activity by reducing the C/OH ratio. Moreover, as reported by Li et al. [167], the scavengers react with hydroxyl radicals, thus resulting in enhanced activity in case of molecules with simplest structure.

Praveen Kumar et al. [130] compared the photocatalytic activity for H_2 evolution in the presence of different scavengers under natural solar light irradiation. Hydrogen production was enhanced with increasing alcohol polarity, due to the different surface properties of the photocatalyst obtained, as well as the adsorption and electron donation properties. Moreover, a great enhancement in hydrogen production was detected by using several organics, such as ethylene glycol, due to the position of its oxidation potential with respect to the valence band potential of titania.

2.8. Hydrogen generation efficiency

Only Cu_2O/TiO_2 materials exhibiting considerable efficiencies for H_2 production under visible light irradiation may be considered for industrial applications. Despite solar energy is a perennial energy source, several issues undermine the photoefficiency of such composites, such as the followings:

1) the recombination reaction seizes a portion of photogenerated charge carriers potentially available for HER;
2) the energy carried by the incident radiation is higher than the bandgap value (E_g), in which case excess energy is dissipated in the form of heath or light;
3) the energy carried by incident photons is lower than E_g, in which case no effective light absorption happens.

As reported in the sections below, different indicators may be used to quantify the efficiency of energy capture depending on the experimental setup adopted. Among the papers found in the literature survey, only a few of them reported data of hydrogen generation efficiency (see Table 1). Overall, this is one of the major weaknesses affecting literature on hydrogen generation through photocatalytic processes.

2.8.1. Photoelectrochemical cells

Dotan et al. [174] defined the solar to hydrogen (STH) conversion efficiency of photoelectrochemical solar cells according to equation (eq. 1), where J_{sc} is the short-circuit photocurrent density, η_F the Faradaic efficiency for H_2 production, and P_i the incident irradiation power density. Such parameters should be estimated under standard solar irradiation conditions (AM 1.5 G), without any sacrificial agents, and pH or electrical bias between counter and working electrodes.

$$\mathrm{STH}=\left[\frac{|J_{sc}(\mathrm{mA/cm^2})|\times 1.23(\mathrm{V})\times \eta_F}{P_i(\mathrm{mW/cm^2})}\right]_{\mathrm{AM1.5G}} \qquad \text{eq. 1}$$

Pan et al. [135] developed a $Cu^0/Cu_2O/Ga_2O_3/TiO_2$/NiMo photocathode with a coaxial nanowire structure based on Cu_2O/Ga_2O_3 – buried p – n junction. Such Cu_2O – based photocathode was employed together with a $BiVO_4$ photoanode for unassisted solar water splitting, thus achieving a STH conversion efficiency value of about 3%. To the best of our knowledge, such value is the highest collected for unbiased PEC devices employing oxide composite materials for water splitting.

Niu et al. [102] synthesized a novel $Cu_2O/Ga_2O_3/TiO_2/RuO_x$ photocathode for water splitting able to achieve a maximum value of thermodynamically based energy conversion efficiency of about 1.9% at around +0.45 V versus RHE. The solar energy conversion efficiency was calculated using equation (eq. 2), where J is the photocurrent under AM 1.5 G irradiation, V_{RHE} is the applied potential versus RHE, $V(H^+/H_2)$ is the Nernst potential for hydrogen evolution (0 V vs RHE), and P_s is the incident solar irradiance (100 mW/cm^2 for AM 1.5 G).

$$\text{Energy conversion efficiency} = \frac{|J| \times \left[V_{RHE} - V(\frac{H^+}{H_2})\right]}{Ps} \times 100 \qquad \text{eq. 2}$$

Such efficiency value, as expressed by equation (eq. 2), was the best found in the literature survey if compared with other Cu_2O/TiO_2 based photocathode structures under the same illumination conditions (i.e., AM 1.5 G), such as FTO/Au/Cu_2O/AZO/TiO_2/Pt exhibiting an efficiency of 1.35% at 0.45 V [175–179].

As reported in Table 1, several further studies [6,9,118,131,139,156,158,159] expressed the maximum photoefficiency for hydrogen evolution in photoelectrochemical cells as photocurrent density (mA/cm^2) at different applied voltage values (i.e., 0.0 V versus reversible hydrogen electrode [118,159]). Such efficiency values are difficult to compare due to different illumination conditions, as in many cases the use of proper UV cut-off filters limiting light irradiation to the visible light spectral range (λ>400 nm) is not considered.

2.8.2. Photocatalytic reactors

When evaluating photocatalytic hydrogen evolution activity over Cu_2O/TiO_2 composite materials, most of the researchers in the literature survey only reported indications on H_2 generation rate, in some cases per unit mass of catalyst, and compare such rate with the one recorded over basic catalyst (e.g., bare TiO_2) [1,64,114,118,120,126–128,136,160,163,164,172,173,180,181]. Due to such inconsistency between photoefficiency expressions and, once again, unequal light irradiation conditions, Cu_2O/TiO_2 photocatalyst performances for hydrogen generation turn out to be hard to compare, as shown in Table 1. To the best of our knowledge, amongst the highest values H_2 generation rate per unit mass of catalyst recorded under solar light irradiation only, Praveen Kumar et al.[130] obtained a value of 79.8 mmol/h·g over a $Cu_2O/Cu^0/TiO_2$ catalyst employed for the photoreforming of ethylene glycol under natural sunlight, with an average light intensity of $1.15 \cdot 10^5$ lx.

As listed in Table 1, column VIII [113,119,156,158] , some authors also reported the values of Apparent Quantum Efficiency (AQE), as expressed by equation (eq. 3), where r_{H_2} (mol/time) the rate of hydrogen generation.

$$\text{AQE} = \frac{2 \times r_{H_2}}{\text{moles of incident photons/time}} \times 100 \qquad \text{eq. 3}$$

Zhen et al. [158] recorded an AQE value for H_2 evolution of 45.7% over EY – sensitized $Cu^0/Cu_2O/Cu^0/TiO_2$ photocatalyst at 520 nm. Such ternary composite, prepared via an *in situ* photoreduction procedure, was tested for the photoreforming of TEOA in the presence of a 420 nm cut – off filter or various band-pass filters.

In general, however, with the aim of accomplishing a consistent comparison among different literature data, values of effective irradiation power should be specified, whereas only nominal power and lamp type were mostly reported in the experimental sections.

Table 1. Literature review of recent studies on Cu_2O/TiO_2 composite materials.

I	II	III	IV	V	VI	VII	VIII	XI
Preparation method	**Cu_2O identification technique**	**H_2 generation mechanism**	**TiO_2 type**	**Co-catalyst**	**Sacrificial agent**	**Lamp filter**	**Efficiency of H_2 generation**	**Reference**
TNTs by hydrothermal method; copper modified TiO_2 by impregnation method	PL, XRD	p-n heterojunction	Home prepared	None	Glycerol	Direct sunlight between 10 a.m. and 3 p.m.	Not reported, best hydrogen evolution rate 48 mmol/h·g	[126]
TiO_2 thin films deposited on quartz glass by electron beam evaporation at T= 200 °C; Cu_2O layers grown by laser ablation	XPS, XRD	p-n heterojunction	TiO_2 thin film	None	None	None (300 W Xenon lamp)	Not reported, highest H_2 production 2.76· 10^{-3} mmol under UV light after 6 h	[180]
TiO_2 by hydrothermal method; CuO_x by wetness impregnation method and calcination at T= 400°C in air	DRIFTS, DRUV, HRTEM, XPS, XRD	p-n heterojunction	Anatase	None	Methanol	None (300 W Xenon simulated solar light)	Not reported, highest H_2 production 0.621 mmol/h·g	[127]
Copper foam-based nanodots composites prepared by immersion-heating procedure and calcination at 300°C	HRTEM, XPS, XRD	p-n heterojunction; Fermi levels formation	Not specified	CFE (Copper foam-based nanodots composite)	None	None	HER onset potential: 18 mV, potential: 114 mV and 10 mA/cm^2	[118]
Cu_2O/TiO_2 catalysts prepared by the alcohol-thermal method	EDX, ICP-OES, STEM−EDS, XPS, XRD	p-n heterojunction	Home prepared	None	Methanol	Cut-off filter λ>420 nm (300 W Xenon lamp)	Not reported, highest H_2 production 24.84 mmol/h·g	[163]
Three different preparation methods: Impregnation and calcination at T=350˚C; Microwave reduction method and several washing with ethanol; Photodeposition method	PL, Raman, TEM, XPS, XRD,	Not reported	Commercial TiO_2 P25	None	Methanol	Sun condition	Not reported, highest H_2 production 0.891 mmol/h)	[128]

Electrodeposition method for Cu_2O film synthesis; $Au/Cu_2O/TiO_2$ electrode fabricated by dip-coating method; $Au/Cu_2O/TiO_2/WS_2$ photocathode fabricated by stirring, centrifugation, and washing procedure	XRD	p-n heterojunction; Fermi levels formation	Not specified	WS_2	None	Cut off filter ($\lambda \geq 420$ nm) (Xenon lamp- Light intensity 100 mW/cm^2)	Not reported, best photocurrent obtained was 10 mA/cm^2 at over-potential of -0.33 V vs RHE under visible light	[9]
TiO_2/Cu_2O core/shell NWAs prepared by hydrothermal method and chemical bath deposition	EDS, HRTEM, XPS, XRD	p-n heterojunction; Fermi levels formation	Rutile	None	None	None (300 W Xenon lamp- Light intensity 100 mW/cm^2)	Not reported, best photocurrent obtained was 2.50 mA/cm^2, with H_2 production 32 $mmol/h \cdot cm^2$	[6]
Bismuth modified TiO_2 prepared by sol-gel method; impregnation of copper on bismuth deposited TiO_2 and calcined at T=400 °C	DRUV, FESEM, XPS, XRD,	Bi_2O_3 minimizes electrone-hole recombination	Commercial TiO_2 P25	Bi_2O_3	Glycerol	Solar simulator (300 W Xenon lamp- Light intensity 40 mW/cm^2)	Not reported, highest H_2 production 3.678 mmol/h	[1]
Cu_2O nanowires prepared by deposition method and coating of a layer of Cu_2O onto Cu_2O nanowire by electrodeposition; TiO_2 coating by deposition method	Raman, XRD	Not reported	Amorphous	$RuOx\text{-}Ga_2O_3$	None	Solar simulator (300 W Xenon lamp- Light intensity 100 mW/cm^2)	solar-to-hydrogen conversion efficiency ~3%	[135]
Cu^{2+}/TNT by impregnation and heating at T=200 °C	XRD	p-n heterojunction	Home prepared	None	Glycerol	1,5 AM solar irradiance of white light (1000 W Hg/Xe- Light intensity 100 mW/cm^2)	Not reported, best photocurrent obtained was 3.40 mA/cm^2 with H_2 production 0.127 $mmol/h \cdot cm^2$	[131]
Cu_2O sheets prepared by thermal oxidation of thin copper foils; Ga_2O_3 and TiO_2 layers deposition by thermal atomic Layer deposition system; RuOx prepared by photoelectrodeposition	XRD	Not reported	Not specified	Ga_2O_3/RuO_x	None	AM 1,5 G filter	1.75% at 0.5 V over $Au/Cu_2O/Ga_2O_3/TiO_2/RuO_x$; 1.9% at 0.45V over Dual Cu_2O-based photocathodes	[102]

Cu_2O sensitized TNAs fabricated by cyclic impregnation growth method	XPS, XRD	Not reported	Home prepared TNAs	None	Glycerol	Cut off filter λ>400 nm (300 W Xenon Lamp)	Not reported, highest H_2 production $4.8 \cdot 10^{-4}$ mmol/h·cm^2	[123]
nanoclusters prepared by green microwave-assisted method with glucose or onion skin waste	DRUV, FESEM, PL, Raman, TEM, XPS, XRD	p-n heterojunction	Commercial TiO_2 P25	None	Glycerol	Not reported (400 W metal halide lamp)	Not reported, highest H_2 production 4.70 mmol/g after 24 h	[64]
Cu_2O grown on Au/Cr/FTO/Glass substrate by potentiostatic electrodeposition; Cu_2O film coated with graphene and TiO_2 layers by atomic deposition; Pt loaded on all the devices	Raman, XPS, XRD	Not reported	Anatase	Pt	None	AM 1,5 G Solar simulator (Light intensity 100 mW /cm^2)	Not reported, best photocurrent obtained was -3 mA/cm^2 at 0.0 V vs RHE	[156]
Cu_2O film fabricated by electrochemical deposition on copper substrate; The Cu_2O/Au film prepared by photodeposition; Cu_2O/TiO_2 and $Cu_2O/Au/TiO_2$ films prepared by painting TiO2 solution onto Cu_2O or Cu_2O/Au films	DRUV, PL, SEM, TEM, XPS, XRD	Z-scheme system	Commercial TiO_2 P25	Au	Methanol, glucose	Cut off filter (300 W Xenon lamp)	Not reported, highest H_2 production *0.0125 mmol/ cm^2	[78]
$Cu^0/Cu_2O/Cu^0/TiO_2$ prepared by selective reduction with hydroxylamine	DRUV, FESEM, HRTEM, PL, Raman, SEM, TEM, XRD	p-n heterojunction	Commercial TiO_2 P25	Cu/Eosyne	Triethanolamine	Cut-off UV filter (300 W Xenon lamp-Light intensity 100 mW/ cm^2)	AQE=45.7 % at 520 nm	[158]
A Cu_2O film prepared by electrochemical deposition on copper substrate and coating with TiO_2	XPS, XRD	Not reported	Commercial TiO_2 P25	None	Methanol	UV-B and UV-C cut-off AM 1,5 filter (Xenon lamp-Light intensity 78 mW/cm^2)	Not reported, highest H_2 production 12.70 mmol/L	[164]
Cu-TiO_2 photocatalysts prepared by Sol-gel method	TPR, XPS, XRD	Not reported	Home prepared Anatase/Brookite	None	Ethanol	None	Not reported, highest H_2 production 3.865 mmol/h·g	[181]
The Cu_2O films were synthesized by electrodeposition method	DRUV, FESEM, XPS, XRD	Not reported	Not specified	Cu	None	Cut off filter AM 1,5	Not reported, best photocurrent obtained	[159]

						(300 W Xenon-Light intensity 100 mW/cm^2)	was −2.04 mA/cm^2 at 0 V vs RHE	
TiO_2–MOF-199 composite prepared by hydrolysis; Cu/Cu_2O over TiO_2 by calcination	DRUV, HRTEM, PXRD, XPS	p-n heterojunction and shifting of the Fermi level due to the presence of copper nanoparticles	Anatase	Cu	Glycerol	None (100 W UV lamp- λ=365 nm)	Not reported, highest H_2 production 15.13 mmol/h·g	[160]
Hydrogen titanate nanotubes prepared by hydrothermal method; $CuOx/TiO_2$ composite prepared by impregnation method and calcination at T=400°C	HRTEM, H2-TPR, XPS, XRD	p-n heterojunction	Anatase, Rutile, Brookite, P25	None	Methanol	None (300 W Solar simulator)	Not reported, highest H_2 production 3.203 mmol/h·g	[129]
Cu/TiO2 thin films deposited on quartz glass substrates by RF reactive magnetron sputtering	XPS, XRD	p-n heterojunction and the Fermi levels formation	Anatase	None	Methanol	None (300 W Xenon lamp)	Not reported, highest H_2 production 2.80· 10^{-3} mmol /h·cm^2	[165]
Cu-loaded photocatalyst prepared by impregnation and calcination	XPS	Cu_2O injects additional photoexcited electrons into the TiO_2 CB, thus TiO_2 produces hydrogen	Commercial TiO_2 P25	CuO	Glycerol	400 nm UV cut-off filter/300 W Xe lamp	Not reported, highest H_2 production 2.240 mmol/h·g under UV-Vis light and 0.100 mmol/h·g under visible light	[136]
TiO_2 nanotubes fabricated by electrochemical anodization; Cu_2O-doped TNAs prepared by square wave voltammetry electrochemical deposition method	SEM, XPS, XRD	p-n heterojunction; Fermi levels formation	Anatase	None	None	None (100 W Hg lamp)	Not reported, highest H_2 production 300 µM/cm^2 after 4 h and photocurrent obtained was 4.50 mA/cm^2 under bias potential of 1 V	[137]
$CuOx/TiO_2$ thin films on quartz glass substrates prepared at T=450°C by RF reactive magnetron sputtering	XPS	Not reported	Anatase	CuO	Methanol	None (300 W Xenon lamp)	Not reported, highest H_2 production *5.30 10^{-3}mmol/h·cm^2	[138]
Metal oxide cluster modified TiO_2 nanoplates prepared by hydrothermal method	XPS, XRD	Not reported	Home prepared	None	Methanol	Cut-off filter 250 nm < λ < 380 nm	Not reported	[182]

						(300 W Xenon lamp)		
TiO_2-Cu_2O NWA grown on FTO glass substrate by hydrothermal synthesis	FESEM, HRTEM, TEM, XPS, XRD	Not reported	Home prepared	None	None	No filter (300 W Xenon lamp)	0.71%, photocurrent density (bias) obtained was 4.66 mA /cm^2	[139]
Cu_xO/TiO_2 composite prepared by impregnation method and calcination at T=350°C	DRUV, PXRD, Raman, XPS	p-n heterojunction	Home prepared TiO_2, Commercial TiO_2 P25 for comparison	Cu	Ethylene glycol-Propanol, ethanol, methanol for comparison	Sun condition Light intensity $1{,}15 \cdot 10^5$lx,	Not reported, highest H_2 production 79.80 mmol/h·g	[130]
Cu_2O photocathode by electrodeposition method on FTO substrates; TiO_2 stabilization layers on Cu_2O photocathodes by ELAMOD process	XRD	Not reported	Home prepared	None	None	Cut off filter 420 nm (ABET Solar Simulators)	Not reported	[140]
Cu-loaded TiO_2 catalysts obtained by chemical reduction deposition method	DRUV, EDS, HR-TEM, NIR, XRD	p-n heterojunction	Home prepared	Cu	Methanol	Cut off filter $360\ nm < \lambda < 780\ nm$ Or $\lambda > 420$ nm (300 W Xenon lamp)	AQE=13.5% at 365 nm	[119]
Cu_2O coating layer deposited onto TiO_2 tube walls by multiple-cycle chemical absorption and reduction method	EDX, XRD	p-n heterojunction; Fermi levels formation	Home prepared	None	Ethylene glycol	AM 1,5G filter (Solar simulator- Light intensity 100 mW/cm^2)	Not reported, highest H_2 production *6.2 mmol/h·cm^2	[122]
Cu_2O microcrystals obtained with autoclaves, heating, precipitation, washing and distillation method	EPR, XRD	Electron-hole pair formation or reduction of formaldehyde and capture of oxygen from Cu_2O	None (commercial TiO_2 P25 as reference)	None	Formaldehyde	Cut off filter $\lambda \geq 420$ nm (Xenon lamp - Light intensity 50 mW/cm^2)	Not reported, highest H_2 value 82.2 µmol after 3 h	[183]

Cu/TiO_2 photocatalysts prepared by photoreduction method	None	Cu/TiO_2 NPs absorbs the whole range of visible light	Commercial TiO_2 P25	None	Glycerol	Cut-off filter $\lambda \geq 420$ nm (500 W Xenon lamp - Light intensity 1,5 mW/cm^2)	Not reported, highest H_2 production 0.24 mmol/h·g	[172]
Cu modified TiO_2 nanorods prepared by wet-impregnation method	None	Electron-hole pair formation	Home prepared	None	Glycerol	Direct sunlight	Not reported, highest H_2 production 0.0503 mmol/h·g	[173]
Not reported, photoreduction of Pt on the catalyst surface	None	Cu_2O as antenna capturing the radiation, electrons are transferred from CB of Cu_2O to Pt	Not specified	Pt	Methanol	None (Tungsten lamp)	Not reported, highest H_2 production *1.82 mmol/h·g	[166]
Cu_2O/TiO_2 nanotube arrays prepared by electrochemical deposition method	None	Not reported	Home prepared	None	None	AM 1.5 G solar simulator (100 mW/ cm^2)	Not reported	[184]
The Cu_2O/TiO_2 photocatalysts prepared by reduction method	DRUV, XPS, XRD,	p-n heterojunction	Commercial TiO_2 P25	None	Methanol, ethanol, glycerol, ethylene glycol	None (500W Xenon lamp)	AQE=4.32%	[185]
The Cu_2O–TiO_2 photoelectrodes prepared by spray pyrolysis process and sputter coating of thin layer of TiO_2	XPS	Not reported	Not specified	None	Glucose	Not reported	Not reported highest H_2 production ~0.122 mmol/h·cm^2	[186]
Cu_2O/TiO_2 particles prepared by glucose solvothermal method	AES spectra, HRTEM, XPS, XR	Similar mechanism to Z-scheme	Commercial TiO_2 P25	None	Ethanol	None (300 W Xenon lamp)	Not reported, highest H_2 production 0.668 mmol/h·g	[114]
Mesoporous TiO_2 beads produced by metal-salt based hydrothermal process; Cu_2O-decorated mesoporous catalysts prepared by chemical bath deposition process	XPS, XRD	The Cu_2O nanocrystals as electron-hole separation centre	Home prepared	None	Methanol	None (400 W high-pressure Hg lamp)	Not reported, highest H_2 production 223 mmol/h·g	[120]

The Cu_2O/TNA composites obtained by electrochemical deposition of Cu_2O in a three-electrode cell	XRD	p-n heterojunction	Home prepared	None	Glycerol	Cut-off filter (Xenon lamp)	Not reported, highest H_2 production 8.9 mmol/h·cm^2	[125]
The Cu_2O grid deposited on TiO_2 thin films by microsphere lithography strategy and Pt addition by deposition method	GIXRD	Not reported	Home prepared	Pt	Methanol	None (Xenon lamp)	Not reported, highest H_2 production 0.06 mmol/ h	[187]
Cu_2O on titania nanotubes by electrodeposition method	XRD	Not reported	TiO_2 nanotubes	None	None	Cut-off filter $\lambda>500$ nm (TS428 lamp 350 nm$<\lambda<$2500 nm)	Not reported	[188]
Cu_2O/TiO_2 composite prepared by ethanol-induced deposition method and calcination at T=350 °C	HR-TEM, XPS, XRD	p-n heterojunction	Commercial TiO_2 P25	None	Ethylene glycol	None (Xe lamp 320 nm $< \lambda <$ 780 nm)	AQE=28.6% at 365 nm	[113]
Cu2O through chemical reduction with ascorbic acid; Au deposition through photo reduction process	XRD, XPS	p-n heterojunction and SPR of Au	Home prepared TiO_2 nanorods	Au	Ethanol	AM 1.5 G filter (300W Xenon lamp)	Not reported, highest H_2 production 8.548 mmol/h·g	[189]
The Cu_2O-TiO_2 prepared by self-assembly approach in presence of AOT except that the addition of TiO2. After stirring for 3h, the solution was kept at 80°C for 4h, then centrifuged, washed, and dried.	XRD, XPS	p-n heterojunction	Home prepared TiO_2	None	Methanol	300 W Xe lamp	Not reported, highest H_2 production 0.5 mmol/h·g	[168]
Cu_2O prepared by oxidation of Cu^0 in 6 h. Au-Cu_2O prepared by partial galvanic replacement reaction. Mixing of Cu_2O or Au-Cu_2O with TiO_2, deposition onto a glass substrate dipped in isopropanol for 10 min, cleaned through plasma for 10 min and drying in oven at 100°C for 15 min.	TEM, SEM, Raman, XPS, UV–Vis absorption, ICP	p-n heterojunction	Anatase	Au	Ethylene glycol	Cut-off filter $\lambda>360$ nm (100 W UV lamp- 8 mW/cm^2). Cut-off filter $\lambda>430$ nm (300 W Xe lamp)	Not reported, highest H_2 production 12 mmol/h·g	[111]

Cu_2O - TiO_2 prepared by sol-gel method; after illumination Cu doped $TiO_2$was redused to Cu_2O - TiO_2.	BET, EDX, TEM, SEM, XRD, DRUV-Vis, Raman, EPR, PL	Reduction of Cu to Cu_2O and p-n heterojunction	Isopropyl titanate	None	Methanol	None (300 W Xe lamp)	Not reported, highest H_2 production 16.25 mmol/h·g	[153]
Cu_2O and Cu_2O/ TiO_2 photocathodes prepared by electrodeposition of Cu_2O and deposition of titanium tetrapropoxide. The rGO/NiFe-LDH composite catalyst was synthesized by hydrothermal method. Cu_2O/ TiO_2/rGO/NiFe-LDH photocathodes prepared by dip-coating method.	XRD, FESEM, SEM, XPS, Raman, R, DRUV–vis	p-n heterojunction	Titanium tetraisopropoxide	rGO/NiFe	0.5 M Sodium sulfate	AM 1.5 G solar simulator (100 mW/ cm^2)	0.41% at 0.25 V vs RHE	[190]
Cu_2O/ TiO_2 prepared by magnetron sputtering method; The deposition temperature was 550 °C for 12 h, obtaining TiO_2 arrays. Deposition of CuO_x by sputtering copper, with controlled flow rate of oxygen.	XRD, XPS, AES	Enhanced performance attributed to metallic Cu, produced during the irradiation	Anatase	None	Methanol	None (300 W Xe lamp - 300 nm ≤ λ ≤ 2500 nm)	Not reported, highest H_2 production $3.7\ 10^{-3}$ mmol/ h·cm^2	[171]
TiO_2 nanostructures via hydrothermal method, followed by thermal reduction strategy, at 300°C for 2 h with H2 flow. Copper-related species were deposited onto TiO_2 via photodeposition route.	XPS	Z-scheme Cu_2O/TiO_2	Anatase	Pt	Methanol	Monochromatic light (350 nm) with filter (300 W Xe lamp)	53.5% at 350 nm	[170]
The (001) TiO_2@ $Ti_3C_2T_x$ was prepared by a hydrothermal method. The Cu_2O/(001) TiO_2@ $Ti_3C_2T_x$ hybrids were synthesized via a modified solvent reduction method.	XRD, TEM, XPS, AES, DRUV-Vis	Migration and spatial separation of photogenerated charge carriers among $Ti_3C_2T_x$, TiO_2, and Cu_2O	Anatase	$Ti_3C_2T_x$	Methanol	None (300 W Xe lamp)	Not reported, highest H_2 production 0.612 mmol/h·g	[169]

2.9. Ball milling as alternative preparation method

As previous discussed (See Section 2.3) several preparations of Cu_2O/TiO_2 composite materials were reported in literature, such as reducing methods, impregnation/calcination, electrodeposition etc. However, each of methods presents advantages and disadvantages, such as the complexity of the methods or high operation costs; sol – gel method for instance, requires very expensive starting materials [191], and hydrothermal method proceeds in presence of high concentration of NaOH (about 10 M), with temperature over 100°C and requires more than 10 hours of treatment [192]. It is thus necessary to develop a different route of preparation. An alternative could be represented by the mechanical mixing of powder materials; among all approaches, mechanical mixing is a simple, low cost and very eco – friendly technique with significant technical advantages for the synthesis of various nanomaterials and nanocomposites, even for the industrial applications. In the field of the chemical synthesis the combination of the solvent – free strategies and the mechanochemical activation has attracted much attention in the last years, in the preparation of organic and inorganic materials. Moreover, the possibility of using a ball miller (See Figure 10) instead of the mortar to mixing the reagent, may effectively reduce the problems of poor reproducibility, which limited the utilization of this method on industrial scale [193].

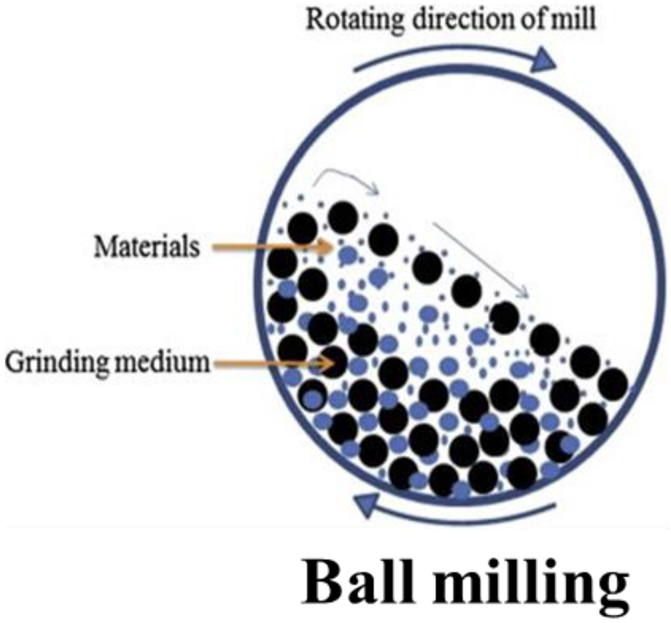

Figure 10. Schematic representation of the mechanical mixing of powder materials in a ball miller.

Generally, mechanochemical synthesis, using high energy collision from the balls, has shown great advantages in material synthesis, by modifying the structure and the electronic properties of catalytic materials (reduction of particle sizes, increase of the specific surface area and change the chemical state of component atoms), giving such properties that influence the activity of the final catalyst, as reported by D.S. Su [194]: He noticed the increase of the specific surface area of V_2O_5 catalyst (from 7 to 32 m^2/g) after 10 hours of milling (150 revolutions for minute), as well as the formation of lattice defects in the structure.

In the area of the photocatalyst synthesis, several studies reported the preparation of composite materials through ball milling as a possible alternative to the common more complicated methods [195–209]:

Chen et al. for instance [196], proposed the preparation of $ZnO/g-C_3N_4$ composite photocatalyst by dispersing the home-prepared powders (ZnO and $g-C_3N_4$) in isopropanol then ball milling for 1 hours at 800 rpm with ZrO_2 beads; the product was collected and dried in an oven at 80°C. The degradation efficiency of RhB under visible light resulted about 51% after 2 hours for $ZnO/ g-C_3N_4$ with 10%wt $g-C_3N_4$.

Among the works concerning the photocatalytic hydrogen production, the ball milling was proposed as preparation method, for instance, by Chen et al. [210], which reported a hydrogen generation of about 1200 micromole/hours in the presence of MoS_2/CdS photocatalyst prepared by mixing $(NH_4)_2MoS_4$ with CdS in an agate jar containing ethanol and a fixed number of agata balls, then calcined at 400 °C for 1 hour in Ar atmosphere. The authors noticed the influence of the milling time on the hydrogen generation, identifying an increasing of the activity up to 4 hours of milling; further increase of the ball-milling time probably causes the occurrence of more defects, which reduce the effective separation of electron and hole pairs.

According to our knowledge, despite the great number of works in which ball milling was used, only few studies have reported the possibility of preparing Cu_2O/TiO_2 composite, for application in photocatalysis, with this technique:

Shifu et al., for instance [211], have used ball milling to prepare p–n junction Cu_2O/TiO_2 photocatalysts aimed to the photodegradation of methyl orange and simultaneous reduction of $Cr_2O_7^{2-}$. In this preparation, TiO_2 powders were mixed in the agate ball milling tank, then a certain amount of Cu_2O was added in the ball miller in presence of water. After mixing at the speed of 500 rpm for selected times (3÷24 hours), the wet powder was removed and dried in air below 110°C, to obtain a dry sample. After the milling, it was observed, as reported also for other works previous presented, an increasing of the specific surface area with the ball milling time, because of agglomerating phenomena of the spherical particles. However, since the presence of oxygen during the preparation leads to oxidation of Cu^+ to Cu^{2+}, the same material could be useless for hydrogen production through visible light irradiation; the presence of Cu^{2+}, able to be reduced to zerovalent copper under UV – visible light conditions, could surely reduce the electron – hole recombination rate of the photocatalyst in the UV – range, but it is unable to extend the light absorption to the visible range. As a confirmation, in a previous work [212] about photocatalytic hydrogen generation in presence of diethanolamine as sacrificial agent using Cu^0/TiO_2 photocatalyst, no activity in terms of hydrogen generation was noticed in the visible range, although the efficiency of hydrogen generation in the UV range was increased with respect to previous results reported in literature with different sacrificial agents [132].

To effectively obtain Cu_2O/TiO_2 photocatalyst, Chen et al. [213] proposed to prepare the sample through ball milling starting from Ti and Cu powders; in their work the materials were mixed along with ZrO_2 (as substrate) in a planetary ball miller at 300 rpm for fixed times (5÷25 hours). Then, two different composite materials were prepared: (i) a Cu_2O/TiO_2 composite, obtained by covering the sample with graphite carbon and oxidizing at 500°C in air atmosphere for 15 hours and (ii) a CuO/ TiO_2 composite, obtained by oxidizing the sample in the air at fixed temperatures (400 ÷ 600 °C) for 15 h. The best photocatalytic performance, in terms of photodegradation of methyl orange under UV radiation, was collected in the case of Cu_2O/TiO_2, probably due to the formation of the p – n heterojunction.

Finally, a different approach was adopted by Basnet et al. [214], which used the ball milling to achieve a desired particle size and crystallinity. In their synthesis, in fact, to effectively obtain Cu_2O/TiO_2 composite photocatalyst, Cu_2O and TiO_2 were mixed and compressed to produce pellets, then heated at 5 °C/min up to 500 °C and then 1000 °C for 2 h under N_2 atmosphere. Finally, the as prepared pellets were ball milled up to 20 hours. The better photocatalytic performance under visible light conditions with respect to the bare TiO_2, indicated the improved charge transfer at the interface of the two semiconductors.

The results reported in the present paragraph require the following considerations:

(i) ball milling represents an interesting new route to prepare a Cu_2O/TiO_2 photocatalyst, due to its simplicity and cost – effectiveness, despite its use is still rarely documented in literature;

(ii) as part of ball milling preparation, it is necessary to develop a different route to prevent the oxidation of the Cu_2O, controlling milling time and the temperature of the process, as well as a solvent – free method, to reduce the costs and the environmental problems.

3. Aim of the thesis

The purpose of the present project **is the development of a visible light active photocatalytic system aimed to hydrogen production through photoreforming of organics, based on copper (I) and prepared by facile method.** As clearly emerged from literature information, several researchers have proposed the utilization of Cu_2O/TiO_2 composite material for hydrogen production, for which different preparation methods – mainly photodeposition and impregnation/calcination – were reported. Based on the results of an extended literature analysis, a *solvent – free* ball milling was chosen as an alternative preparation method, due to its simplicity and industrial applicability.

The system was analyzed in terms of hydrogen generation at varying chosen operating parameters. Among the goals of this study:

1. Evaluation of the effect of adopting various oxygenated organic substrates as sacrificial organic agents.
2. Evaluation of the best performing conditions in terms of milling time and rotation rate of the miller. A thorough catalyst characterization (X-Ray diffraction, Diffuse Reflectance UV Spectroscopies, Photoluminescence, Transmission Electron Microscope, Scanning Electron Microscopy analyses, Fourier-transform infrared spectroscopy, X-ray photoelectron spectroscopy, Transmission electron microscopy energy-dispersive X-ray spectroscopy) provides the basis for the correlation between the photocatalytic activity and the physical – chemical properties of the catalyst.
3. Evaluation of the effect of the temperature and pH of the suspension on the photocatalytic hydrogen production efficiency.
4. Development of a suitable mathematical model capable of simulating hydrogen production over the same catalyst (Cu_2O/TiO_2) when methanol was adopted as sacrificial agents.
5. Evaluation of the photocatalytic performance of the best photocatalytic system studied under solar radiation.

4. Materials and methods

4.1. Materials

TiO_2 nanopowder (commercial grade, Aeroxide TiO_2-P25, average particle size 21 nm, specific surface area 50 ± 15 $m^2 \cdot g^{-1}$, 80/20 anatase/rutile) was purchased from4 Sigma Aldrich, while cuprous oxide (Cu_2O, powder) and methanol (99.9%) were purchased from Carlo Erba Reagents. All reagents were used as received. Doubly glass–distilled water was used throughout this study.

4.2. Photocatalysts preparation

The preparation of the photocatalyst is performed by using two different methods:

1. A simple mixing of the two powders, in which a fixed amount of TiO_2 (nanopowder, <50 nm, Sigma Aldrich – 0 ÷ 1500 mg) and a fixed amount of Cu_2O (0÷150 mg) are mixed in a vial.
2. A fixed amount of TiO_2 (nanopowder, <50 nm, Sigma Aldrich – 0 ÷ 1500 mg) is mixed in the agate ball milling tank (PM100, RETSCH), with agate balls and a fixed amount of Cu_2O (0 ÷ 150 mg). The operative parameters evaluated, to carry out an optimization of the method, are the rotation rate (rpm) and the milling time.

Several samples were prepared through impregnation method. The milled sample, at fixed Cu_2O percentage, milling time and rotation rate was calcined under nitrogen atmosphere for 2 h at 500°C.

4.3. Experimental set-up

Photocatalytic tests are performed in an annular glass batch reactor (see Figure 11 (a – c) for the schematic illustration of the reactor and the real experimental set – up), with the following characteristics:

- Outer diameter of 6.5 cm;

- Volume of 300 ml;
- Optical length of 1.1 cm;
- Height of 40 cm.

The reactor is equipped with a lamp located in a quartz sleeve, in which a cooling solution is circulated; the temperature of the reactor, adjusted between 25 and 80°C, is controlled with a thermostat. An inlet allows a nitrogen stream bubbled into the solution, an outlet is used to taking of the liquid and gas samples. A high pressure Hg lamp is adopted as radiation source for the experiments; the specific powers of the lamp, mainly emitting at 305, 313 and 366 nm in UV range, and at 404.7 nm and 435.8 nm in the visible range, calculated as reported in literature [215,216], are $6.08 \cdot 10^{-7}$ $E \cdot s^{-1}$, $2.05 \cdot 10^{-6}$ $E \cdot s^{-1}$, $1.18 \cdot 10^{-6}$ $E \cdot s^{-1}$, $2.96 \cdot 10^{-7}$ $E \cdot s^{-1}$, $1.97 \cdot 10^{-6}$ $E \cdot s^{-1}$, respectively. To evaluate the activity under visible light conditions, in almost all runs a filter solution with $NaNO_2$ (0.5 M) is circulated through the quartz sleeve to prevent radiation with a wavelength lower than 400 nm, as reported in literature [217].

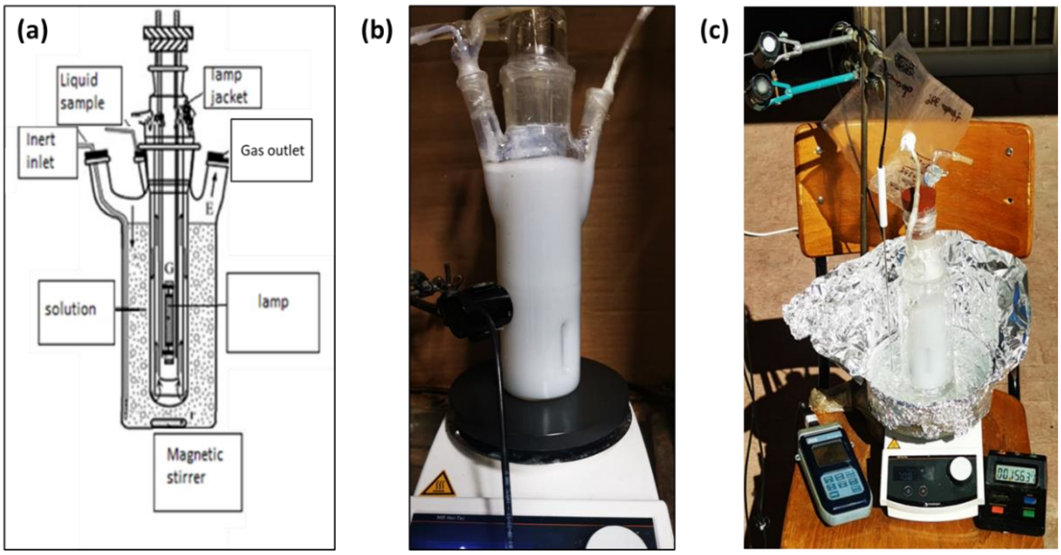

Figure 11. (a) Schematic illustration of the annular batch reactor. (b) Experimental set-up for the experiments conducted under artificial UV and/or Visible light source. (c) Experimental set-up for the experiments conducted under the solar source.

4.4. Experimental procedures

In a typical run, a fixed amount of catalyst is suspended in a doubly distilled aqueous solution, at fixed pH, containing chosen concentrations of the sacrificial species. To prevent the reaction between dissolved oxygen and copper species as well as the photogenerated electrons, a N_2 stream is bubbled into the solution starting from 40 min before the introduction of the photocatalyst; after that, the photocatalytic run is carried out. During photocatalytic experiments nitrogen is continuously bubbled into the reactor, at a fixed flow rate. In some cases, nitrogen bubbling is interrupted to allow hydrogen accumulation in the reactor. The effect of the temperature was evaluated by increasing the temperature of the system up to 80°C (in this case a condenser, located on the reactor, is used to prevent the evaporation of the organic species). To evaluate the photocatalytic activity by using solar source, in some cases the suspension, containing a fixed concentration of the sacrificial agent (2.5 M) and a fixed amount of the photocatalytic material (1000 ppm) was exposed under solar radiation (See the Figure 11 (c) for the experimental set – up). To evaluate the effect of pH, in some cases the solution pH is adjusted to the chosen value by adding diluted solution of KOH as well as $HClO_4$.

4.5. Recovery of the photocatalysts

In some cases, at the end of the run the photocatalyst was recovered as described below. The suspension, under inert atmosphere, was let settle overnight, until the solid phase was perfectly separated from aqueous solutions and deposited on the bottom. Finally, after removing the surfactant liquid, the solid phase was dried under inert atmosphere.

4.6. Analytical methods

To estimate hydrogen production, gaseous samples were collected by means of Tedlar gas sampling bags (1 L) at different reaction times. These samples were analysed in a gas-chromatograph (Agilent 7820A), equipped with a HP-PLOT Molesieve 5A column (Agilent) and a TCD detector using argon as carrier gas. The pH of the solution was monitored through an Orion 420 p pH – meter (Thermo). Minitab software (Version 19) was used to analyse the experimental data.

4.7. Catalyst characterization

The UV-vis diffusive reflectance spectra were collected using a Shimadzu UV-2600 UV/vis spectrophotometer, with an integrating sphere attachment and $BaSO_4$ as the reflectance standard. Scanning electron microscopy (SEM) coupled with energy-dispersive X-ray spectroscopy (EDX) was performed using a Nova NanoSEM to observe the morphology of samples and to estimate the amount of Cu. Transmission electron microscopy (TEM) was carried out by using TecnaiG2 microscope at 200 kV. TEM samples were obtained by using the same procedure reported elsewhere [218]. In this case, a Forvar/Carbon 400-mesh Au grid was used to support the specimen. The X-ray Diffraction (XRD) patterns of the solid samples were recorded by an Empyrean Panalytical diffractometer employing a CuKα source (40 kV, 30 mA) and operating at diffraction angles 2θ ranging between 20 and 80° with a scan rate of 0.02° 2θ/s. The photoluminescence (PL) spectra in emission mode with an excitation at 300 nm were recorded using a Perkin Elmer LS 55 spectrometer between 320 and 580 nm (100 nm/min scan rate). Fourier transform infrared (FT – IR) analysis was carried out by using a Bruker Vertex 80 v FT-IR in the 4000 cm^{-1} – 400 cm^{-1} region. XPS measurements were conducted with an Ulvac-Phi Quantera II spectrometer, using Al Karadiation. Powder samples were pressed onto adhesive carbon tape, placed on insulating glass slide. Two measurements were conducted on each sample: Quick survey measurement of full spectral range, 16 min/sample and details on selected peaks with higher resolution, 2h15min/sample. The measurements were conducted under constant neutralisation with low energy e^- and Ar^+, which guarantees a stable measurement, but not absolute energy scale. Charge referencing is required. The measurement spot for details was 100 µm in diameter (200 µm for survey scans).

5. Results I. Cu_2O/TiO_2 composites prepared by facile mechanochemical synthesis for visible light driven hydrogen production

5.1. Introduction

As previously discussed, the activity of many researchers was directed during the last decades to improve the efficiency of TiO_2 through the combination with an additional semiconductor, thus extending the light absorption to the visible range through the formation of a heterojunction. Many preparation methods were proposed, even if the high costs of the reagents and the low productivities recorded limit at present their applicability on industrial scale. As alternative preparation method, ball milling was chosen in this work, due to its simplicity and industrial applicability.

To evaluate the effectiveness of this choice, preliminary studies were conducted by comparing the hydrogen production in presence of bare TiO_2 (P25), bare Cu_2O and TiO_2/Cu_2O composites prepared by manual mixing of the two commercial powders. In addition, the effect of the sacrificial agent used was analysed, and, to detect the factors further influencing photocatalytic system, a two – level 3 – factorial design approach was followed; based on this analysis, an in-depth evaluation of the activity of the photocatalyst by varying the percentage of Cu_2O and the operating conditions (milling time and speed rate) for the preparation of the composite is performed.

5.2. Results and discussion

5.2.1. Preliminary results

5.2.1.1. Effect of mixing

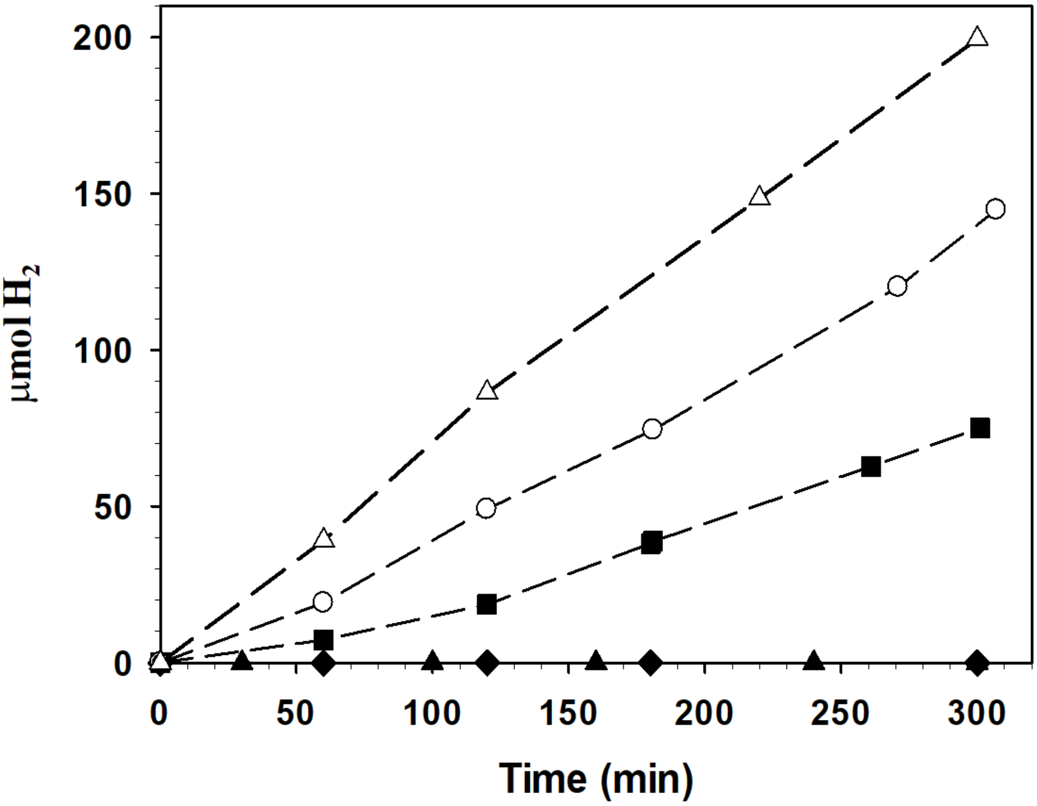

Figure 12. Comparison of hydrogen production with different mixed commercial semiconductors. Experimental conditions: [Methanol]=2.5 M; V=0.30 L; C_{Cat}= 1000 ppm; T=35 °C; P=1 atm; pH≈8.5; Cu_2O percentage in TiO_2: (■) 0 % Cu_2O; (Δ) 1% Cu_2O; (○) 2% Cu_2O; (◆) 98% Cu_2O; (▲) 100% Cu_2O; (All samples were prepared by manual mixing).

In Figure 12 the produced hydrogen amount at varying the relative percentage of Cu_2O and TiO_2 prepared by manual mixing was plotted; no hydrogen generation was recorded in presence of bare Cu_2O as well as in presence of a larger amount of Cu_2O than TiO_2, probably due to its unfavourable valence band position and the low stability in aqueous solution, as reported by others [219–221]. Moreover, in the presence of Cu_2O/TiO_2 composites higher values of hydrogen were obtained with respect to that recorded in presence of bare TiO_2, due to the formation of the heterostructure. The different reactivity observed in presence of 1% and 2% of Cu_2O in the composite materials demonstrates the influence of the relative percentage of each of the two semiconductors in the composites. These results indicated the effectiveness of the combination of Cu_2O and TiO_2 through a simple manual mixing, thus suggesting the possibility to maximize hydrogen generation if a deeper contact between the two powders is achieved by means of a more energetic mechanical mixing, as that obtained using a ball miller (See description in the experimental section). In the next sections, (i) chosen specific parameters (milling time and rotation rate) of the miller, the effect of the sacrificial agents was evaluated and (ii) the effects of the variables specifically related to the mixing operation – milling time and rotation rate – were discussed by using of a factorial design approach.

5.2.1.2. Effect of sacrificial agent

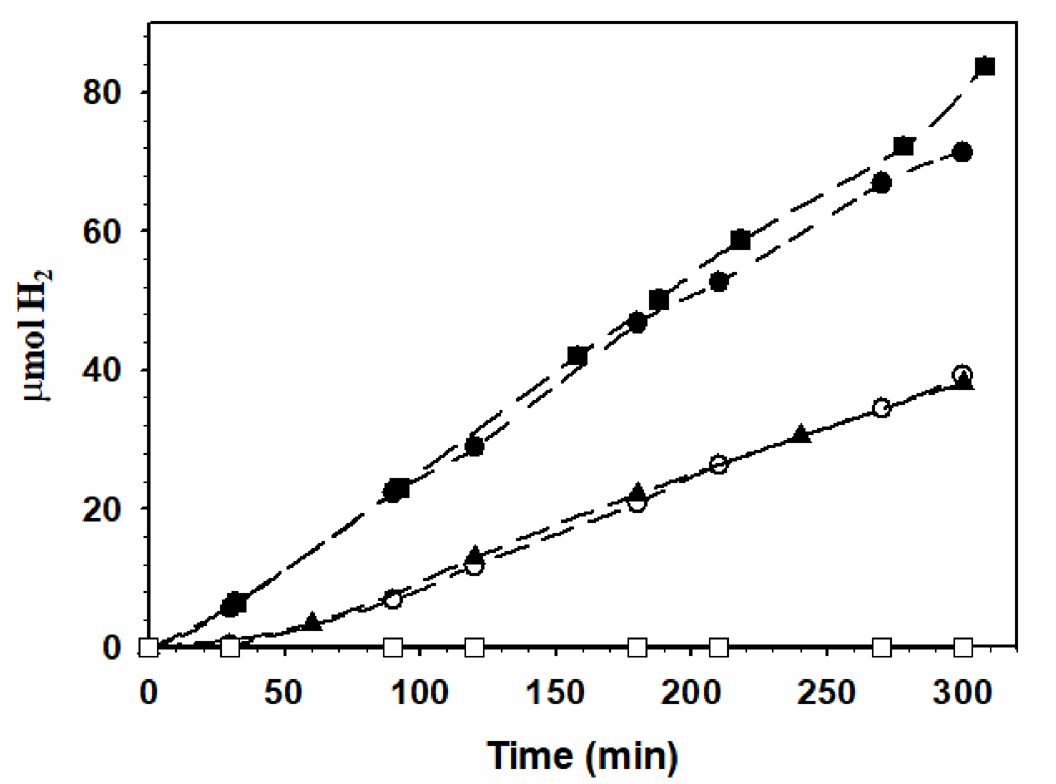

Figure 13. Effect of sacrificial agents (alcohols) on hydrogen production. Experimental conditions: [Organic]=2.5 M; V=0.30 L; T=35 °C; P=1 atm; pH≈ 6.0-8.5; Ccat (ppm)= 1000 ppm; Cu_2O percentage in TiO_2 = 1% wt; Milling time= 10 min; rotation rate= 500 rpm. Organic: No (Water splitting) (□); Methanol (▲); Ethanol (o); Glycerol (●); 1,2- Ethandiol (■).

To evaluate the effect of the scavenger used on the photocatalytic hydrogen production in presence of the Cu_2O – TiO_2 photocatalyst, prepared by using mechanical mixing, several runs, at fixed milling time and rotation rate of the miller (10 min, 500 rpm), were carried out at varying the sacrificial alcoholic agent used.

As reported in the Figure 13, glycerol and 1,2 – Ethandiol were the best candidates for hydrogen production in presence of Cu_2O – TiO_2 photocatalyst, according with literature findings in which Cu based TiO_2 were used to produce hydrogen through photoreforming [162]. On the contrary, no hydrogen production was detected in case of pure water, as well as using a solution containing sulphite (data not shown). An attempt to explain the results may be done if one considers the reactivity of the organics with photogenerated positive holes, which depends on both the nucleophilicity of the groups in the molecular structure of the sacrificial agents and the capability of organics to adsorb on the catalyst surface. The four species present similar nucleophilicity [222]. Moreover, as regards the adsorption phenomena, in case of glycerol and 1,2-ethanediol, the formation of the bidentate (and tridentate) complexes can be proposed, while the formation of weaker monodentate complexes can be supposed for ethanol and methanol, according with their structures. Based on these considerations, it is clear the reason why glycerol resulted the best sacrificial agent tested in this study. However, in the present investigation, it was chosen to study the system in the presence of methanol, which is the most reported sacrificial agent in literature findings.

5.2.2. Factorial design approach

The effects of two additional variables specifically related to the mixing operation – milling time and rotation rate – and of the Cu_2O percentage have to be taken into account and experimentally investigated. To this purpose, a two – level factorial design approach was followed to *(1)* plan the experimental runs to easily achieve a characterization of the photocatalytic activity of the system and *(2)* understand the interaction between the different factors, upon which hydrogen generation depends.

Each of the three factors (Cu_2O/TiO_2 ratio, milling time and rotation rate) may influence in a different way the system behaviour, and an extended experimental campaign was carried out to investigate it. However, a first attempt to understand the photocatalytic system behaviour may be done with a two – level factorial design approach [94,223], considering as response the hydrogen production rate (µmol/h). The chosen factors were: **A** for the Cu_2O percentage (wt. %), **B** for the milling time (min) and **C** for the rotation rate (rpm). Each of them was studied at low (-1) and high (1) levels, as reported in Table 2. For the Cu_2O percentage, the levels (1%, 10%) were chosen considering literature information [224], as well as the preliminary results reported in Figure 12, from which the need of using small amounts of Cu_2O may be derived. For the milling time, the values of the two levels (1 min, 30 min) were chosen to avoid an uncontrolled increase of temperature in the miller during the preparation of the material. Finally, the level values of the rotation rate were fixed at 100 and 500 rpm after considering the specifications of the instrument manufacturer. The response Y studied may be represented through the following polynomial function (eq. 4):

$$Y = a_0 + a_1A + a_2B + a_3C + a_{12}AB + a_{13}AC + a_{23}BC + a_{123}ABC \qquad \text{eq. 4}$$

where the a_0 represents the average response, a_1, a_2 and a_3 represent the principal effects of the factors studied (A, B, C) and a_{12}, a_{13}, a_{23} and a_{123} represent the interaction effects between the factors.

Table 2. Coded and un-coded values and levels of the factors.

Factors	Factor level	
	(-1)	(1)
Cu_2O percentage (%wt.)	1	10
Milling time (min)	1	30
Rotation rate (rpm)	100	500

In Table 3, the design table for the factors, along with the experimental and predicted responses in terms of hydrogen production rate, were reported; all the experiments were carried out twice. Moreover, the effect of the chosen parameters (Factors – A, B, C) and of the main and interaction effect plots on the response were discussed by using a Pareto chart [225]. To confirm the normality of the experimental data collected, a normal probability plot was reported and discussed.

As clearly shown in Table 3, the developed mathematical regression model resulted in agreement with the experimental data, as indicated by the comparison between the replicated and predicted responses, as well as by the value of the coefficient of determination (R – squared = 99.88%).

Table 3. Design table for the chosen factors and statistical factorial design. The coefficient of determination (R-squared) is equal to 99.88%.

Run	(A) Cu_2O Percentage (% wt.)	(B) Milling time (min)	(C) Rotation rate (rpm)	Mean hydrogen production rate (µmol/h)		
				Replicate 1	Replicate 2	Calculated response
1	-1	1	-1	10.82	8.93	9.87
2	1	1	1	0.00	0.00	0.00
3	-1	-1	1	37.15	37.09	37.12
4	1	1	-1	4.61	3.80	4.20
5	1	-1	1	3.88	4.85	4.36
6	1	-1	-1	5.05	4.81	4.93
7	-1	-1	-1	38.45	39.8	39.85
8	-1	1	1	6.47	5.38	5.92

As confirmation to what is reported above, in Figure 14 the normal probability plot for hydrogen production is reported. As clearly shown, all the points are distributed close to the straight line, confirming the good agreement of the data.

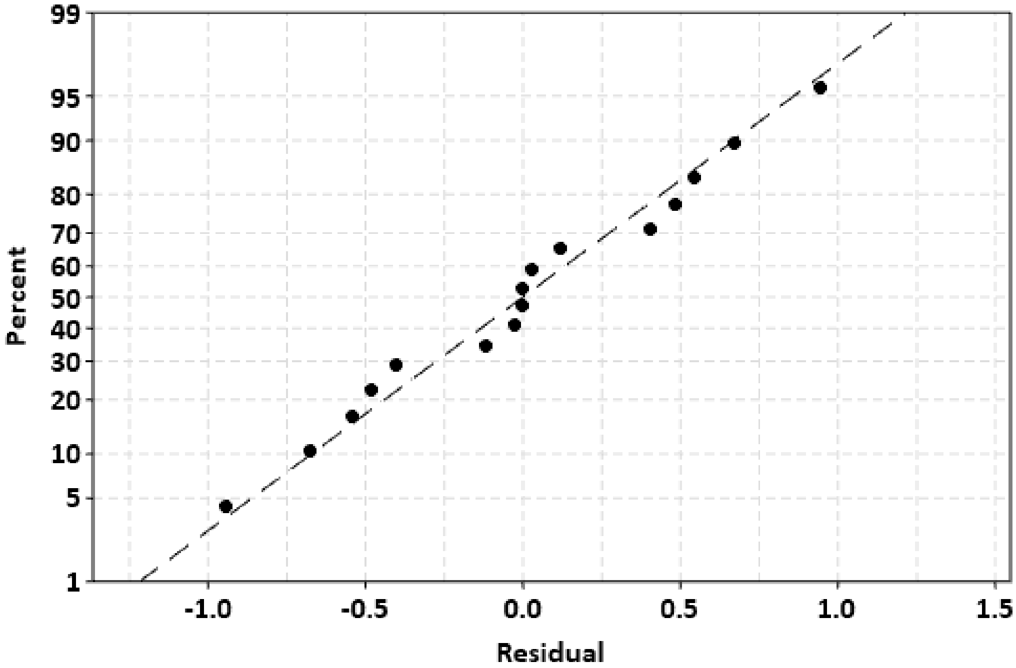

Figure 14. Normal probability plot of the residuals for hydrogen generation.

Regarding the Pareto chart, reporting the absolute values of the effects of the main factors and the effects of their interaction, it allows the identification of the relative importance of the factors. Specifically, considering Figure 15, only the factors exceeding the red line are statistically significant and can potentially affect the system. Among these values, the higher is the effect of the factor (or of the interaction between different factors), the higher is the value represented on the diagram.

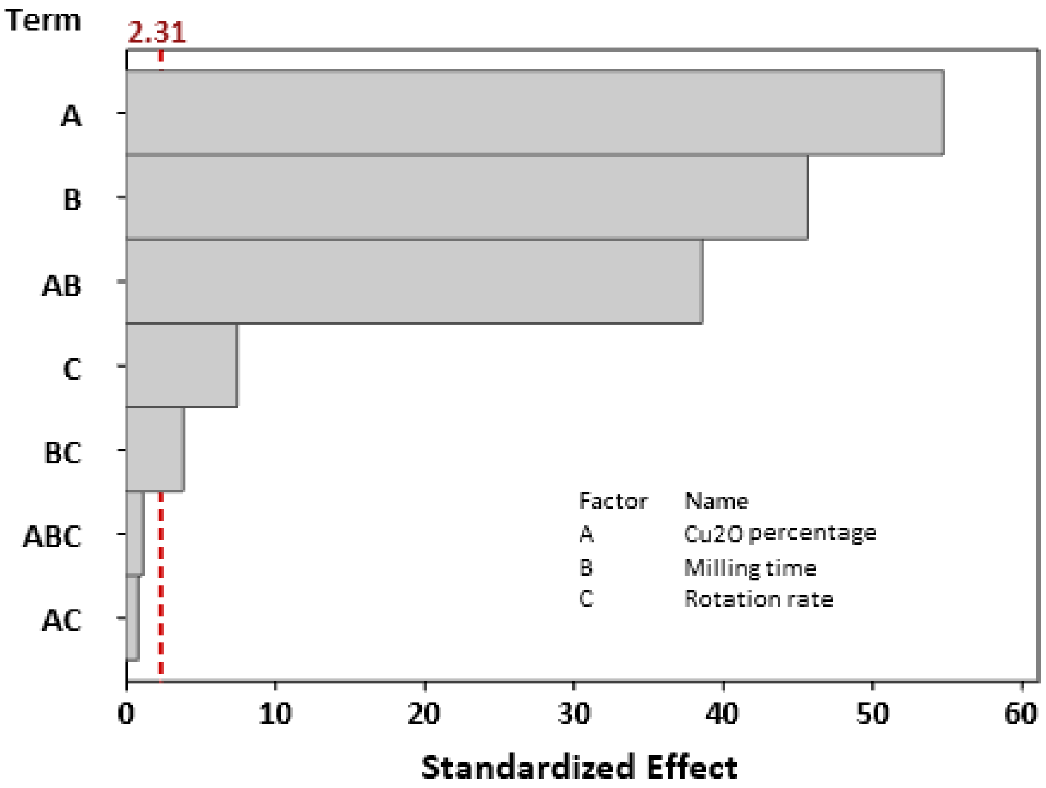

Figure 15. Pareto chart for standardized effects for hydrogen production, considering as response hydrogen production rate. Significance level α=0.05. Factors: A – Cu_2O percentage; B – Milling time; C –Rotation rate.

Hence, as clearly shown in the figure, a strong influence was observed for Cu_2O percentage, followed by the milling time and their interaction, while small effects were shown by the rotation rate factor and the milling time/rotation rate interaction. As for the interaction between rotation rate and Cu_2O percentage, the results indicate a not – statistically significant effect.

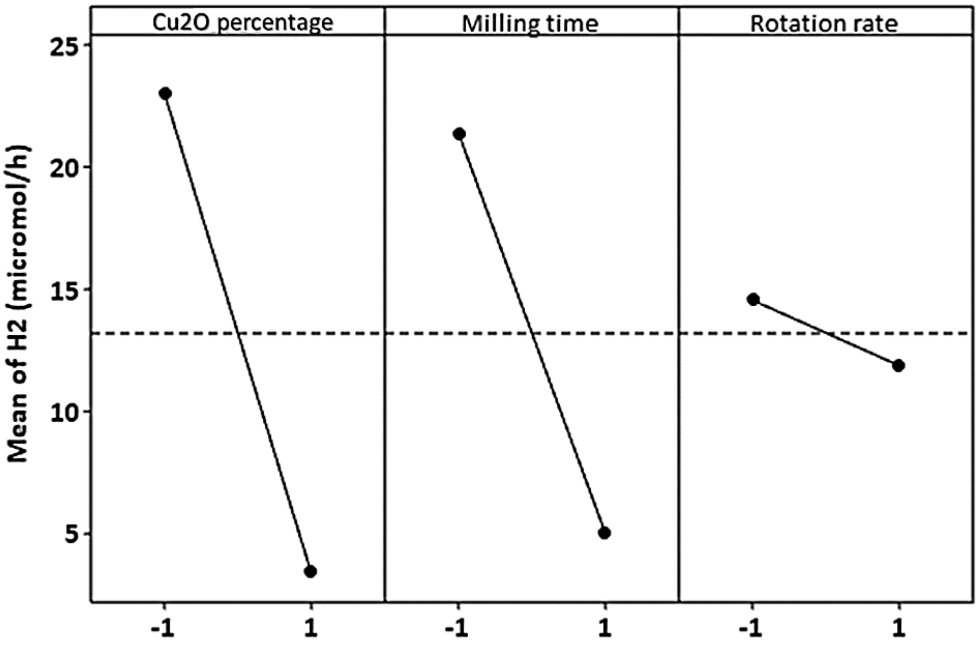

Figure 16. Main effects plot for Cu_2O percentage, milling time and rotation rate of the miller considering the hydrogen production rate as response.

To better understand the effect of the parameters, in Figure 16 the main effect plot is reported. An increase of all the three single factors has a negative influence on the hydrogen generation, and the more evident one was detected for Cu_2O percentage, confirming the Pareto chart analysis. Moreover, the photocatalytic activity of the composite material is weakly and negatively influenced by the rotation rate, while a stronger negative effect was detected for the milling time. Finally, and excluding the interaction between rotation rate and Cu_2O percentage (due to not – statistically significant results as discussed above), the strongest interaction effect was detected in the case of the Cu_2O percentage and milling time (Figure 17).

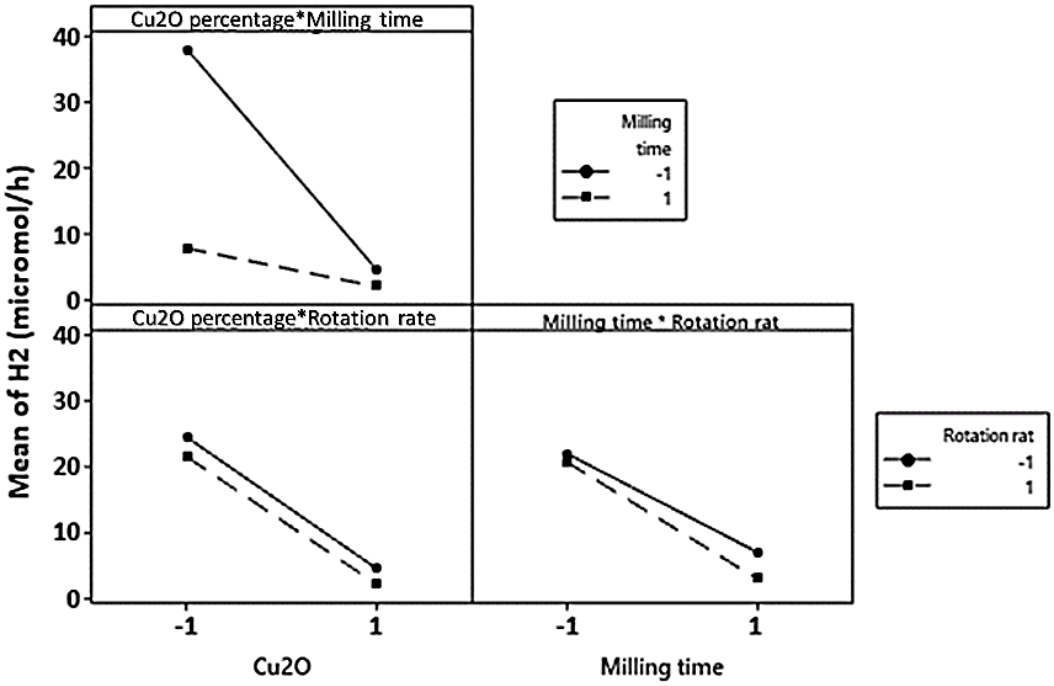

Figure 17. Interaction effects plot for the three factors, considering the hydrogen production rate as response.

In the next sections, an attempt will be done to explain the effect of Cu_2O percentage, milling time and rotation rate based on the results of a physico-chemical characterization of the composite materials prepared and used.

5.2.3. Physico – chemical characterization

The photocatalysts prepared by means of ball milling were submitted to the physico-chemical characterization. Results of the XRD, diffusive reflectance, XPS, SEM, TEM, and PL characterizations are presented and discussed below.

Table 4. Detailed information about the materials on which XRD, diffusive reflectance, XPS, SEM, TEM, FT-IR and PL characterizations were performed. The calculated bandgaps and crystallite sizes are also reported.

Details of the tested samples					**Characterization results**				**Produced H_2 after 5 hrs* (μmol)**
Sample	**Comment**	**%Cu_2O**	**Milling time (min)**	**Rotation rate (rpm)**	**Band gap (eV)**	**Anatase (nm)**	**Rutile (nm)**	**Cu_2O (nm)**	
A	RECOVERED	1%	10	500	2.98	26.9	20.3	-	-
B	RECOVERED	1%	10	500	2.97	24.2	30.5	-	-
C	MILLED	1%	10	500	3.02	17.3	22.1	-	100
D	MILLED	1%	120	500	2.94	12.1	13.5	-	Not detected
E	MILLED	1%	30	500	2.99	22.0	34.8	-	32
G	MILLED	1%	1	500	3.08	16.2	30.5	-	180
H	RECOVERED	1%	1	500	3.04	22.0	30.5	-	-
I	RECOVERED	2%	30	500	2.95	34.7	30.5	-	-
J	MILLED	2%	30	500	3.00	20.2	30.5	-	3
K	MILLED	2%	30	200	3.22	22.0	40.6	-	87
L	MILLED	100%	10	500	1.47	-	-	71.2	Not detected
M	COMMERCIAL GRADE	100%	No	No	1.57	-	-	102.4	Not detected
N	MILLED	0%	10	500	3.01	24.3	34.8	-	8
O	COMMERCIAL GRADE	0%	No	No	3.30	24.3	22.2	-	76
P	MILLED	2%	1	500	3.08	27.0	40.7	-	161
Q	MILLED	5%	1	500	3.08	23.1	27.1	-	80
R	MILLED	10%	1	500	3.10	23.1	27.1	33.3	23
S	RECOVERED	5%	1	500	ND	23.1	40.7	-	-
T	RECOVERED	10%	1	500	ND	23.1	32.5	41.6	-

*Experimental conditions: [Methanol]=2.5 M; V=0.30 L; Cat= 1000 ppm; T=35 °C; P=1 atm; pH≈8.5

XRD patterns of the composites did not show any diffraction peaks for Cu_2O at low percentage of Cu_2O in the TiO_2 samples (1% – 2%, see Figure 18 (a, b)).

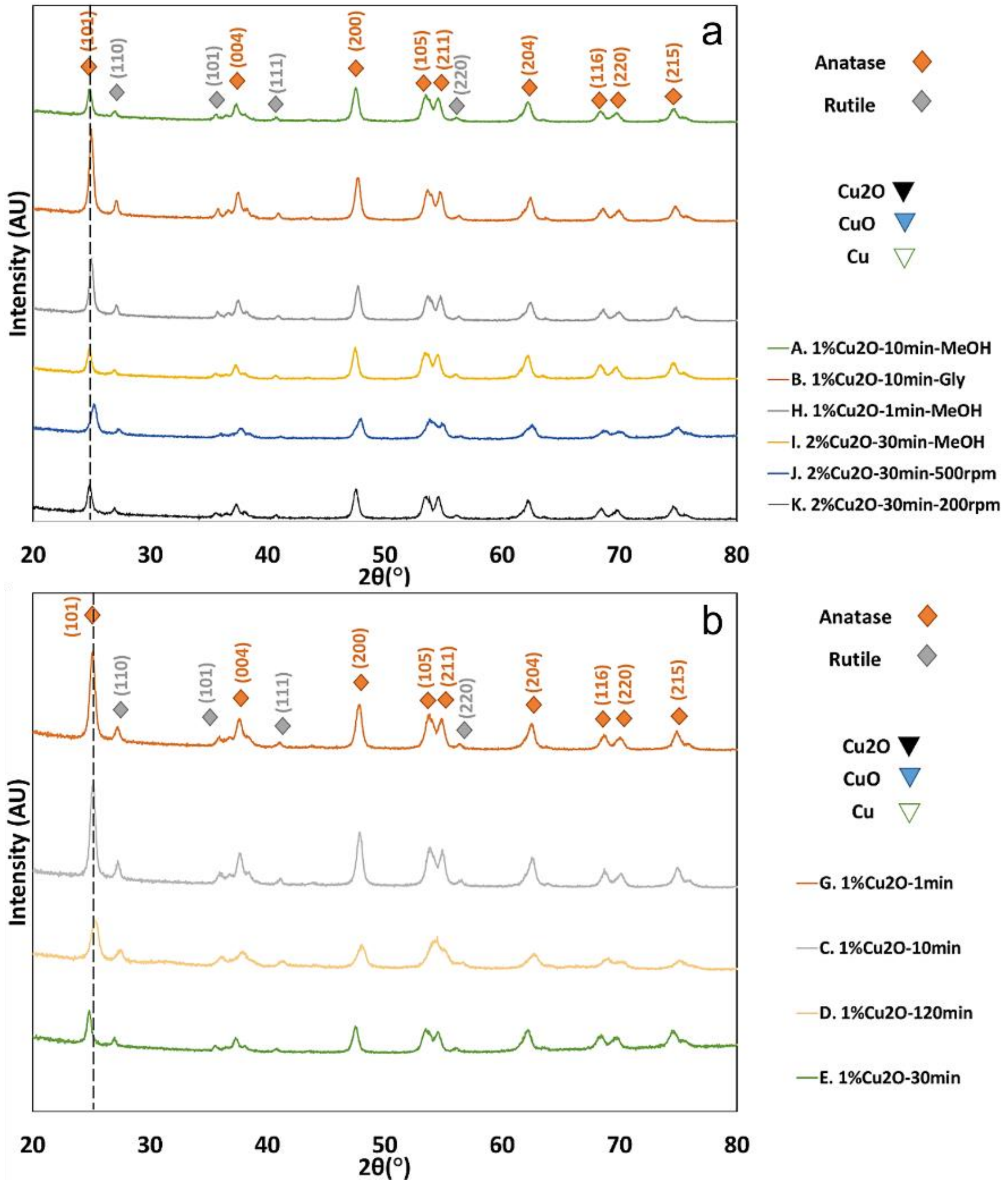

Figure 18. XRD patterns of several 1% and 2% Cu_2O – TiO_2 composite materials tested.

On the other hand, at high Cu_2O loading (5% – 10%), Cu_2O diffraction peaks were clearly identified, even in the recovered sample, as clearly shown in the Figure 19.

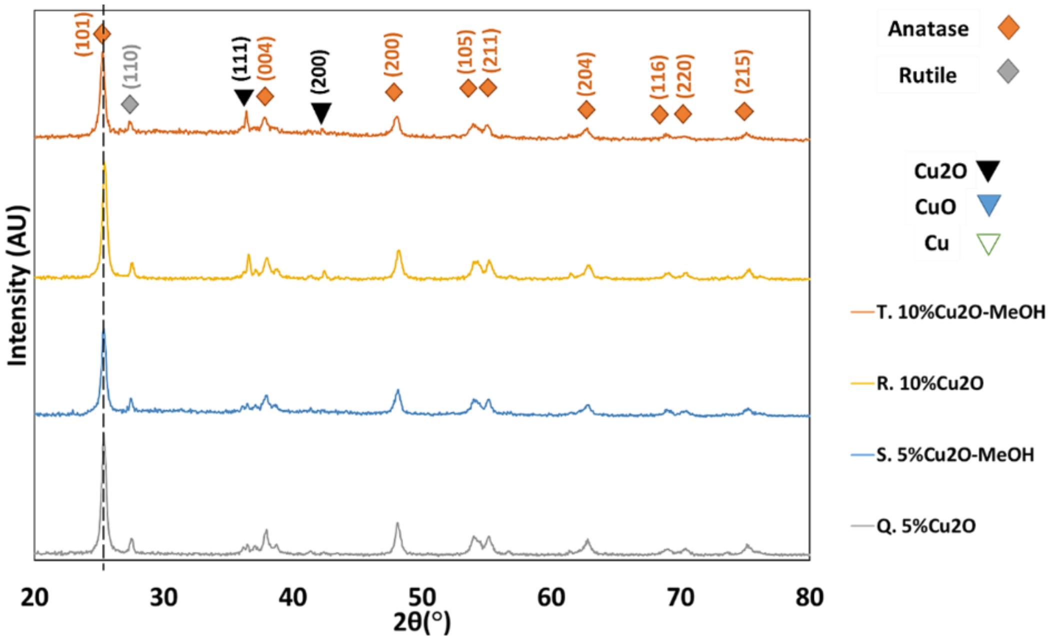

Figure 19. XRD patterns of several 5% and 10% Cu_2O – TiO_2 composite materials tested, before and after the reaction.

In case of bare Cu_2O, the peaks obtained demonstrate that the sample contains traces of metallic Cu and CuO and indicate a higher degree of crystallinity compared to TiO_2; moreover, the peaks obtained in case of bare TiO_2 demonstrate that the titanium dioxide used consists mainly of the anatase phase, as shown in the Figure 20.

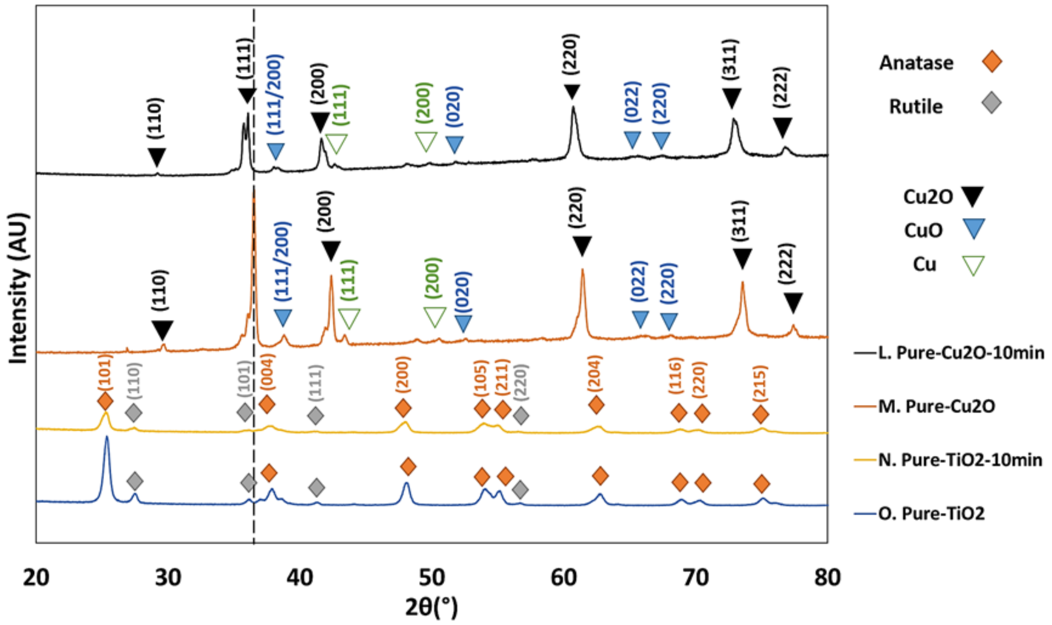

Figure 20. XRD patterns of the bare TiO_2 and Cu_2O samples.

From the crystallite size of the samples, which was determined by using the Debye-Scherrer equation with respect to the anatase and rutile major peaks, the following considerations may be realized:

1. Milling seems to increase the crystallite size of rutile TiO_2 (see samples N/O in the Table 4) and increase the width of the diffraction peak. The increase in rutile crystallite size is probably due to nanoparticle agglomeration, while the broadening of the diffraction peak reveals the probable creation and accumulation of lattice defects. As for Cu_2O, milling seems to decrease the crystallite size of the material (see samples L/M in the Table 4).
2. By increasing the milling time, an increase in crystallite size (anatase) is detected, again probably because of the agglomeration. However, at very high milling times, i.e., at 120 mins, the crystallite size significantly drops (see samples C to G in the Table 4). Additionally, with increasing milling time, an increase in the of presence of defects in the lattice structure may be inferred from the broadening of the diffraction peaks.
3. At higher speed rates, smaller TiO_2 crystals and more lattice defects (as may be inferred from the broadening of the diffraction peak) were obtained (see samples J/K in the Table 4).
4. Finally, increasing the Cu_2O content from 2 to 5% reduced the crystallite size of TiO_2 (see samples P/Q in the Table 4). A further increase to 10% Cu_2O, however, showed no effect on the crystallite size of TiO_2 (see samples Q/R in the Table 4).

The diffuse reflectance spectra of the catalysts are shown in Figures 21 (A – D). The presence of Cu_2O semiconductor resulted in an enhanced visible – light absorption (i.e., low reflectance) compared to bare TiO_2 – P25, thus demonstrating the effectiveness of the combination of Cu_2O and TiO_2 (See Figure 21 (A)).

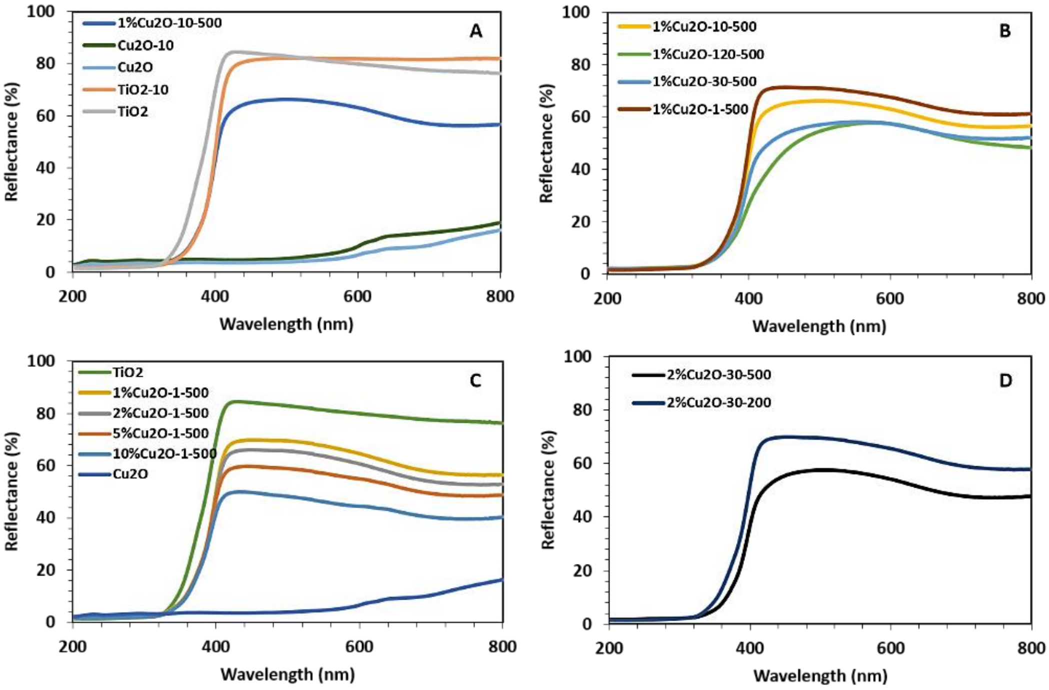

Figure 21. Diffusive reflectance spectra of several A%Cu_2O-B-C samples, with: (A) Cu_2O percentage, (B) milling time, (C) rotation rate. The bare TiO_2 and Cu_2O are indicated as: Cu_2O (and TiO_2) for the commercial samples and Cu_2O-B (and TiO_2-B) with B=milling time and rotation rate = 500 rpm.

The optical band gap values, which are reported in Table 4, were calculated through the onsets of the plots of the modified Kubelka – Munk function, that is $(F(R)\ h\nu)^{1/2}$ for indirect semiconductors, versus the energy of the exciting light. Considering the results in the table, the following considerations may be also realized:

i. The milling seems to significantly narrow the band gap (see samples L/M and N/O in Figure 21 (A) and Table 4), with the band gap decreasing further as the milling time increases (see samples C to G in Figure 21 (B) and Table 4).

ii. Introducing Cu_2O (1%, 2%, 5%, or 10%) does not seem to significantly affect the band gap of TiO_2 (see samples G/P/Q/R in Figure 21 (C) and Table 4). However, as clearly shown in Figures 18 (A) and Figure 21 (C), an enhancement in the absorbance of visible light, with new bands appearing between 400 and 600 nm, took place. The enhancement in visible light absorption increased with the amount of Cu_2O added. This result could lead to higher reactivity of the composite with respect to the bare TiO_2.

iii. The band gap decreases significantly with increase of the rotation rate of milling (see samples J/K in Figure 21 (D) and Table 4), possibly due to the larger particles obtained at lower rpm. The decrease of the band gap with increasing rotation rate could result in a greater photocatalytic activity.

Along with XRD measurements, the XPS analyses were performed to clearly identify the oxidation state of copper species in the photocatalytic samples. As clearly shown in the Figure 22, in the case of the bare Cu_2O: *(i)* the typical Cu^{1+} peaks of Cu_2O are individuated at 932.2 and 952.0 eV; however, as reported in the previous section, the peak position of about 932 eV agrees also with literature value of zerovalent copper; *(ii)* the shoulder and satellite peaks between 940 eV and 945 eV indicate that CuO is also present in sample.

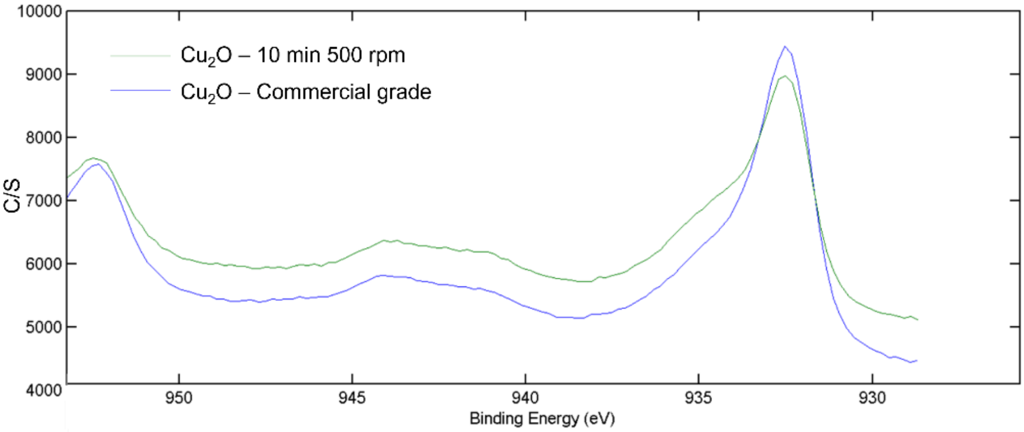

Figure 22. XPS spectra of Cu_2O powders: green line (commercial grade), blue line (sample prepared through ball milling: milling time=10 min; rotation rate=500 rpm).

Moreover, in the Figure 23 the Cu2p region for the 1% Cu_2O-TiO_2 composite material (prepared through ball milling with a milling time of 1 minute and rotation rate of 500 rpm) is reported, for the fresh and the reacted sample.

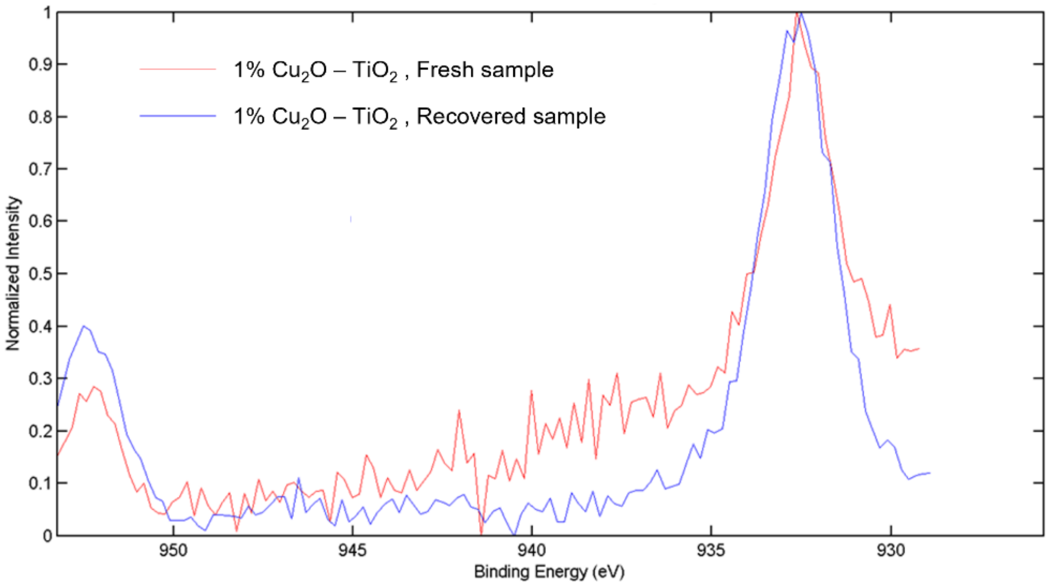

Figure 23. XPS spectra of 1% Cu_2O – TiO_2 composite material (prepared through ball milling: milling time=1 min; rotation rate=500 rpm): (red line) Fresh sample, (blue line) reacted sample.

As clearly shown in the diagram, due to the low percentage of Cu_2O in the composite, the spectra present low signals; however, the comparison between the peaks (at 932.2 and 952.0 eV) for the fresh and the recovered samples does not indicate the oxidation of the copper species (Cu^{1+}, Cu^0) to Cu^{2+}.

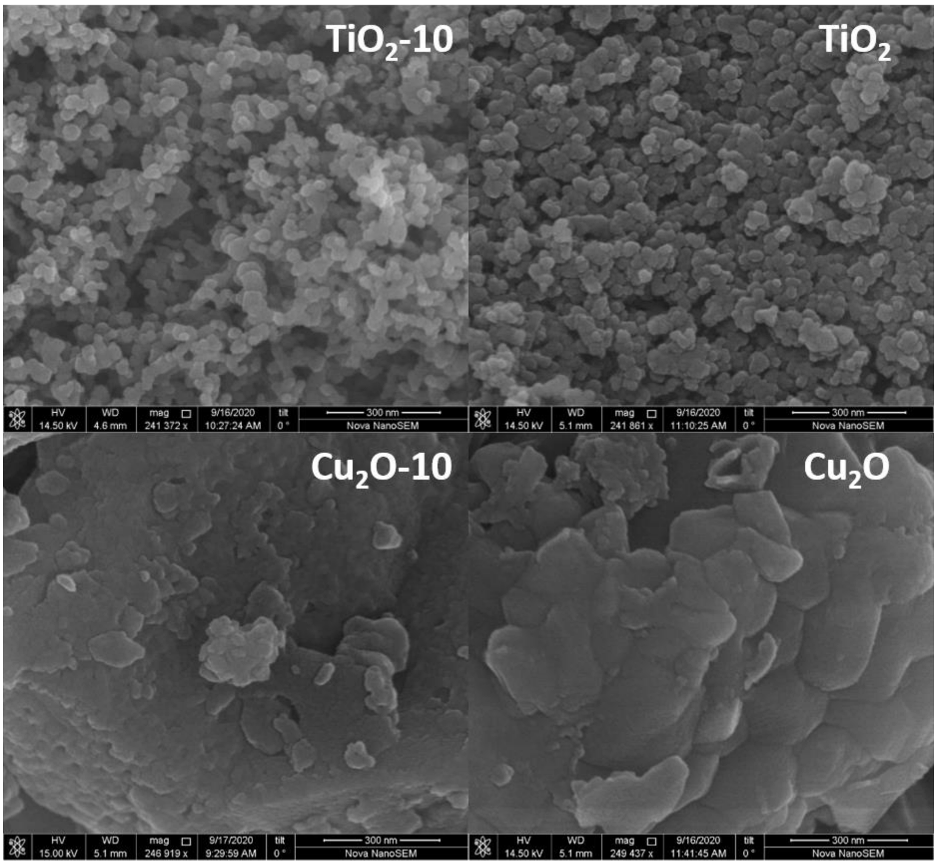

Figure 24. SEM analysis of bare Cu_2O and TiO_2. TiO_2 – 10: sample prepared through ball milling (Milling time = 10 min; rotation rate = 500 rpm); Cu_2O – 10: sample prepared through ball milling (Milling time = 10 min; rotation rate = 500 rpm).

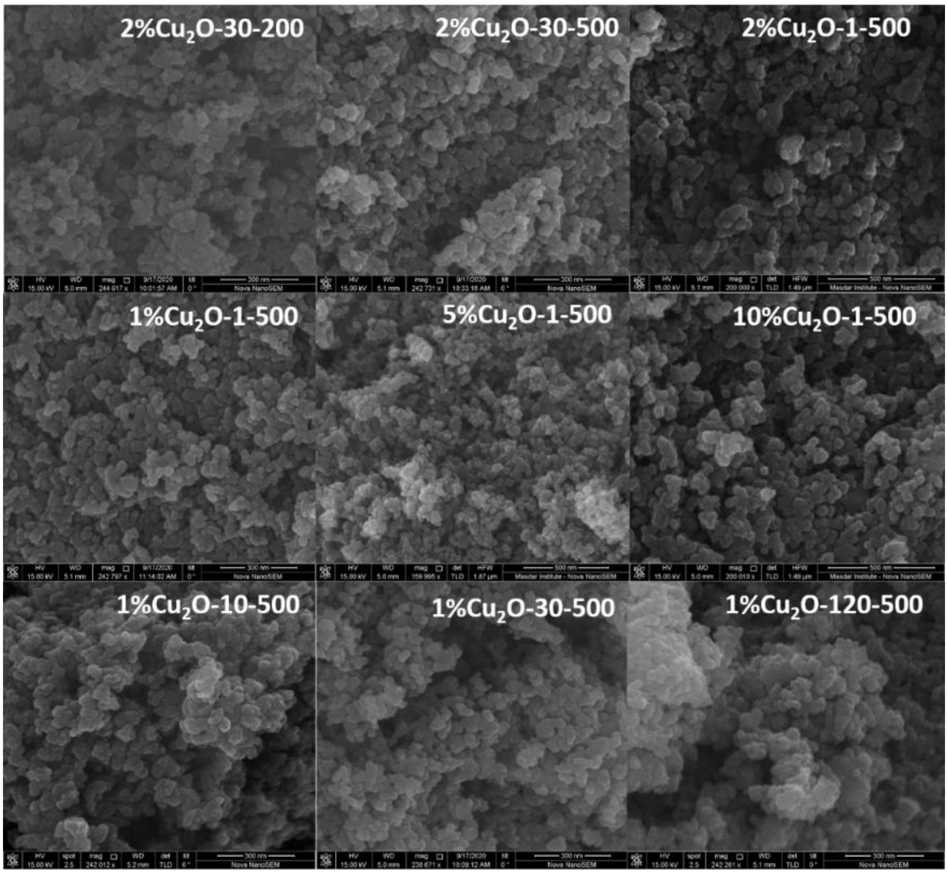

Figure 25. SEM analysis of several A%Cu_2O-B-C samples, with: (A) Cu_2O percentage, (B) milling time, (C) rotation rate.

Figures 24 – 28 show SEM (Scanning Electron Microscopy) analysis and the TEM (Transmission Electron Microscopy) micrographs of the bare photocatalysts and Cu_2O/TiO_2 composite materials. The morphology of the samples did not change significantly with doping, time and rotation speed used during the treatment, even if a slightly higher agglomeration was detected after milling. This result may be associated with the lower reactivity recorded at increasing the milling time at fixed rotation rate. Moreover, TiO_2/Cu_2O particles exhibited irregular shapes mainly composed of anatase with dominant (101) planes as confirmed by TEM, while the presence of metallic copper with dominant (111) planes was detected in the recovered sample. Metallic copper is probably also present in the fresh composite samples, but due to the very low amounts used of cuprous oxide, it is not detectable by characterization techniques. The traces of metallic copper in the fresh composite samples are almost negligible compared to the composition of other constituents. In the 2% Cu_2O sample the Cu species was detected, and the amount measured by SEM/EDX was about 2%. The EDX spectra for the 2% Cu_2O samples displayed energy peaks at 0.93 and 8.04 keV, which are characteristic to Cu Lα and Cu Kα, respectively. SAED (selective area electron diffraction) patterns were also acquired but these did not show any group of lattice planes belonging to Cu_2O. This is probably due to the low concentration of Cu_2O (1-2 wt.%) or to the overlapping with anatase and rutile signals in P25 (data not shown).

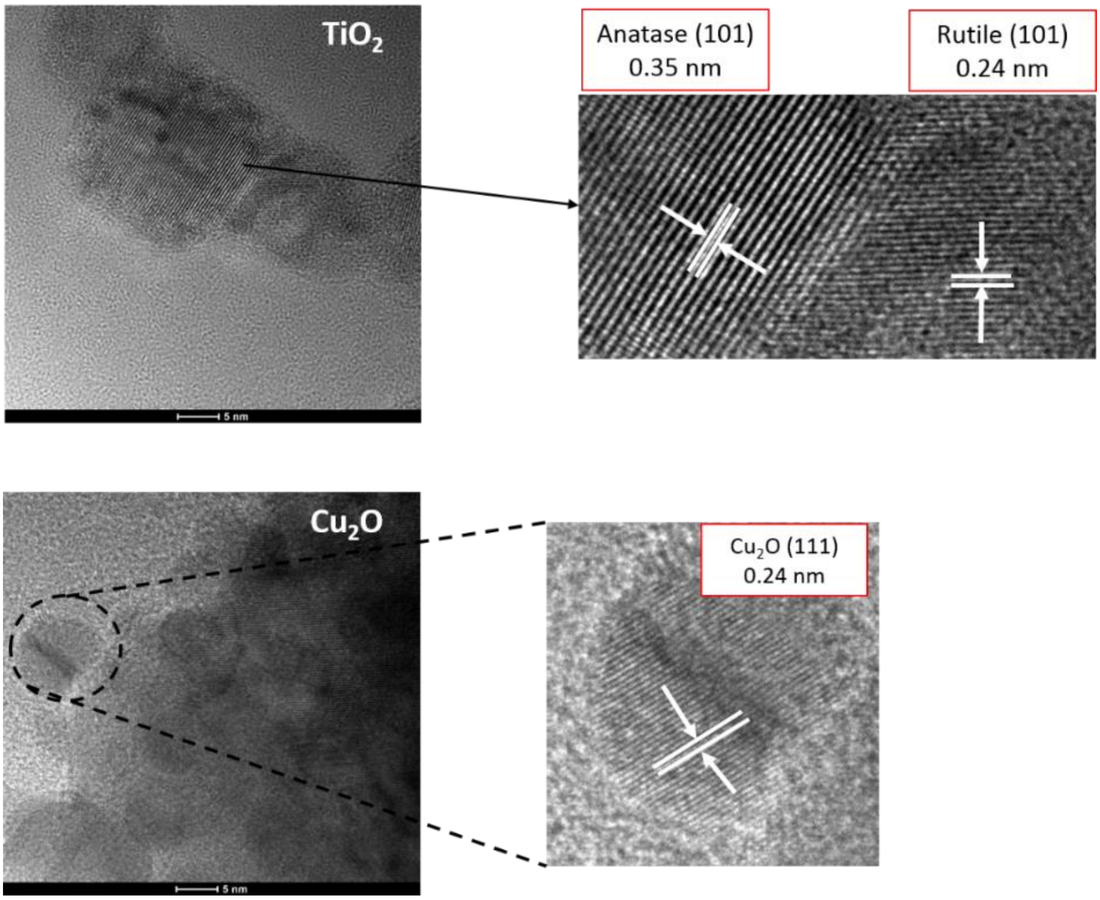

Figure 26. TEM micrographs of the bare TiO_2 (P25) and Cu_2O.

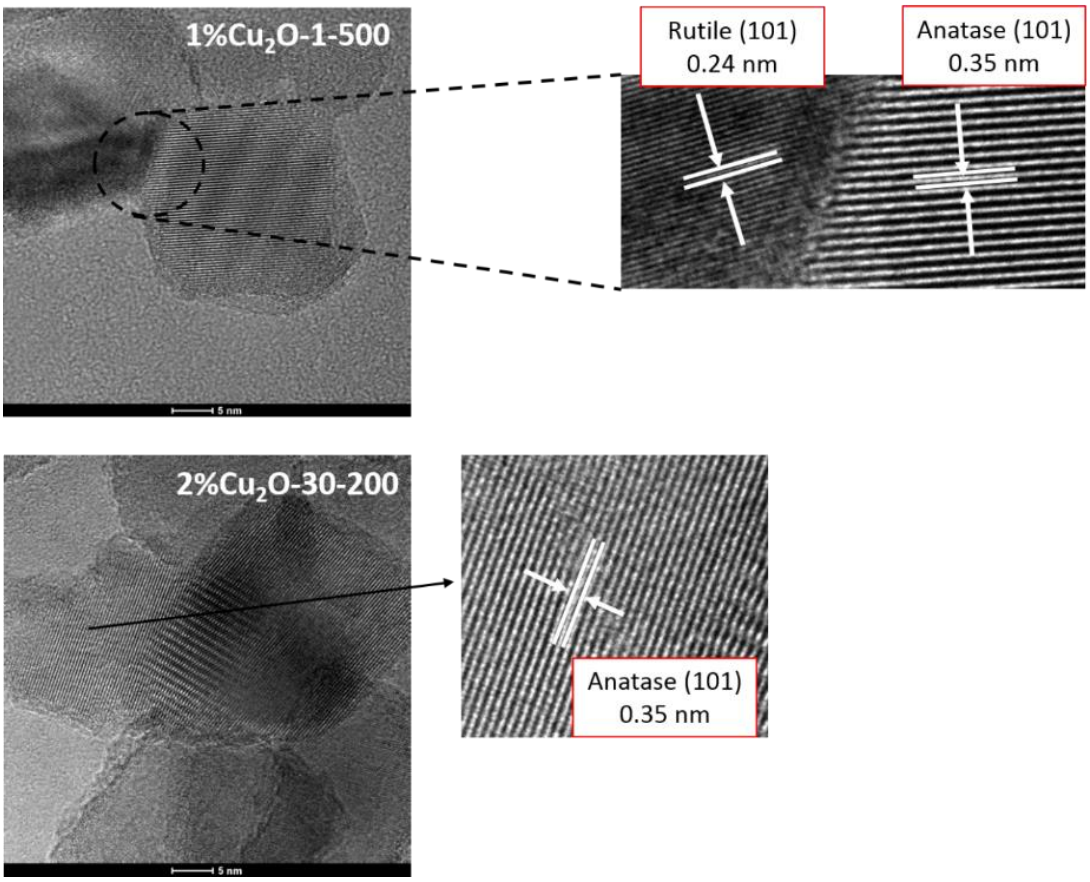

Figure 27. TEM micrographs of some A%Cu_2O-B-C samples, with: (A) Cu_2O percentage, (B) milling time, (C) rotation rate.

TEM/EDX results, which are presented in the Figure 28 and Table 5 (See appendix A for EDX spectra), show an increase in the Cu to O ratio after reaction. The higher content of Cu after the reaction is indicative of the diffusion of Cu from the bulk of the photocatalyst to the surface. While a low amount of metallic copper leads to a more efficient electron – hole separation, excess metallic Cu (Cu^0) on the surface of the catalyst may act as recombination centers and can block the absorption of light, as reported by others [226]. Thus, a high Cu^0 content would be detrimental to the photocatalytic activity. These results, along with the shielding effect of Cu_2O on the titanium dioxide surface, may help to explain the lower hydrogen yields obtained as the Cu_2O content was increased, as reported in the previous section (5.2.3). The higher the Cu_2O content, the higher the Cu^0 on the surface and the lower the hydrogen yield.

Table 5. Ratio of Cu to O calculated on the fresh and the recovered samples.

Sample	Ratio of Cu to O*
1% Cu_2O-TiO_2 before reaction	0.58
1% Cu_2O-TiO_2 after reaction	0.83
10% Cu_2O-TiO_2 before reaction	0.34
10% Cu_2O-TiO_2 after reaction	0.50

* Note that TEM/EDX was performed on the same sample twice, where each time a different area of the sample was analysed. The values in the table represent the average values of the two analyses. Ratio was calculated as weight %. All the fresh samples are prepared through the ball milling (1 min, 200 rpm).

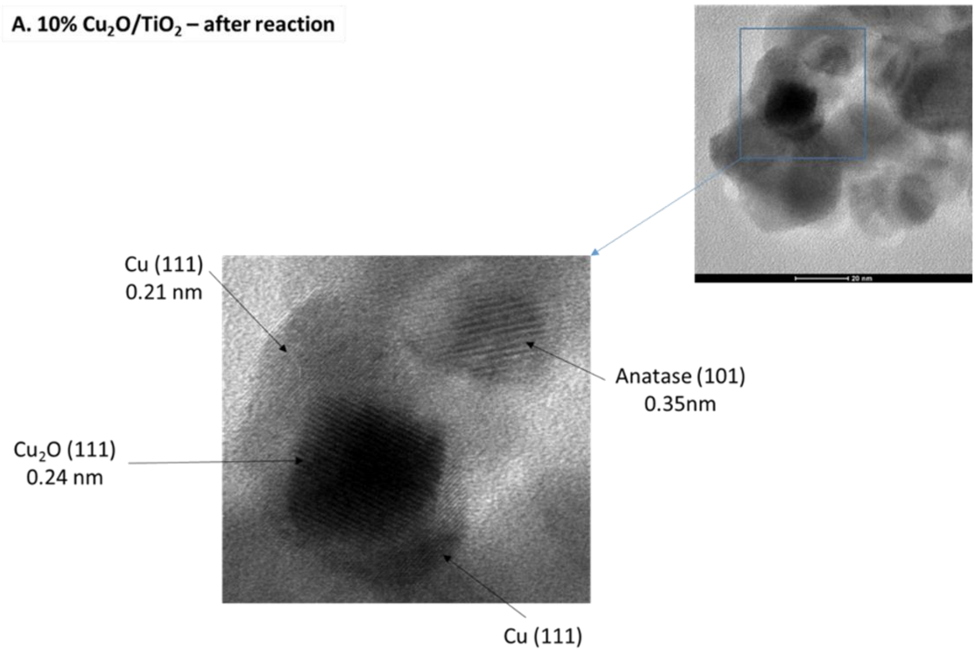
A. 10% Cu_2O/TiO_2 – after reaction

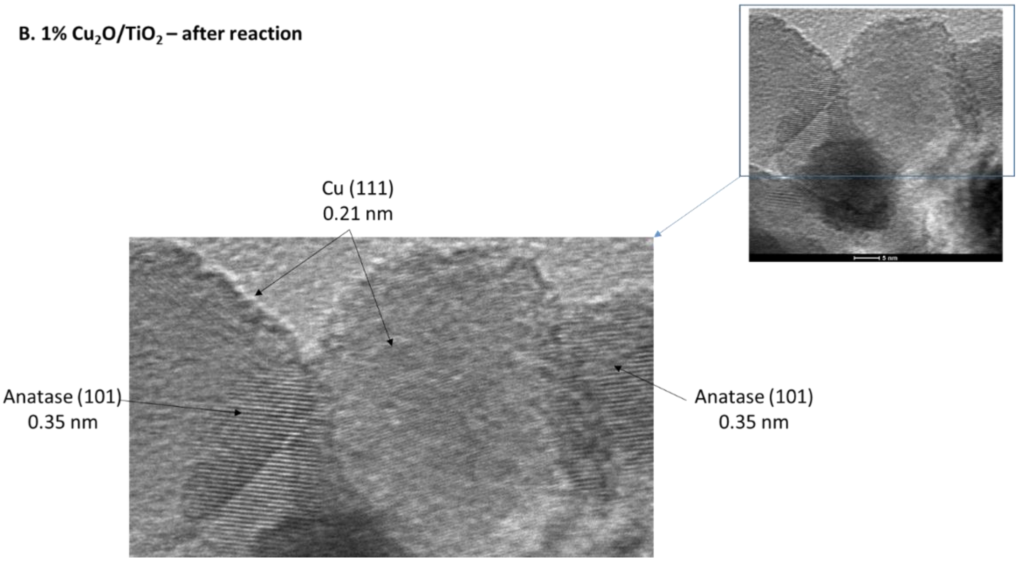
B. 1% Cu_2O/TiO_2 – after reaction

Figure 28. TEM micrographs of some (a) 10%Cu_2O-TiO_2 and (b) 1%Cu_2O-TiO_2 samples prepared through ball milling (1 min, 200 rpm), after the reaction.

Finally, the investigation on absorption/emission properties was carried out through the photoluminescence studies on some Cu_2O – TiO_2 materials tested. In the Figure 29 the PL measurements on the samples at different rotation rate (Figure 29 (A)) and milling time (Figure 29 (B)) were reported.

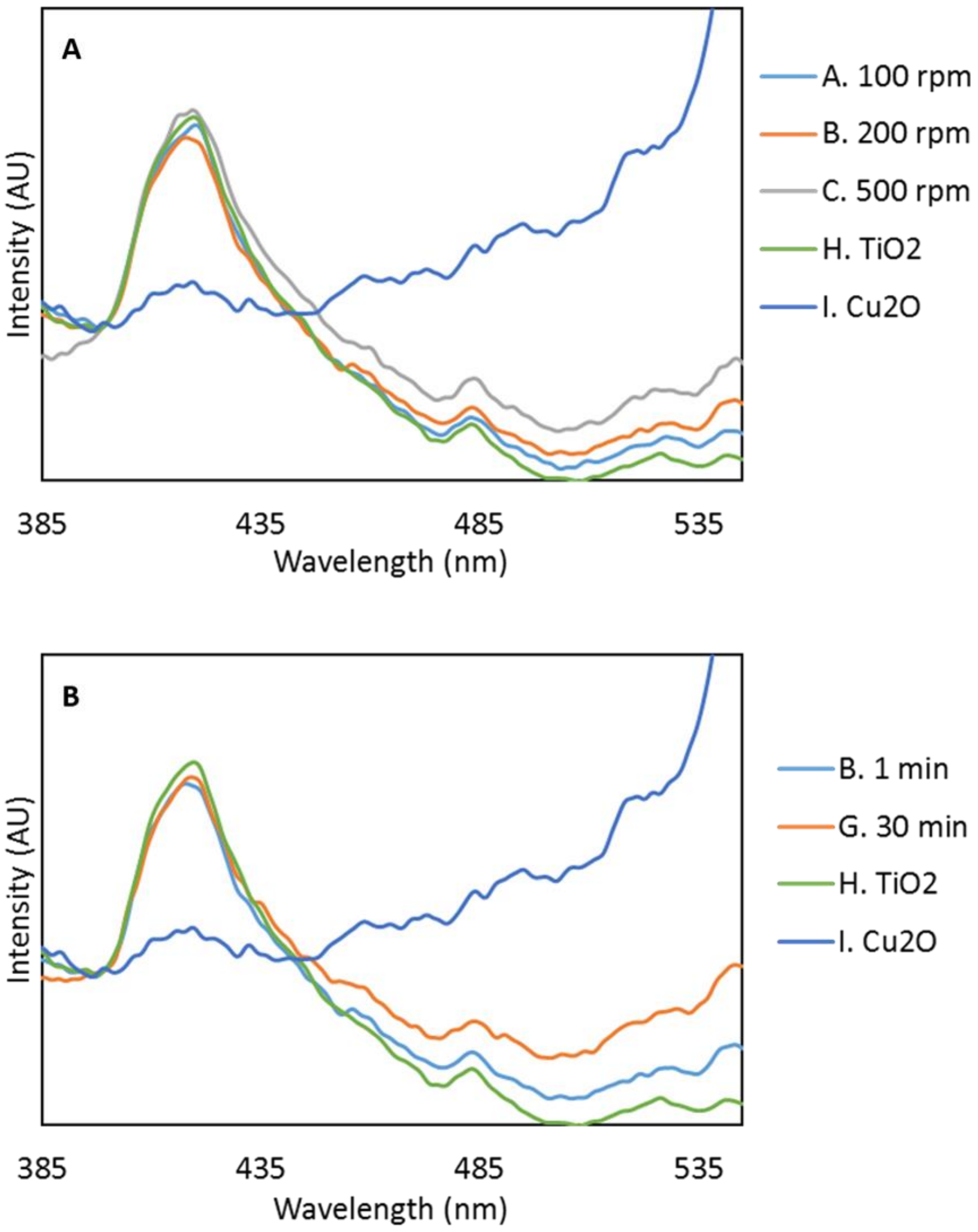

Figure 29. PL spectra of some Cu_2O – TiO_2 composites, (A) at different rotation rates and (B) at different milling times.

The main peak at ca. 420 – 425 nm may be attributed to electron migration from conduction band back to valence band, while the emission at lower energy is mainly due to excitonic PL resulting from lattice defects of the crystal. Considering the Figure 29 (A), the lowest charge recombination was observed at intermediate rotation rate (i.e., 200 rpm), while the high recombination rate was detected at high milling rotation rate, probably due to the formation of defects in the structure. As for the milling time (Figure 29 (B)), an increasing of the milling time seems to increase the recombination of charges, probably due to more structural defects forming at higher milling times.

5.2.4. Photocatalytic tests

5.2.4.1. Effect of Cu_2O percentage

The increase of the Cu_2O loading in the composite photocatalyst within the range explored in this study has a negative impact on hydrogen generation: this is clearly shown in Figure 30, where experimental (full circles) and calculated (empty circles) data for H_2 production at constant milling time and rotation rate are reported as a function of the Cu_2O loading. The experimental data show a classic volcano-like behaviour with a maximum value in correspondence of 1% wt. Cu_2O, similarly to the results reported by others [227,228]. It can be argued that the addition of small amounts of Cu_2O leads the formation of the heterojunction – structure, thus improving hydrogen generation, whereas too large contents of cuprous oxide in the TiO_2/Cu_2O nanoparticles reduce the light energy absorbed by TiO_2 surface, due to its excessive coverage and the formation of higher content of Cu^0 during the reaction, as confirmed by EDX/TEM analyses on the recovered samples (See Table 5 and Figure 28 in the section 5.2.4). Moreover, the comparison between the experimental results and the data calculated by the model obtained by the factorial design analysis confirms the reliability of the simulation used and the negative effect on the generation of hydrogen at increasing Cu_2O percentage.

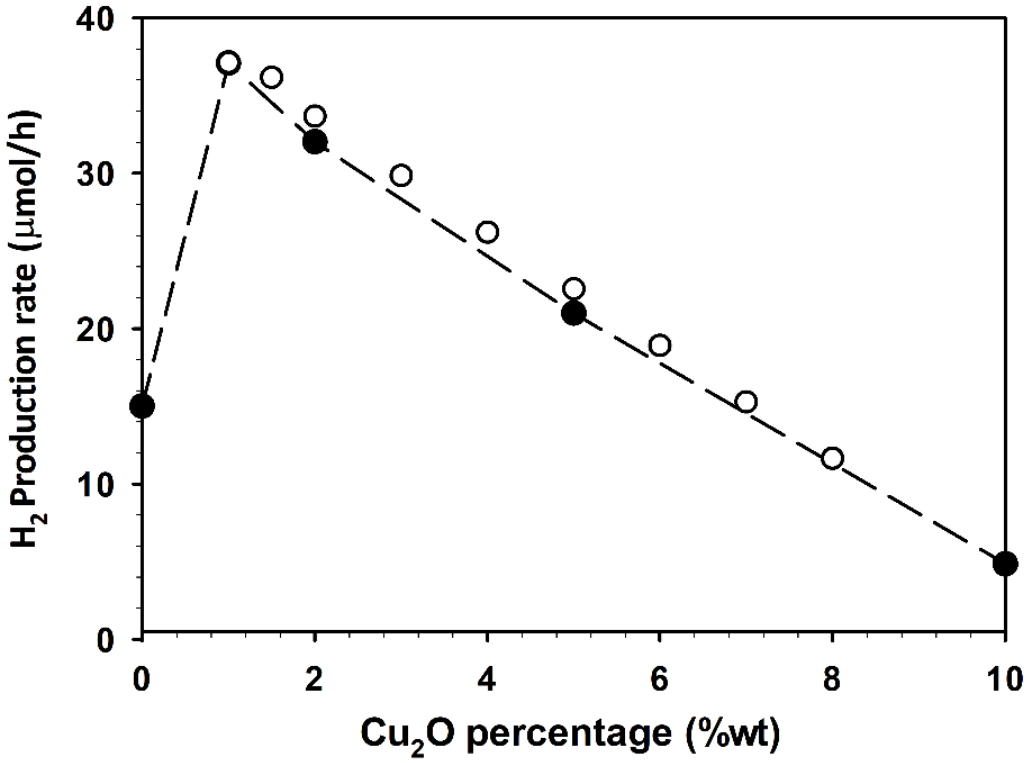

Figure 30. Effect of commercial Cu_2O percentage in TiO_2 on hydrogen production. Experimental conditions: [Methanol]=2.5 M; V=0.30 L; Cat= 1000 ppm; T=35 °C; P=1 atm; pH≈8.5; milling time= 1 min; speed rate = 500 rpm. Comparison between experimental data (full symbols) and calculated data (empty symbols).

5.2.4.2. Effect of milling time and rotation rate

The preliminary factorial design analysis indicated that the increase of either the milling time and the rotation rate negatively affects the hydrogen generation rate, as well as their interaction. To better understand the behaviour of the photocatalytic system under investigation, an in-depth evaluation of these effects was carried out. Therefore, additional experimental runs were performed on Cu_2O/TiO_2 samples prepared at various milling time – at fixed rotation rates and Cu_2O percentage – and the results were compared with those predicted by the model.

As shown in Figure 31, at any fixed rotation rate, a progressive reduction of hydrogen productivity was obtained with increasing the milling time: this corresponds to an increase of presence of defects in the lattice structures detected by XRD measurements, which, in turn leads to a high electron – hole recombination rate, as confirmed by PL measurements. The agreement between the regression model and the novel data set is satisfactory, even though the experimental hydrogen production was in some cases overpredicted by the model. On contrary, at any fixed milling time, the hydrogen generation passed through a maximum for at a rotation rate of 200 rpm and then decreased. It should be noticed that the simple regression model employed does not include the possibility of a non – linear trend in hydrogen production as varying one of the factors. This is probably due to the occurrence of two main contrasting phenomena affecting the activity of the photocatalysts, such as: *(i)* the decrease of the crystallite size of anatase and, in turn, the reduction of the band gap value of the composite; *(ii)* the increase of structural defects detected by XRD, to whom a higher electron-hole recombination rate may be attributed, as confirmed by PL measurements.

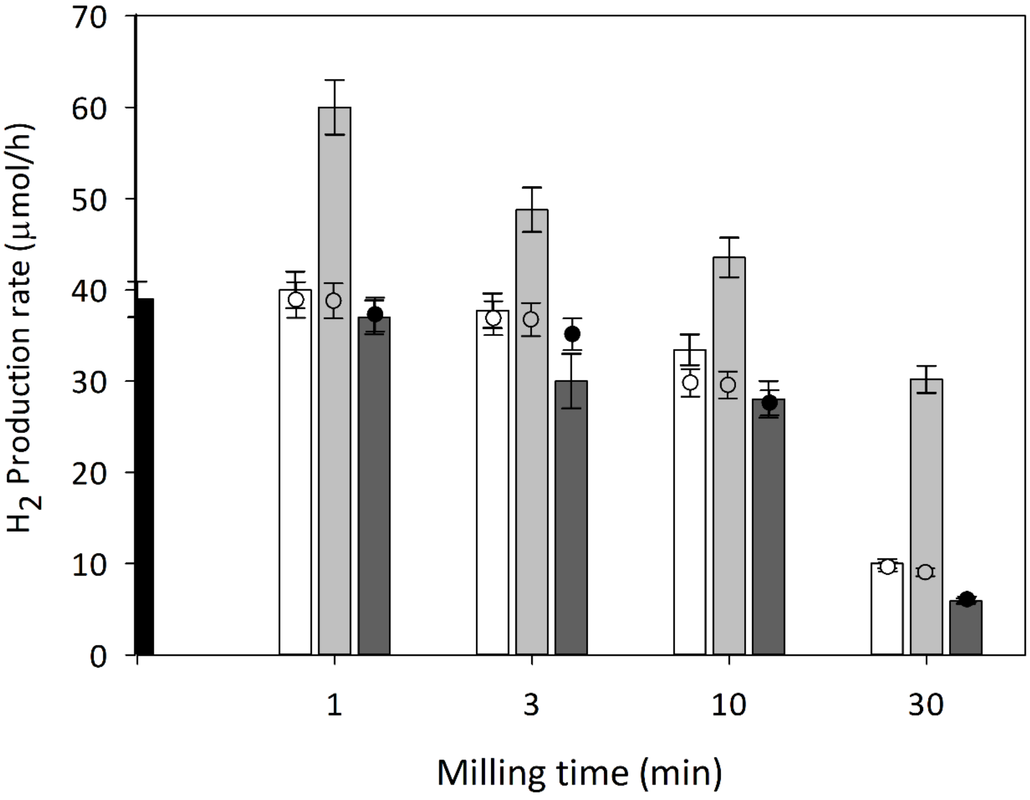

Figure 31. Hydrogen production after 5 hours of reaction at varying the operative variables during the preparation of the photocatalyst. Experimental conditions: [Methanol]=2.5 M; V=0.30 L; T=35 °C; P=1atm; pH≈8.5; C_{cat}(ppm) = 1000 ppm; Cu_2O percentage in TiO_2 = 1% wt.

Milling rotation rate (rpm): (empty bars) 100; (light grey bars) 200; (grey bars) 500. Comparison with a simple manual mixed composite material (Full black bar). Data predicted through the regression model, at varying milling rotation rate (rpm): (○) 100; (●) 200; (●) 500.

5.2.4.3. Effect of calcination

To evaluate the possibility to improve the efficiency, in terms of hydrogen production, of the best identified photocatalyst prepared through the ball milling, a calcination of the photocatalytic powder was carried out, as reported in the materials and methods section.

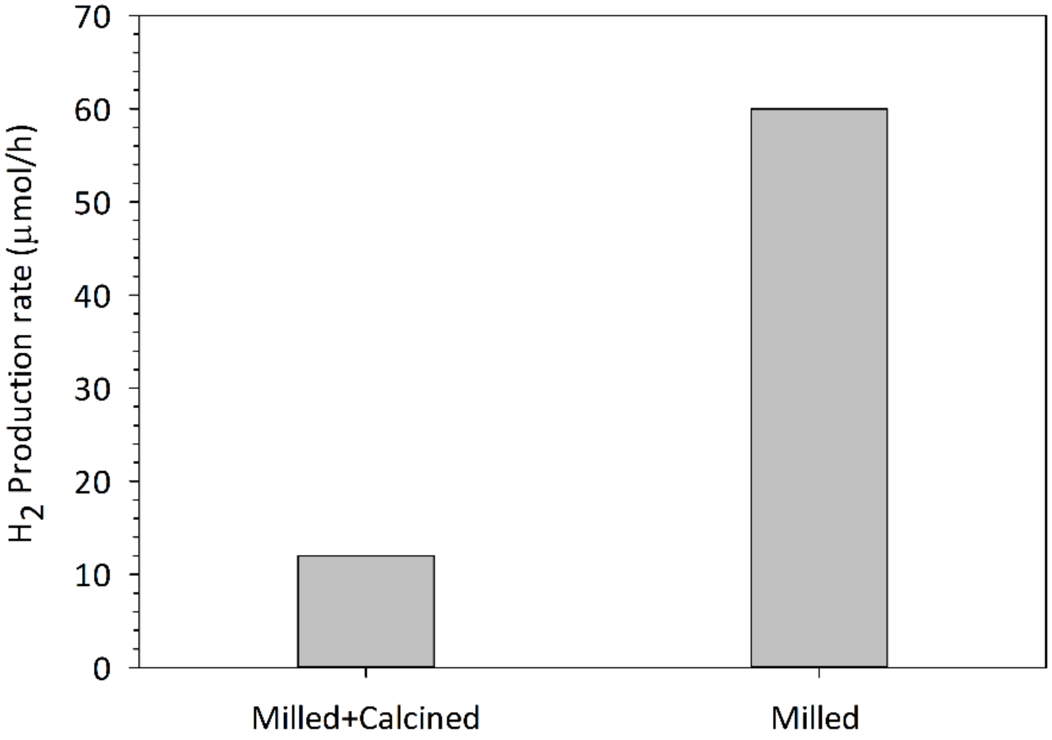

Figure 32. Comparison between the hydrogen production after 5 hours of irradiation in presence of the best photocatalyst analysed calcined under nitrogen atmosphere or used as prepared. Experimental conditions: [Methanol]=2.5 M; V=0.30 L; T=35 °C; P=1 atm; pH≈8.5; Cu_2O percentage in TiO_2 = 1% wt.; Milling time: 1 min; Rotation rate (rpm): 200 rpm. Calcination temperature: 500°C; Calcination time: 2 hrs.

In Figure 32 the comparison, in terms of hydrogen production rate, in the case of the best simple milled photocatalyst and of the same material for which a calcination under nitrogen conditions was performed, are reported. As clearly shown by the diagram, the photocatalytic activity resulted about six times lower in the case of the calcined material with respect to the simple milled material. The reason may be probably ascribed to some modification occurred during the calcination, as reported by others [229]. The Figure 33 displays the XRD pattern of as prepared and calcined Cu_2O/TiO_2 composite.

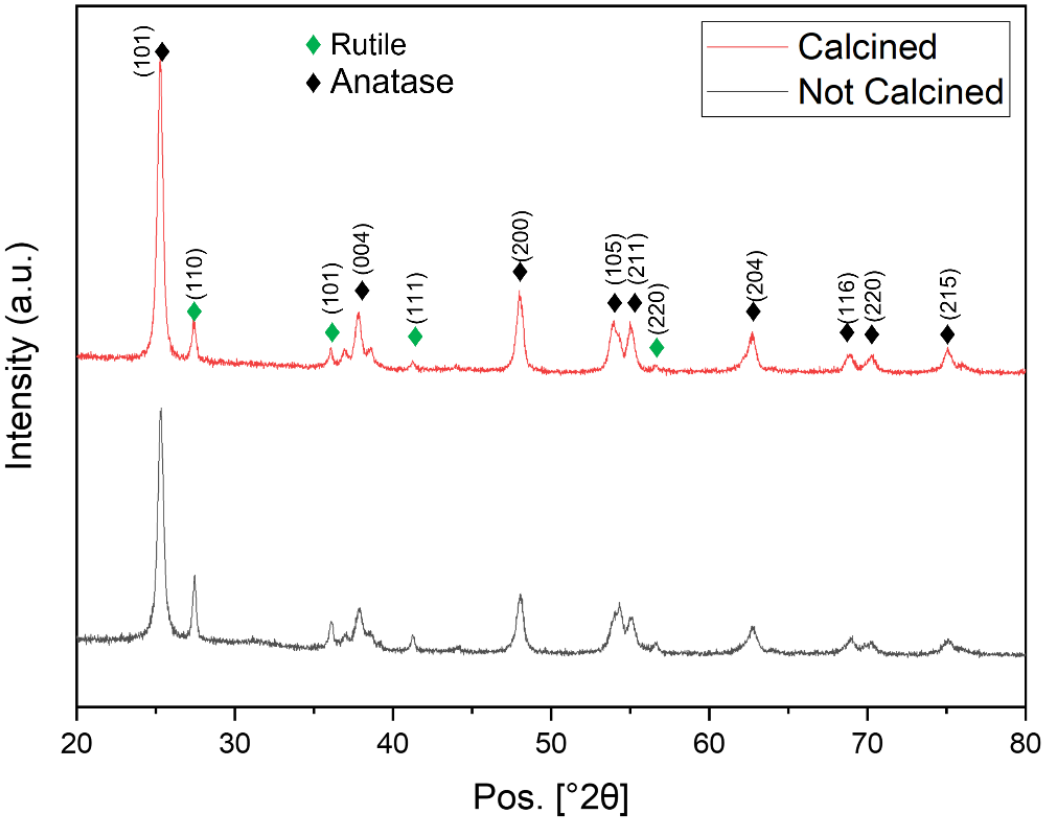

Figure 33. XRD patterns of the 1% Cu_2O – TiO_2 composite materials prepared through ball milling (1 min, 200 rpm) not calcined (black line) and calcined (red line).

Calcination seems to improve the crystallinity and strengthening of anatase TiO_2 along with the crystal sizes, as shown by the diffraction peaks, which become sharper and stronger [228,230]. On contrary, the broadening of the diffraction peak for the rutile phase, probably indicated the creation and accumulation of lattice defects, which can reduce the photocatalytic activity of the material.

5.3. Summary

Photocatalytic hydrogen generation under visible light conditions was preliminary studied in presence of a manually mixed Cu_2O/TiO_2 photocatalyst, starting from commercial TiO_2 and Cu_2O. The produced hydrogen resulted about 3 – fold higher than that obtained using bare TiO_2. Based on this observation, ball milling method was adopted as photocatalyst preparation. Firstly, the effect of the sacrificial agent used is evaluated, recognizing glycerol as the best candidate to produce hydrogen among the tested organics.

Moreover, for a good characterization of the catalysts, it was necessary to consider that three variables could affect the structure of the catalyst, namely the percentage of Cu_2O, the milling time and the rotation speed of the miller. To identify, with a minimum number of runs, the influence of that factors on photocatalytic hydrogen production, a two-level factorial design approach was used. Based on the results of this investigation campaign, 1% wt. of Cu_2O with respect to TiO_2 was chosen to analyze the system behavior, and the best hydrogen production (about 60 µmol/h) was obtained with a milling time of 1 minute and rotation rate of 200 rpm.

6. Results II. Investigations on the best performing photocatalyst

6.1. Introduction

The results of the analysis reported in the Results I allowed the identification of the best photocatalyst that can be prepared for hydrogen generation by mixing Cu_2O and TiO_2 (i.e., 1%wt. Cu_2O in TiO_2 photocatalyst material prepared through ball milling method at rotation rate of 200 rpm and milling of 1 min). To characterize this material, the effect of the catalyst load and the organic concentration, chosen methanol as sacrificial agent, were evaluated. Additionally, to evaluate the best performance achievable by the system the effect of temperature in the presence of methanol and glycerol as sacrificial agents was estimated; moreover, the quantum yield and the light – to – chemical energy calculations were performed. Finally, being the aim of the present work the development of a visible light active photocatalytic system, the possibility of using it by exploiting the solar light was evaluated.

6.2. Results and discussion

6.2.1. Effect of catalyst load

A first attempt to characterize this catalyst was carried out exploring the effect of the catalyst load on hydrogen production. In Figure 34 the data collected during a set of runs at varying the catalyst load are shown.

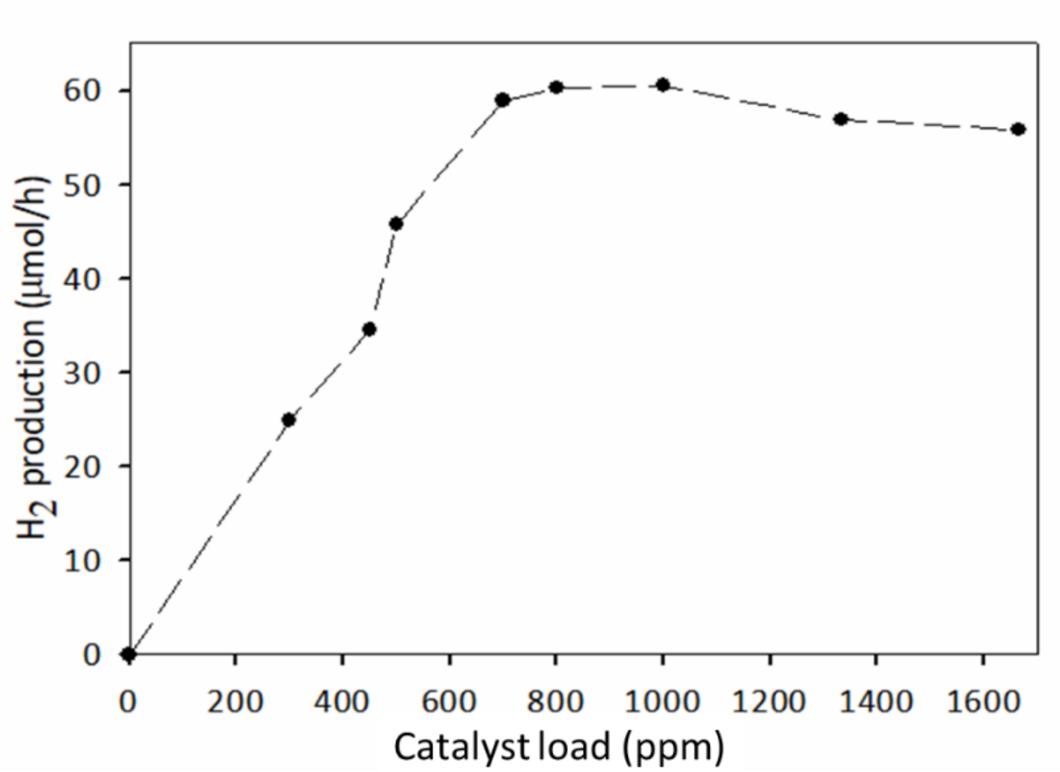

Figure 34. Hydrogen production rate at varying the catalyst load. Experimental conditions: [Methanol]=2.5 M; V=0.30 L; T=35 °C; P=1 atm; pH≈8.5; Cu_2O percentage in TiO_2 = 1% wt.; milling time: 1 min; rotation rate (rpm): 200 rpm.

As expected, from the experimental data it was possible to identify the existence of a range of loads in which the hydrogen production linearly increases with it. In the present case, this behavior was observed up to 1000 ppm of photocatalyst load. Beyond this value, a slight decrease of hydrogen production was observed, probably due to some scattering effects exerted by the photocatalyst particles on incident radiation and/or a partial sedimentation of the particles in the aqueous mixture.

6.2.2. Effect of organic concentration

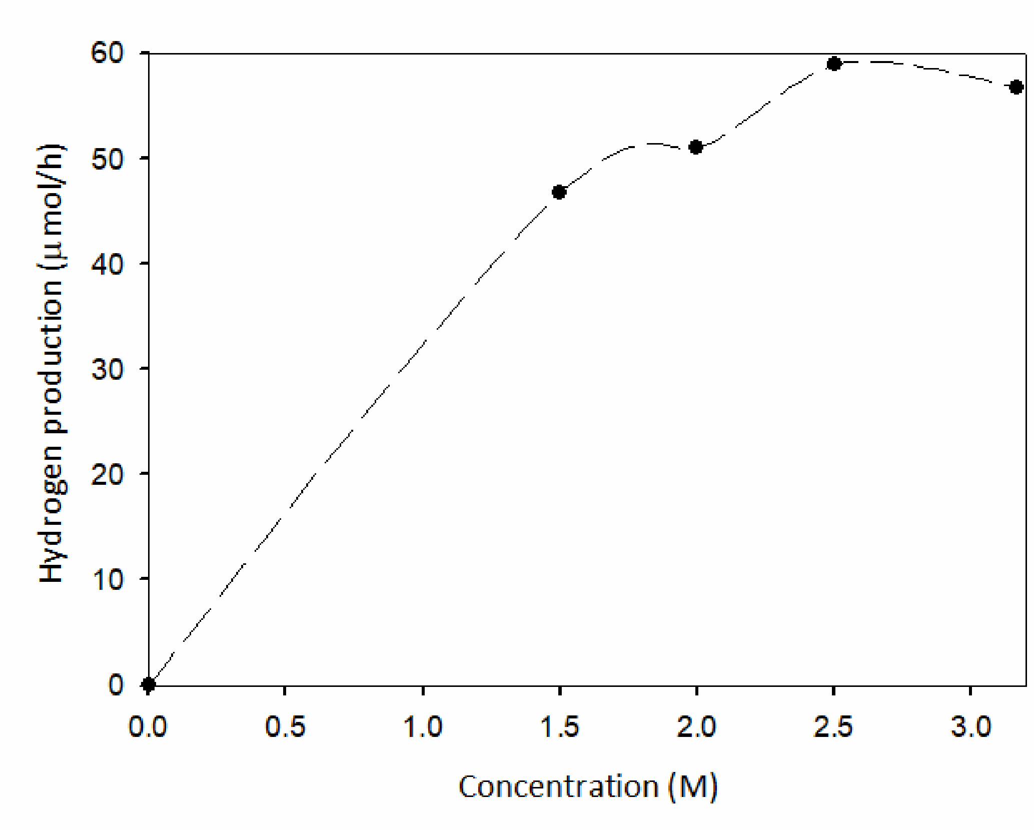

Figure 35. Hydrogen production rate at varying the organic concentration (methanol). Experimental conditions: [Catalyst]=700 ppm; V=0.30 L; T=35 °C; P=1 atm; pH≈8.5; Cu_2O percentage in TiO_2 = 1% wt.; milling time: 1 min; rotation rate (rpm): 200 rpm.

In the Figure 35 hydrogen production rates recorded during photocatalytic runs at varying methanol concentration are reported; from the figure it is clear that the organic species are adsorbed according with the Langmuir-Hinshelwood model.

The concentration of the adsorbed species may be obtained through the equilibrium reaction r.10 and the equation eq. 5, in which K_{ads} (M^{-1}) is the adsorption equilibrium constant, and C_t (M) is the total concentration of active sites on the catalyst surface for a fixed catalyst load q (g/L).

$$CH_3OH + C_t \overset{K_{ads}}{\longleftrightarrow} CH_3OH_{ads} \qquad \text{r. 10}$$

$$K_{ads} = \frac{[CH_3OH_{ads}]}{C_t[CH_3OH]} \qquad \text{eq. 5}$$

The term C_t was calculated through the following equation (eq. 6):

$$C_t = N \cdot q \qquad \text{eq. 6}$$

where N is the total moles of active sites per unit mass of catalyst (mol/g).

To obtain a value of the adsorption constant (K_{ads}) for methanol over Cu_2O/TiO_2 composite photocatalyst, a Langmuir – Hinshelwood – type model expressing hydrogen generation rate was adopted (eq. 7):

$$r_{H_2} = k' \frac{K_{ads}[CH_3OH]}{1 + K_{ads}[CH_3OH]} \qquad \text{eq. 7}$$

where k' and K_{ads} are the apparent kinetic constant of substrate oxidation and the organic adsorption constant, respectively.

An optimization procedure based on the comparison between data reported in Figure 35 and data calculated through equation eq. 7 allowed to estimate the adsorption constant of the organic species on the catalyst surface. A value of 0.967 M^{-1} was obtained in the presence of the best photocatalyst tested in the present work.

6.2.3. Effect of temperature

Is well known that the photocatalytic activity is poorly influenced by the temperature, being the electron – hole generation dependent on the radiation intensity. However, the temperature may be used to improve the photocatalytic activity, being able to increase the reaction rate, to improve the desorption of the products on the catalyst surface as well as to provide a higher electron transfer in valance band to higher energy levels [231]. Thus, it facilitates the electron – hole formation that could be utilized in initiating oxidation and reduction reactions, respectively, and helps the reaction to compete more effectively with the recombination of the charge carriers, as reported by different authors [232,233]. For this reason, some experimental runs were performed at varying the temperature of the suspension between 25°C and 80°C, in presence of methanol and glycerol as sacrificial agents.

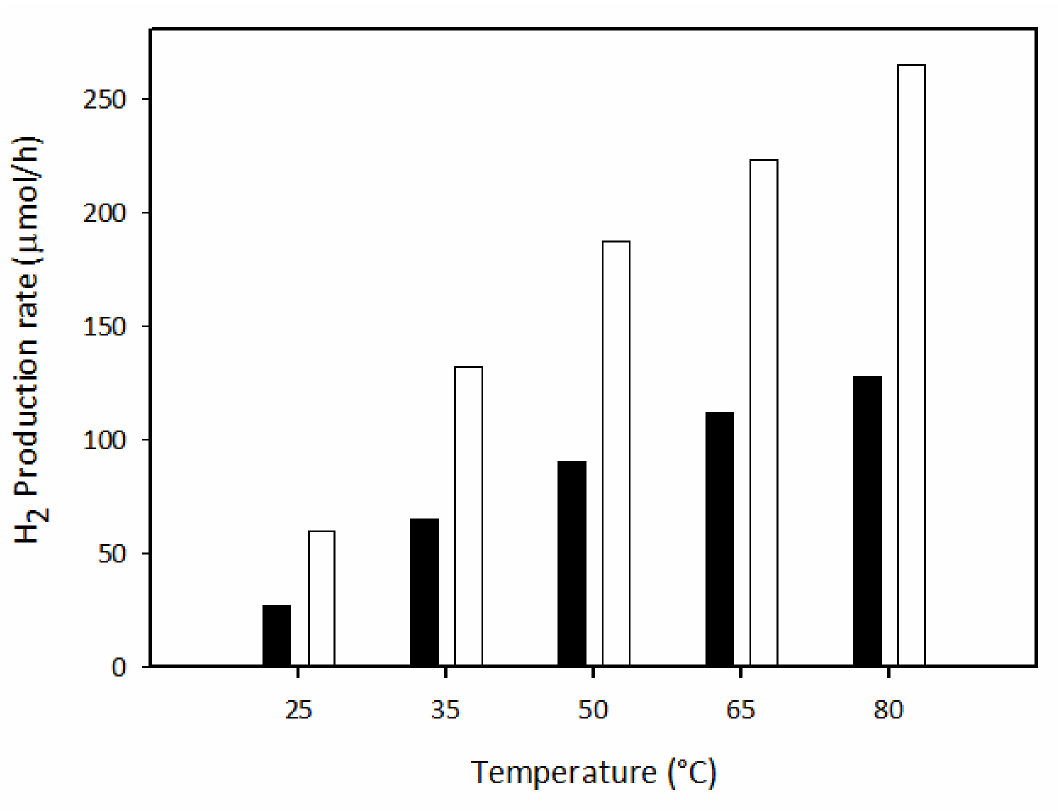

Figure 36. Hydrogen production rate at varying the temperature of the system. Experimental conditions: [Catalyst]=1000 ppm; V=0.30 L; P=1 atm; pH≈8.5; [Organic] = 2.5 M; Cu_2O percentage in TiO_2 = 1% wt.; milling time: 1 min; rotation rate (rpm): 200 rpm; visible range. (■) Methanol; (□) Glycerol.

The main results are reported in the Figure 36; as clearly sown by the diagram, when the temperature passes from 25°C to 80°C, hydrogen production rate achieves a value about 4.5 times higher than that obtained at the lowest temperature, thus demonstrate the positive effect of temperature on the system.

6.2.4. Effect of pH

As reported in the previous section, some authors have noticed a considerable influence of the pH of the suspension on the photocatalytic hydrogen generation [224]. To evaluate the effect of this variable on the photoactivity, several runs, at varying the pH of the solution in which the catalyst is dispersed, were carried out.

In the Figure 37, where the mean hydrogen production rate collected at different pH values are reported, a higher reactivity may be recognized under alkaline conditions.

The results may be probably ascribed *(i)* to the higher stability of the copper species on the surface of TiO_2 particles under alkaline conditions, as reported by others [162], *(ii)* to the fundamental properties of both the sacrificial agent (i.e., methanol) and the composite photocatalyst: in particular, methanol is protonated, being its pKa about 15.0, while the photocatalyst surface is positively or negatively charged depending on the pH value; at increasing the pH of the suspension, a higher concentration of negative charges is localized on the catalyst surface, resulting in a more efficient adsorption of the organic compound, as well as in an improved photocatalytic activity.

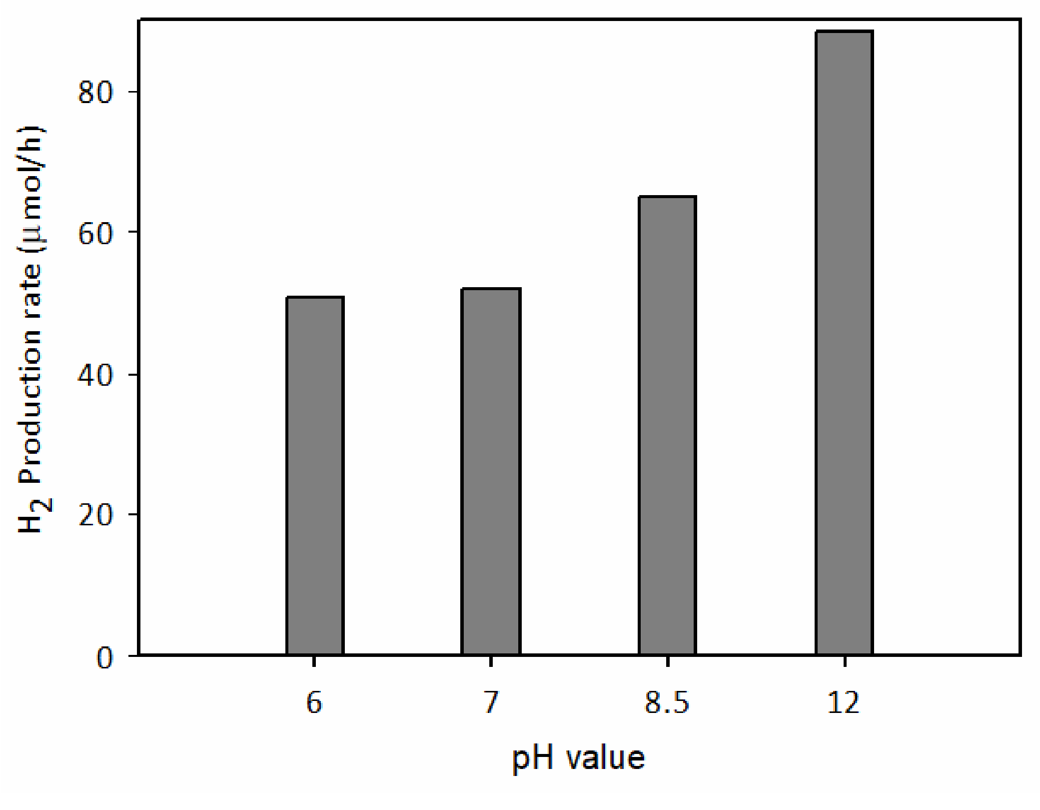

Figure 37. Hydrogen production rate at varying the pH of the suspension. Experimental conditions: [Catalyst]=1000 ppm; V=0.30 L; P=1 atm; T=35°C; [Organic] = 2.5 M; Cu_2O percentage in TiO_2 = 1% wt.; milling time: 1 min; rotation rate (rpm): 200 rpm; visible range.

6.2.5. Quantum yield and light-to-chemical energy efficiency calculation

To make easier the comparison of the results of the present investigation with those reported by others, the apparent quantum efficiency (AQE) and the light – to – chemical energy efficiency (η) were calculated on the data collected on the best photocatalyst (eq. 8 – eq. 9):

$$\text{AQE (\%)} = \frac{2 \cdot r_{H_2}}{\text{moles of incident photons/time}} \cdot 100 \qquad \text{eq. 8}$$

$$\eta = \frac{r_{H_2}\,(-\Delta H^0_{comb})}{I \cdot S} \qquad \text{eq. 9}$$

Where:

- r_{H_2} (mol·s^{-1}) is the hydrogen production rate;
- ΔH^0_{comb} is the standard enthalpy change for the combustion reaction between oxygen and hydrogen ($-$ 282.0 · 10^3 J/mol);
- I (W·cm^{-2}) is the specific irradiance of the light source;
- S (cm^2) is the irradiated area.

Table 6. Mean hydrogen production rate, apparent quantum efficiency, and light to chemical energy efficiency obtained using a manually mixed catalyst (Cu_2O% in TiO_2= 1% wt.) and the milled catalyst (best conditions: Cu_2O% in TiO_2= 1% wt.; Milling time = 1 min; rotation rate = 200 rpm) under visible (λ>400 nm) and UV-A + Visible light conditions.

Experimental conditions	Mean hydrogen production (μmol/h)	AQE(%)	η(%)
Manually mixed; T=35°C; P=1 atm; pH≈8.5; C_{cat} (1%wtCu_2O-TiO_2)=1000 ppm; [Methanol]=2.5 M; visible light conditions	38	0.96	0.35
Milled catalyst (1 min, 200 rpm); T=35°C; P= 1 atm; pH≈8.5; C_{cat} (1%wtCu_2O-TiO_2)=1000 ppm; [Methanol]=2.5 M; visible light conditions	60	1.51	0.60
Milled catalyst (1 min, 200 rpm); T=35°C; P= 1 atm; pH≈8.5; C_{cat} (1%wtCu_2O-TiO_2)=1000 ppm; [Methanol]=2.5 M; UV+visible light conditions	253	2.31	0.83
Milled catalyst (1 min, 200 rpm); T=80°C; P= 1 atm; pH≈8.5; C_{cat} (1%wtCu_2O-TiO_2)=1000 ppm; [Methanol]=2.5 M; visible light conditions	128	3.17	1.14
Milled catalyst (1 min, 200 rpm); T=80°C; P= 1 atm; pH≈8.5; C_{cat} (1%wtCu_2O-TiO_2)=1000 ppm; [Glycerol]=2.5 M; visible light conditions	264	6.54	2.36

In table 6 the most significant results are reported. Using a high – pressure Hg lamp, a maximum AQE under visible light radiation of 1.61% was calculated in presence of Cu_2O(1%wt.)/TiO_2 composite prepared through ball milling method (200 rpm, 1 min), when the temperature of the system is about 35°C. In the same conditions, a maximum light – to – chemical energy efficiency value of 0.60% was obtained.

These are more than 1.5 – fold higher than that obtained in presence of the manually mixed material with identical composition (about 1%, about 0.35%, respectively), and only about 1.4 – fold lower than the maximum efficiencies obtained under the same conditions using UV – A + Visible light radiation (about 2.3% and 0.8%, respectively). In fact, as reported in the table, despite the large difference between hydrogen production rate obtained with and without UV – A radiation, the different light intensities induced rather similar activities in terms of quantum yield and light – to – chemical energy efficiency.

Moreover, it is interesting noticing that these values are 2 – fold higher when the temperature of the system is about 80°C, and 4 – fold higher when, at 80°C, glycerol is used as scavengers.

6.2.6. Photocatalyst recycling

For a complete characterization of the behaviour of the selected photocatalyst, the photostability of the material and the possibility of recycling it in successive runs were evaluated and the results are presented in Figures 38, where the produced hydrogen amount (Figure 38 (a)) and the hydrogen production rate (Figure 38 (b)) are reported. First, a set of three repeated runs (empty symbols) was carried out on the same aliquot of photocatalyst, each one lasting for about 5 hours. At the end of the run 1 and 2, the photocatalysts was separated, recovered, and weighed before its reuse. As it is clear from the diagrams, in the second run (open triangles) a lower productivity with respect to that recorded in the first one (open circles) was observed, and the same trend was recorded between the third (open squares) and the second run, thus indicating a reduction of the reactivity. To understand the reasons for this behaviour, a second aliquot of the photocatalyst was used in a run carried out for 10 hours (full circles in Figures 38).

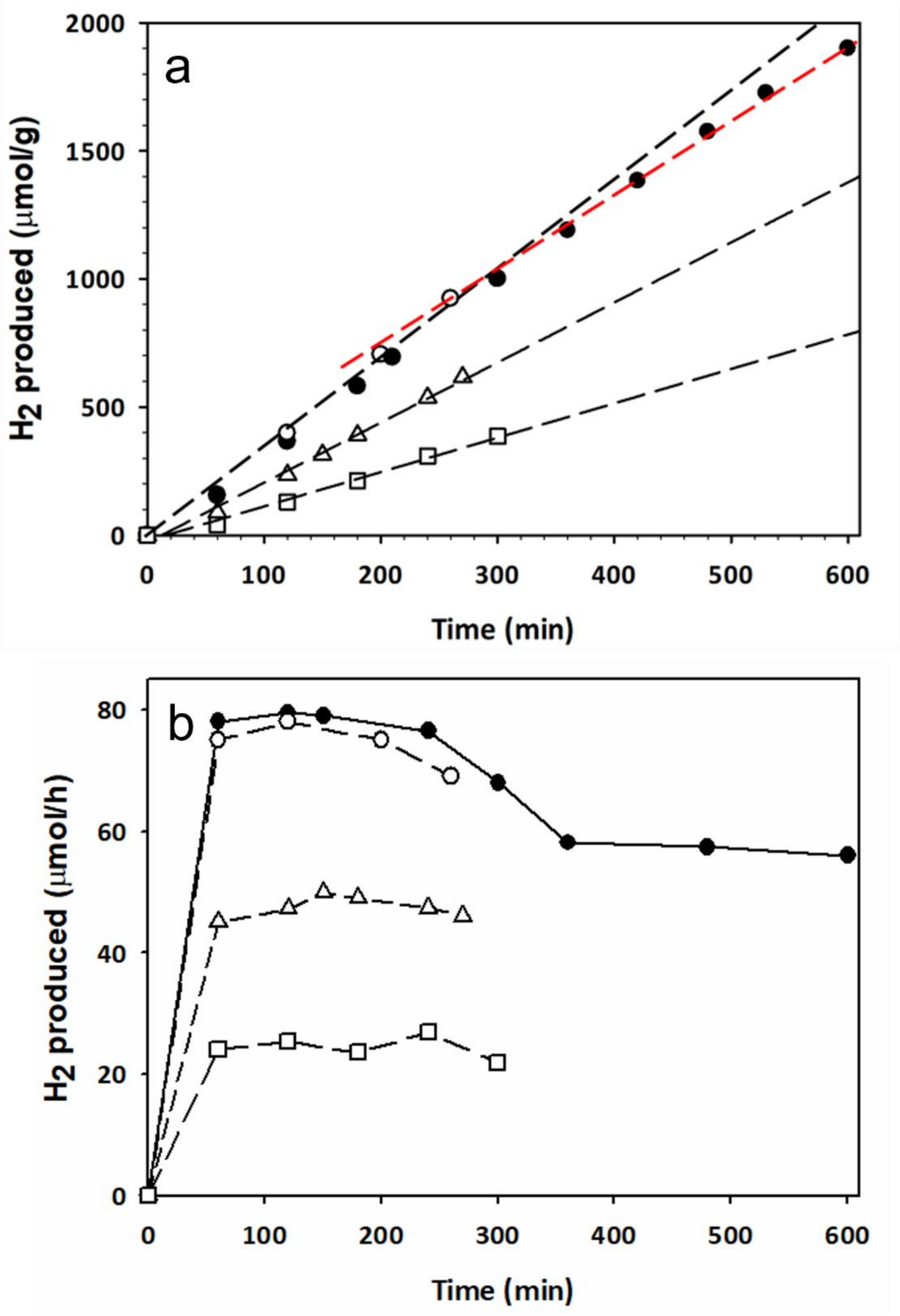

Figure 38. (a) Produced hydrogen amount and (b) mean hydrogen production rate during a single run (●) and 3-runs by using the recovered material: (○) first cycle; (Δ) second cycle; (□) third cycle. Experimental conditions: [Methanol]=2.5 M; V=0.30 L; T=35 °C; P=1 atm; pH≈8.5; Cu_2O percentage in TiO_2 = 1% wt.; Milling time: 1 min; Rotation rate (rpm): 200 rpm.

The data collected during the first five hours of this new run were consistent with those recorded at the beginning of the first set of investigation (open and full circle). Notably, only a moderate reduction of hydrogen productivity was recorded extending the reaction time between 5 and 10 hours, as indicated by the slope in the Figure 38 (a), indicating a good photostability of the composite catalyst during a single photoreforming experiment. On the other hand, the same data suggest that some physico – chemical modifications in the photocatalyst composition should happen, especially during its separation and recovery.

An attempt to explain this phenomenon may be done by considering *(1)* the formation of zerovalent copper on the TiO_2 surface during the reaction, as confirmed by the TEM and TEM/EDX measurements on the recovered samples reported in the Figure 28 and Table 5, respectively (See appendix A for the EDX spectra), *(2)* the FT-IR measurements, reported in the Figure 39, in which the occurrence of an OCO asymmetric and symmetric stretching vibration was detected in the recovered samples, probably due to the presence of adsorbed species not fully eliminated during the recovery of the material, which irreversibly modify the photocatalyst and *(3)* the XRD measurements (Samples R/T in Table 4), in which an increase in the crystallite size of the material is detected, probably due to the nanoparticle agglomeration occurred during the recovery of the material.

As for the point *(1)*, the reduction of Cu^{1+} to Cu^0 following the reaction r.8 was considered by some authors as a possible reason for the decrease of hydrogen productivity [113,224,227]; a successive reoxidation of the metallic copper (See r.9), and the achievement of an equilibrium condition between the two species, were also proposed, confirming the trend observed between 5 and 10 hours during the single run (full symbols in the Figures 38). Moreover, the TEM/EDX results show an increase in the Cu to O ratio after the reaction. The higher content of Cu after the reaction is indicative of the diffusion of Cu from the bulk of the photocatalyst to the surface. Excess metallic Cu (Cu^0) on the surface of the catalyst may act as a recombination center and block the light absorption. Thus, a high Cu^0 content would be detrimental to the photocatalytic activity. These results may also help to explain the lower hydrogen yields obtained as the Cu_2O content was increased, as reported in the section 5.2.5. The higher the Cu_2O content, the higher the Cu^0 on the surface and the lower the hydrogen yield.

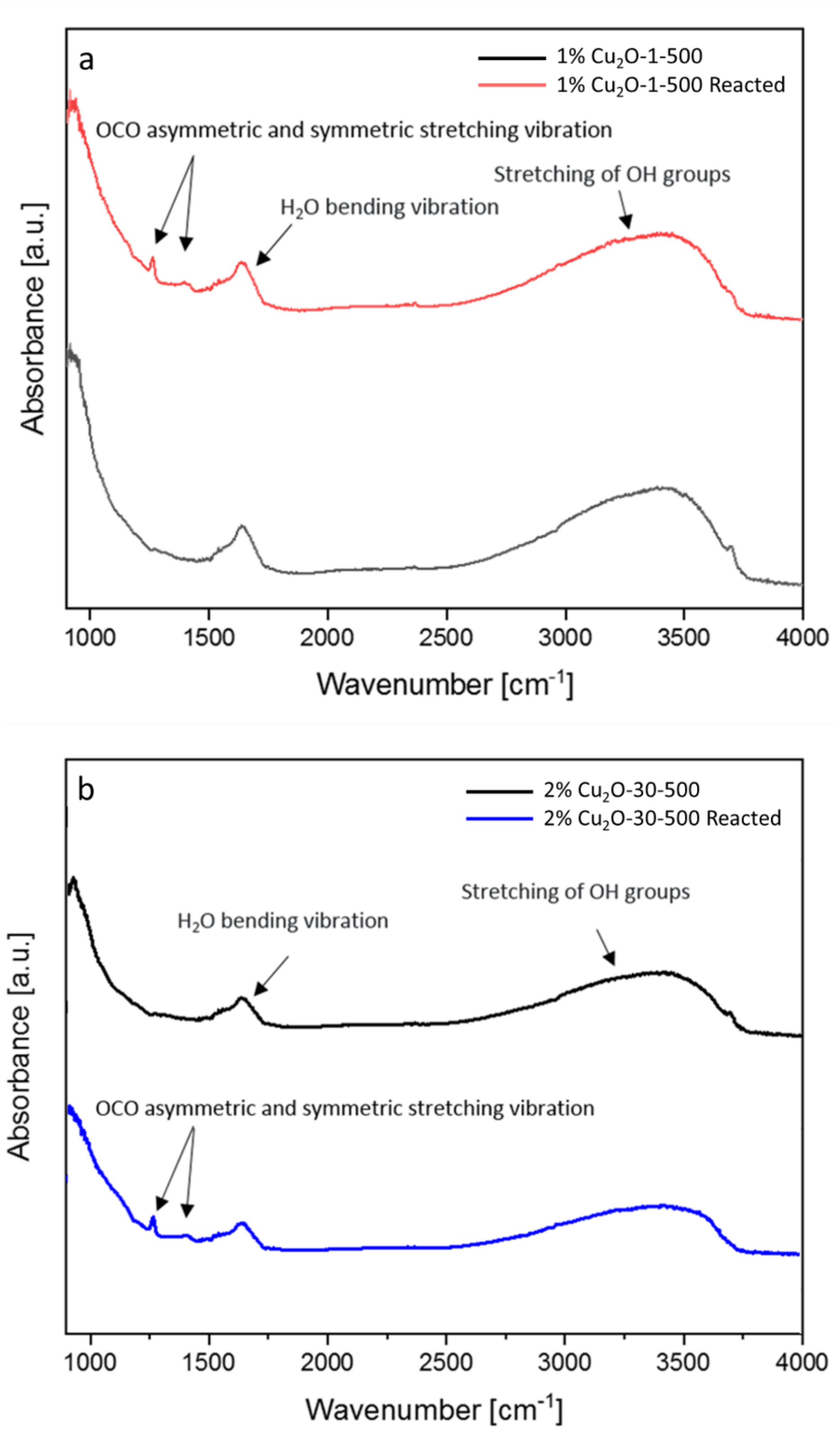

Figure 39. (a) FTIR spectra of 1%Cu_2O-TiO_2 photocatalyst prepared through ball milling (1 min, 500 rpm), before and after the reaction; (b) FTIR spectra of 2%Cu_2O-TiO_2 photocatalyst prepared through ball milling (30 min, 500 rpm), before and after the reaction.

6.2.7. Photocatalytic activity under solar conditions

To conclude the experimental campaign of the present project, a set of experiments were performed under direct solar radiation using the apparatus shown in the Material and methods section (Figure 11 (c)). The runs were carried out in the early September 2021 in Naples, between 11.00 and 13.00 hours under clear sky conditions. To evaluate the contribution of the UV and visible radiations in the hydrogen production, some photocatalytic runs, in which a cut – off filter was adopted to eliminate the radiation under 400 nm ($NaNO_2$ 0.5 M, see Materials and methods section), were carried out.

In the Figure 40 the main results from the photocatalytic runs conducted under solar radiation are reported.

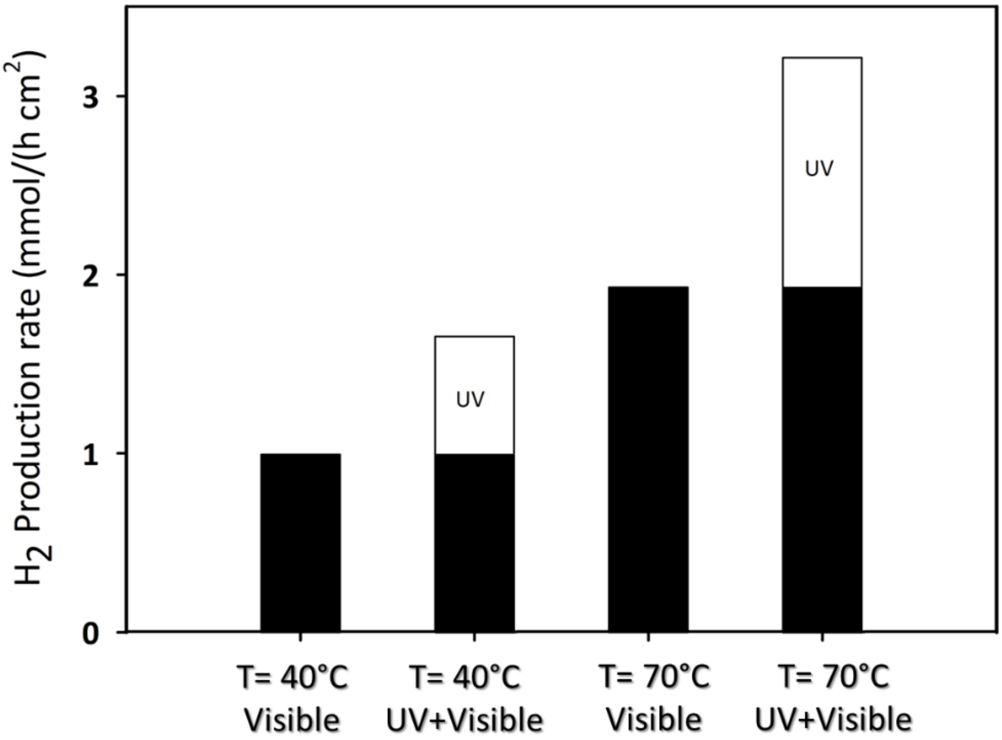

Figure 40. Hydrogen production rate during experimental runs conducted under solar radiation. Experimental conditions: [Catalyst]=1000 ppm; V=0.30 L; P=1 atm; pH≈8.5; [MeOH] = 2.5 M; Cu_2O percentage in TiO_2 = 1% wt.; Milling time: 1 min; Rotation rate (rpm): 200 rpm.

The hydrogen production rate was about 1 mmol/(h·cm^2) when the temperature is about 40°C and the suspension was submitted only to visible light irradiation. The hydrogen generation increases of about 1.6 – fold when the total solar spectrum is used. The result indicated that the contribute of the visible light represents about 3/5 of the hydrogen production under solar radiation, while the improvement in terms of hydrogen generation obtained without any cut – off filter may be ascribed to the UV contribute. Moreover, the hydrogen production rate achieves a value of about 3 mmol/h·cm^2 when the temperature was increased at 70°C, thus confirming the positive effect of this variable on the photocatalytic activity.

The efficiencies of the catalytic system adopted in the present investigation for hydrogen generation were calculated using the data for irradiation collected during the experimental runs. The ranges of irradiation considered are 315 – 400 nm and 380 – 550 nm, where the mean values of the specific irradiance were about 15.56 W/m^2 and 95.75 W/m^2, respectively.

Based on that reported above, in the Table 7 the values of the light – to – chemical energy efficiency are reported. A value of about 6.5% was obtained considering the contribution of the UV range when the temperature was about 70°C. As for the light to chemical energy efficiency in the total solar range, the low calculated values have to be related to the overestimation of the specific irradiance collected under the visible range (380 – 550 nm): in fact, wavelength higher than about 420 nm should be neglected, due to the bandgap value of about 3 eV of the composite, to which correspond the activation of the photocatalyst at a wavelength lower than that above – mentioned.

Table 7. Mean hydrogen production rate and light to chemical energy efficiency (in the UV and total solar range) obtained using the milled catalyst (best conditions: Cu_2O% in TiO_2= 1% wt.; Milling time = 1 min; rotation rate = 200 rpm) under solar conditions.

Experimental conditions	Mean hydrogen production (μmol/h)	η(%) in the UV range	η(%) in the total solar range
Milled catalyst (1 min, 200 rpm); T=40°C; P= 1 atm; pH≈8.5; C_{cat} (1%wtCu_2O-TiO_2)=1000 ppm; [Methanol]=2.5 M; Solar light	331	3.33	1.16
Milled catalyst (1 min, 200 rpm); T=70°C; P= 1 atm; pH≈8.5; C_{cat} (1%wtCu_2O-TiO_2)=1000 ppm; [Methanol]=2.5 M; Solar light	642	6.47	2.22

6.3. Summary

The evaluation of the photocatalytic activity of the best performing material at varying the organic concentration allows the identification of an adsorption equilibrium constant of 0.967 M^{-1}. As for the temperature, a great positive effect was recorded, showing a hydrogen productivity about 4.5 – fold higher than that obtained at the lowest temperature; the alkaline conditions have also demonstrated to have a positive effect on the photocatalytic hydrogen generation. In terms of efficiency, the apparent quantum efficiency and the light – to – chemical energy efficiency values calculated, at 35°C, in the presence of the best tested photocatalyst were equal to 1.51% and 0.6%, respectively; these values resulted about 1.5 – fold higher than that obtained in presence of the manual mixed material; moreover, values of about 6.5% and 2.36% were obtained when glycerol was used as scavengers and the temperature of the system was about 80°C. Finally, under solar conditions, the maximum hydrogen production rate obtained was about 642 micromoles/h when the medium temperature of the suspensions was about 70°C and the mean UV and visible irradiance values were respectively 15 and 95 W/m^2; this value was about 5 – fold higher than that collected under simulated solar conditions (with high pressure mercury lamp – see materials and methods section).

7. Results III. Kinetic modeling of H_2 production over Cu_2O/TiO_2 catalyst through photoreforming of methanol

7.1. Introduction

In the previous sections, the photocatalytic hydrogen generation from different sacrificial agents in presence of Cu_2O/TiO_2 composite material – prepared through ball miller – was investigated. The development of a suitable mathematical model capable of simulating the hydrogen production over the same catalyst (Cu_2O/TiO_2 composite material), when methanol was adopted as sacrificial agents, is herein presented.

7.2. Kinetic model

Based on previous literature findings, a reaction network was proposed to develop a simple suitable kinetic model able to simulate the photocatalytic system behaviour at varying the organic concentration and the catalyst load. At least in principle, it was chosen to develop the model using the data collected on the best tested photocatalyst ((1%wt) Cu_2O/TiO_2, milling time = 1 min, rotation rate = 200 rpm). Moreover, as discussed in the Section 6.2.6., during the photocatalytic run a decrease of hydrogen productivity was recorded, due to the reduction of Cu^{1+} to Cu^0 following the reaction r.8; then, a successive reoxidation of the metallic copper was assumed, and the achievement of an equilibrium between Cu^{1+} to Cu^0 was also proposed, thus confirming the trend observed after 5 hours of irradiation (See Figure 38). Based on these considerations, it was chosen to analyze the photocatalytic activity using the data collected after 5 hours of irradiation, being at this time reasonably the catalyst form stabilized. To simplify the analysis, the following hypothesis were done:

I. It was chosen to consider the (1%wt) Cu_2O/TiO_2 composite material as a single photocatalyst, with a single quantum yield ϕ and a single recombination rate constant k_r;

II. The adsorption of the organic could be considered only on TiO_2 surface, on which the photooxidation occurs. Even if a moderate adsorption may occur on

Cu_2O, the position of the valence band of this semiconductor with respect to the redox potential couple for the methanol oxidation does not allow the oxidation of the organic; the decrease of hydrogen generation for increasing the percentage of cuprous oxide, discussed in the Section 5.2.5, is consistent with the hypothesis.

III. It was chosen to analyze the system at pH of about 8.5. In this condition, as reported in the section 6.2.4, methanol is protonated; as for the photocatalyst surface, similarly to the P25, at the pH=8.25 it may be considered negatively charged.

IV. The adsorption phenomena occur following a Langmuir – Hinshelwood mechanism, as discussed in the Section 6.2.2.

In the first step the electron – hole pairs are generated under visible light irradiation of the composite material, following the reaction r.11; the reaction depends on the photon adsorption by the photocatalyst in the visible light range.

$$Cu_2O/TiO_2 \overset{h\nu}{\rightarrow} Cu_2O/TiO_2(h^+) + Cu_2O/TiO_2(e^-) \qquad \text{r. 11}$$

The electron – hole pairs may recombine through radiative and/or non – radiative processes, producing light and heat (See r. 12), following a second – order kinetic law, where k_r is the electron – hole recombination rate constant.

$$Cu_2O/TiO_2(h^+) + Cu_2O/TiO_2(e^-) \overset{k_r}{\rightarrow} Q + \text{light} \qquad \text{r. 12}$$

The organic species used as sacrificial agent (i.e. methanol), adsorbs on the catalyst surface forming a monodentate complex (r. 13), following a Langmuir – Hinshelwood model with K_{ads} representing the adsorption equilibrium constant for methanol; then, the adsorbed species may react with the photogenerated holes producing protons and oxidation by – products, following the r. 14, in which k_{h^+} represents the kinetic constant associate to the oxidation of the organic; despite the oxidation by – products may react with the photogenerated holes, the reactions will be neglected due to the high concentration of methanol used.

$CH_3OH + \theta_{TiO_2} \overset{K_{ads}}{\longleftrightarrow} CH_3OH_{ads}$ r. 13

$CH_3OH_{ads} + Cu_2O/TiO_2(h^+) \xrightarrow{k_{h^+}} CH_3OH^{\bullet}_{ads} + Cu_2O/TiO_2(h^+) + H^+ \xrightarrow{Fast} P + 2H^+$ r. 14

Finally, the produced protons react with the photogenerated electrons, thus generating hydrogen gas (r. 15):

$2H^+ + 2Cu_2O/TiO_2(e^-) \xrightarrow{Fast} 2H^{\bullet} \xrightarrow{Fast} H_2$ r. 15

According to the above reported kinetic scheme, a mathematical model based on a set of mass balance equations for the main species involved in the process was developed (eq. 10 ÷ eq. 13):

$$\frac{d[h^+]}{dt} = G_{vis} - r_r - 2r_{h^+} \quad \text{eq. 10}$$

$$\frac{d[e^-]}{dt} = G_{vis} - r_r - 2r_{h^+} \quad \text{eq. 11}$$

$$\frac{d[CH_3OH]_{tot}}{dt} = -r_{h^+} \quad \text{eq. 12}$$

$$\frac{d[H_2]}{dt} = r_{h^+} \quad \text{eq. 13}$$

Where the reaction rate of the photochemical step G_{vis}, may be expressed as follow (eq. 14):

$$G_{vis} = \frac{\phi_{vis}}{V} \sum I_i^0 (1 - \exp(-2.3\, L\, \varepsilon_{vis}\, [TiO_2])) \quad \text{eq. 14}$$

And the amount of methanol $[CH_3OH]_{tot}$ is expressed as a function of the free and the adsorbed species, as follow (eq. 15):

$$[CH_3OH]_{tot} = [CH_3OH] + [CH_3OH]_{ads} \quad \text{eq. 15}$$

With:

ϕ_{vis} = quantum yield in the visible range, L = optical pathway, 1.1 cm, V = volume of the suspension, I_i^0 is the specific powers of the lamp, $E \cdot s^{-1}$ and ε_{vis}= extinction coefficient of the composite material in the visible range, 265.5 M^{-1} cm^{-1}, calculated as reported in literature [234].

Moreover, the electron – hole recombination rate and the reaction regulating the substrate oxidation, may be expressed by the eq. 16 and 17, respectively.

$$r_r = k_r[h^+][e^-] \qquad \text{eq. 16}$$

$$r_{h^+} = k_{h^+}[CH_3OH]_{ads}[h^+] \qquad \text{eq. 17}$$

As concerns the concentration of the adsorbed methanol $[CH_3OH]_{ads}$, a Langmuir – Hinshelwood is assumed, as previously discussed, which depends on the active sites (θ_{TiO_2}) of the TiO_2 catalyst, as follows (eq. 18):

$$[CH_3OH]_{ads} = K_{ads}[CH_3OH][\theta_{TiO_2}] \qquad \text{eq. 18}$$

The active sites of TiO_2 may be calculated as reported below (eq. 19):

$$[\theta]_{tot} = N_{TiO_2}[TiO_2] = \left[\theta_{TiO_2}\right] + [CH_3OH]_{ads} \qquad \text{eq. 19}$$

Where N_{TiO_2}represents the moles of active sites per unit mass of TiO_2.

By combining the eq. 18 and eq. 19, the following expression was obtained for the number of active sites of titanium dioxide (eq. 20):

$$\left[\theta_{TiO_2}\right] = \frac{N_{TiO_2}[TiO_2]}{1 + K_{ads}[CH_3OH]} \qquad \text{eq. 20}$$

The mathematical model is able to describe the evolution of the concentration with time of each species, at varying the initial operative conditions. At this purpose it is necessary to numerically solve the mathematical system, by adopting proper values of the kinetic parameters ϕ_{vis}, k_r, k_{h^+}, K_{ads}, N_{TiO_2}. The following initial conditions may be associated to the set of ordinary differential equations:

$$[h^+]_{t=0} = 0\ ;\ [e^-]_{t=0} = 0;\ [\ CH_3OH]_{tot,\ t=0} = [CH_3OH]_{tot,\,0};\ [H_2]_{t=0} = 0$$

All the kinetic parameters above indicated resulted unknown, and an iterative optimization procedure [235] was necessary to estimate them, starting from the literature information available for similar systems [212,236].

7.3. Results and discussion

As earlier discussed, according to the previous literature findings on similar systems [236] it was chosen to assume as zero – time data for modeling the photocatalytic hydrogen production rate collected after 5 hours of irradiation, being at this time reasonably the catalyst form stabilized. As for the unknown kinetic parameters (ϕ_{vis}, k_r, k_{h^+}, K_{ads}, N_{TiO_2}), it was chosen to adopt, in the current modelling, the literature information available for a similar system (Cu^0/P25 [236]) as starting values for the optimization procedure. Based on the above – mentioned starting values, Matlab software was used to solve the set of mass balance equations reported in the section 7.2 (eq. 10 ÷ eq. 13), by means of a proper numerical optimization procedure, focusing the attention on the analysis of the data collected during methanol photoreforming experiments performed at varying the catalyst load and starting concentration of the organic species (See Table 8).

Table 8. Experimental conditions used in the optimization (A – D, F – H) and validation (E) procedures. For all runs: pH=8.50; T=35°C; Cu_2O percentage = 1%wt; milling time = 1 min; rotateon rate = 200 rpm.

	Catalyst load (g/L)	**Methanol [M]**
A	0.30	2.50
B	0.45	2.50
C	0.50	2.50
D	0.70	2.50
E	0.80	2.50
F	0.70	1.50
G	0.70	2.0
H	0.70	2.50

The values of the unknown parameters were hence estimated through an iterative optimization procedure (Marquardt approach), that minimized the square of the differences between the calculated and measured data for hydrogen generation rate (objective function, eq. 21) [235]:

$$\phi = \sum_{i=1}^{l} \sum_{j=1}^{m} \sum_{k=1}^{n} (Y_{k,j,i} - C_{k,j,i})^2 \qquad \text{eq. 21}$$

in which:

- Y and C represent the calculated and experimental data,
- l, m and n are the number of experimental data recorded for each experiment, the number of the involved species and the number of the experiments used in the optimization procedure, respectively.

The development of the model allowed the identification of the following parameters (confidence interval 97%) (See Table 9):

Table 9. Values obtained for the unknown kinetic constants. Reference values adopted in the current investigation reported by Clarizia et al. [236].

Kinetic rate constants		**Reference value (Cu^0/P25)**	**Equilibrium adsorption constants**		**Reference value (Cu^0/P25)**
k_r ($M^{-1}s^{-1}$)	$8.89 \cdot 10^3 \pm 3.83 \cdot 10^2$	$3.91 \cdot 10^6$	**$K_{ads,MeOH}$(M^{-1})**	$0.967 \pm 8.17 \cdot 10^{-2}$	0.24
k_{h^+} ($M^{-1}s^{-1}$)	$2.23 \cdot 10^3 \pm 8.17 \cdot 10^1$	$1.13 \cdot 10^4$	**Active sites per unit mass of the photocatalyst**		**Reference value (Cu^0/P25)**
Quantum yield		**Reference value (Cu^0/P25)**			
ϕ_{vis}(mol ein^{-1})	$3.53 \cdot 10^{-3} \pm 1.50 \cdot 10^{-4}$	0.19	**N_{TiO_2} (mol g^{-1})**	$1.74 \cdot 10^{-5} \pm 7.58 \cdot 10^{-7}$	$3.69 \cdot 10^{-4}$

The model accuracy was evaluated by employing the results coming from the experimental runs under the conditions reported in Table 8. The comparison between the experimental results and the modelling data obtained are reported in Figure 41.

Moreover, the estimated parameters were used in a validation procedure; In particular, the model was validated by predicting the hydrogen generation rate after 5 h of irradiation in presence of a different operative condition (See E in the Table 8). As clearly shown in the Figure 41, the modelling outputs allowed to effectively predict hydrogen generation in the presence of methanol as sacrificial agent under the mentioned operating conditions.

As concerns the kinetic parameters, the electron – hole recombination rate constant results about 500 times lower than the reference value ($Cu^0/P25$), probably due to the presence of Cu_2O (the combination with TiO_2 leads a p – n heterojunction, thus (i) absorbing the radiation within the solar spectrum and (ii) increasing the photogenerated charge carriers separation, leading to higher photocatalytic efficiencies), while the reaction constant of the organic with the holes is about 10 – fold lower than that reported in literature for $Cu^0/P25$. The quantum yield results two orders lower than the value reported for the $Cu^0/P25$ under UV + Visible light radiation. Finally, as concerns the number of active sites of the photocatalyst, it results lower than the reference value (related to P25), probably due the effect of the milling on the catalyst surface: in fact, as demonstrated by XRD analyses (See Table 4 in the section 5.2.4), SEM and TEM images (See Figures 24 – 28 in the section 5.2.4), milling leads to a higher crystallite size and an agglomeration of the particles, thus reducing the sites on which the photocatalytic process occurs.

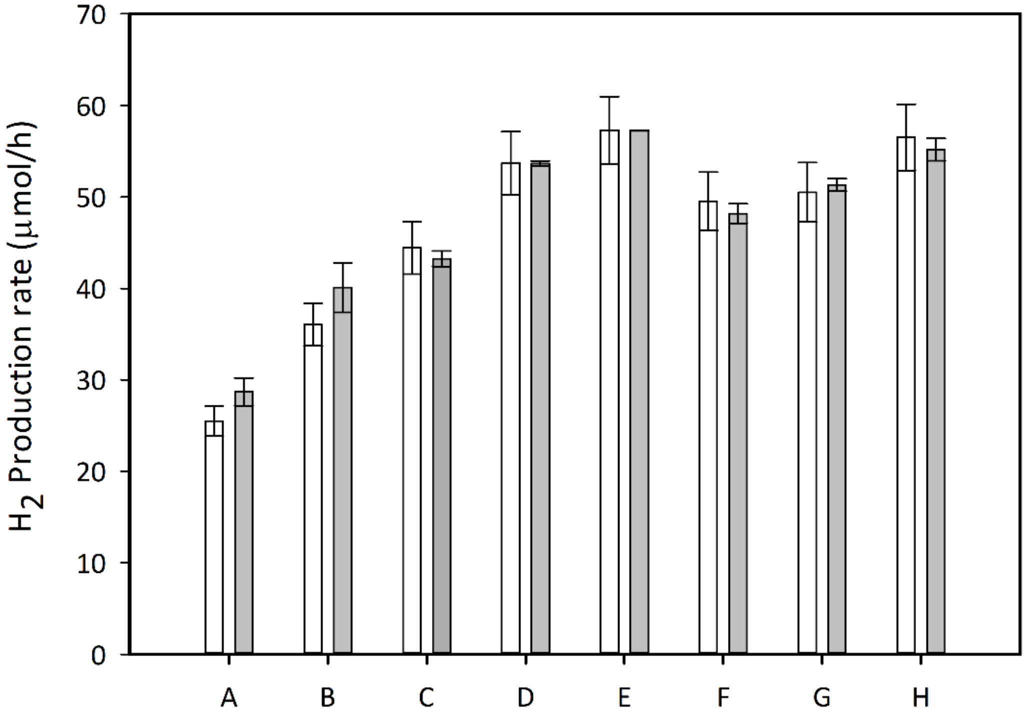

Figure 41. Comparison between experimental results (□) and data obtained through the mathematic model (■). The experimental conditions for each photocatalytic run are reported in Table 9.

7.4. Summary

Methanol was used in the photocatalytic reforming for hydrogen production on Cu_2O – TiO_2 composite material prepared through a simple mixing of the two powders by means of a ball miller. Starting from the mass balance equations for the main species involved in the photocatalytic process, a kinetic model was developed capable to simulate the photocatalytic hydrogen generation. The model was run on the data collected during the experimental campaign at various substrate concentrations and catalyst loads.

As a result, the best values of the unknown parameters were estimated, such as (*i*) the electron – hole recombination rate constant, (*ii*) the adsorption equilibrium constant, (*iii*) the reaction constant of the sacrificial species with the photogenerated hole and (*iv*) the primary quantum yield under the visible light range. Based on the estimated values, it is clear that:

(a) the electron – hole recombination rate constant results lower than that reported for the Cu^0/P25 photocatalyst, probably due to the presence of Cu_2O in the structure;
(b) the adsorption constant is comparable to that obtained for similar systems;
(c) for the first time, an indication about a quantum yield for hydrogen generation under the visible light radiation is reported.

Conclusions

In this work, a visible light active photocatalytic system aimed to hydrogen production through photoreforming of organics, based on Cu_2O/TiO_2 photocatalyst prepared by a facile method, was developed and analyzed in details.

Firstly, starting from the results of an extended literature analysis, a *solvent – free* ball milling was chosen as a simple alternative preparation method, obtaining a photocatalyst suitable to hydrogen production under visible light radiation in the presence of different oxygenated organic substrates as sacrificial organic agents.

The three main variables affecting the structure and performance of the catalyst, namely the percentage of Cu_2O, the milling time and the rotation speed of the miller, were studied: a two – level factorial design approach was used to identify with a minimum number of experiments the influence of those factors on the photocatalytic hydrogen production via photoreforming of methanol under UV and visible radiation: 1 and 10 % wt. of Cu_2O, milling time of 1 and 30 minutes, and rotation rate of the miller of 100 and 500 rpm were chosen as minimum and maximum levels of the factors. Based on the results of this investigation campaign, 1% wt. of Cu_2O with respect to TiO_2 was identified as the best formulation for the composite catalyst and this was selected to further analyze in detail the system behavior. Moreover, the best hydrogen production (about 60 µmol/h after 5 hours of irradiation) was obtained with a milling time of 1 minute and rotation rate of 200 rpm. Through a thorough catalyst characterization, the correlation between the photocatalytic activity and the physical – chemical properties of the catalyst was obtained.

The evaluation of the photocatalytic activity of the best performing material at varying organic concentration allowed the identification of an adsorption equilibrium constant of 0.967 (M^{-1}), and the alkaline conditions have demonstrated a positive effect on the photocatalytic hydrogen generation. As for the temperature, a great positive effect was recorded, arising hydrogen productivity about 4.5 – fold higher than that obtained at the lowest temperature. The apparent quantum efficiency and the light – to – chemical energy efficiency values were 1.51% and 0.6%, respectively, in the presence of the best tested photocatalyst when the temperature was about 35°C, while these values reached about 6.5% and 2.36%, respectively, when glycerol is used as scavengers at 80°C. Moreover, the photocatalytic performance of the best system studied under solar radiation resulted about 5 – fold higher than that collected under simulated solar conditions. Despite the great number of studies on the Cu_2O – TiO_2 composite photocatalyst, only a few of them reported the results in terms of AQE, thus making difficult the direct comparison with the results obtained by others. However, based on the performed literature analysis, the studied system may be assumed as competitive due to *(i)* the simplicity of the photocatalyst preparation and *(ii)* the AQE values obtained considering only the radiation at wavelength higher than 400 nm.

Finally, the development of a suitable mathematical model capable of simulating hydrogen production allowed the estimation of the unknown parameters, in particular an indication of the quantum yield for hydrogen generation under the visible light radiation was obtained for the first time.

This work lays the foundation to the development of a competitive visible – light active photocatalytic process, able to produce hydrogen, by using a simple photocatalyst under solar radiation, in presence of organic pollutants contained in wastewater.

Appendix

1% Cu_2O-TiO_2 before reaction

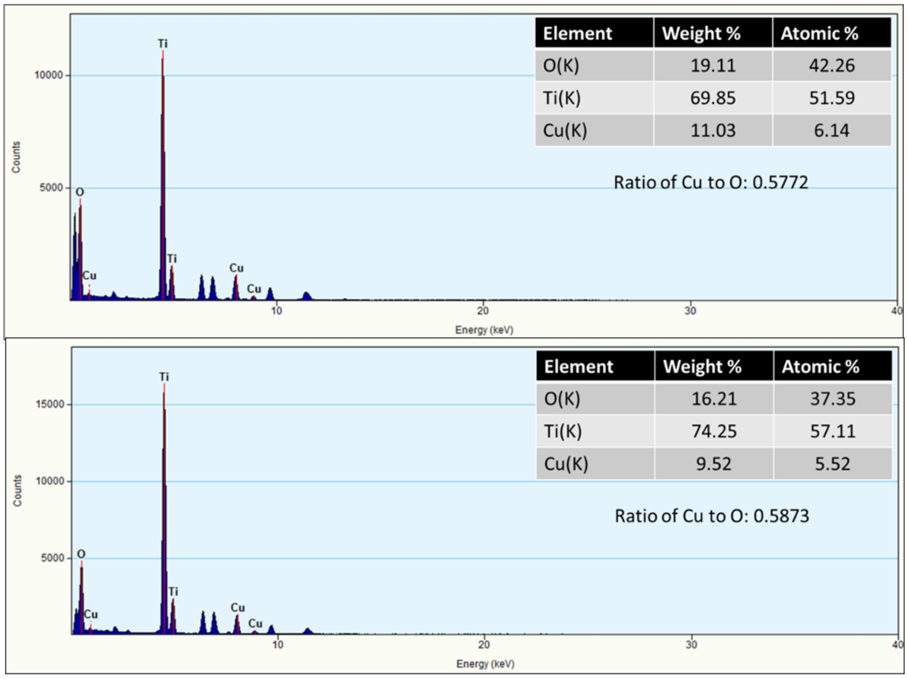

Element	Weight %	Atomic %
O(K)	19.11	42.26
Ti(K)	69.85	51.59
Cu(K)	11.03	6.14

Ratio of Cu to O: 0.5772

Element	Weight %	Atomic %
O(K)	16.21	37.35
Ti(K)	74.25	57.11
Cu(K)	9.52	5.52

Ratio of Cu to O: 0.5873

1% Cu_2O-TiO_2 after reaction

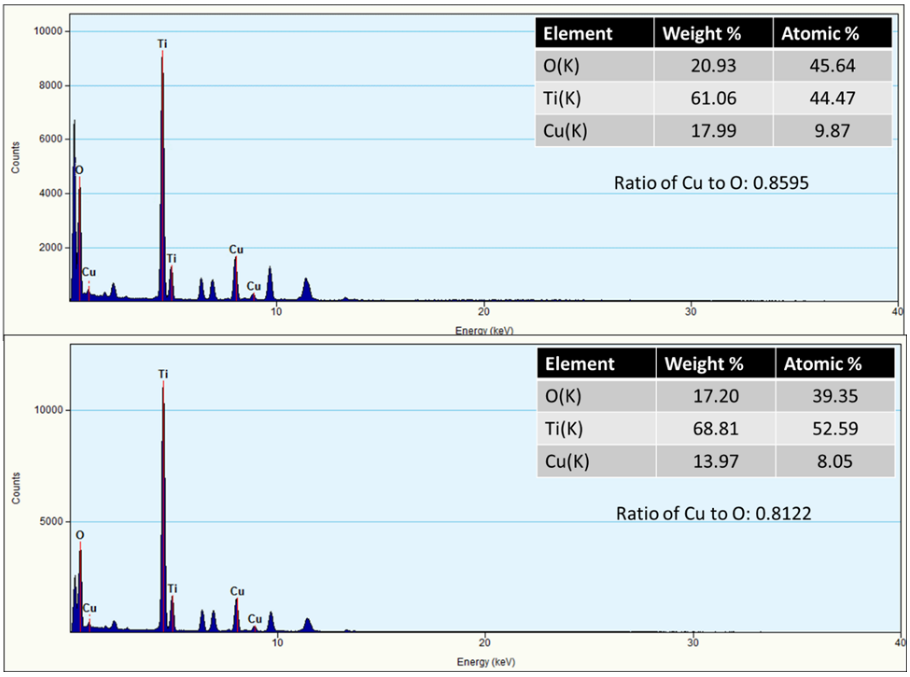

Element	Weight %	Atomic %
O(K)	20.93	45.64
Ti(K)	61.06	44.47
Cu(K)	17.99	9.87

Ratio of Cu to O: 0.8595

Element	Weight %	Atomic %
O(K)	17.20	39.35
Ti(K)	68.81	52.59
Cu(K)	13.97	8.05

Ratio of Cu to O: 0.8122

Figure 42. EDX spectra on the (1%wt) Cu_2O-TiO_2 composite material before and after the reaction.

10% Cu_2O-TiO_2 before reaction

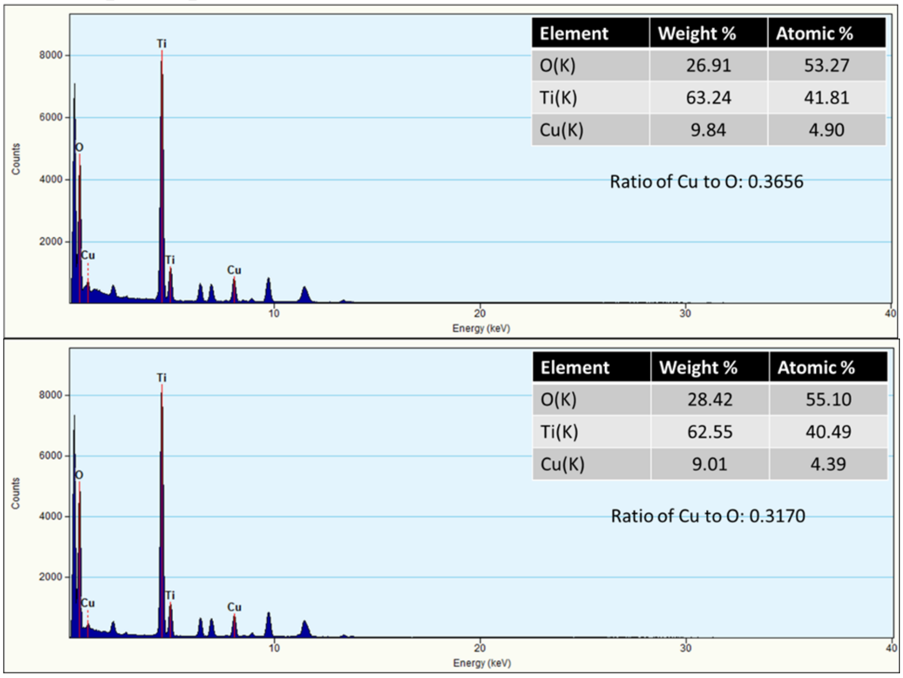

Element	Weight %	Atomic %
O(K)	26.91	53.27
Ti(K)	63.24	41.81
Cu(K)	9.84	4.90

Ratio of Cu to O: 0.3656

Element	Weight %	Atomic %
O(K)	28.42	55.10
Ti(K)	62.55	40.49
Cu(K)	9.01	4.39

Ratio of Cu to O: 0.3170

10% Cu_2O-TiO_2 after reaction

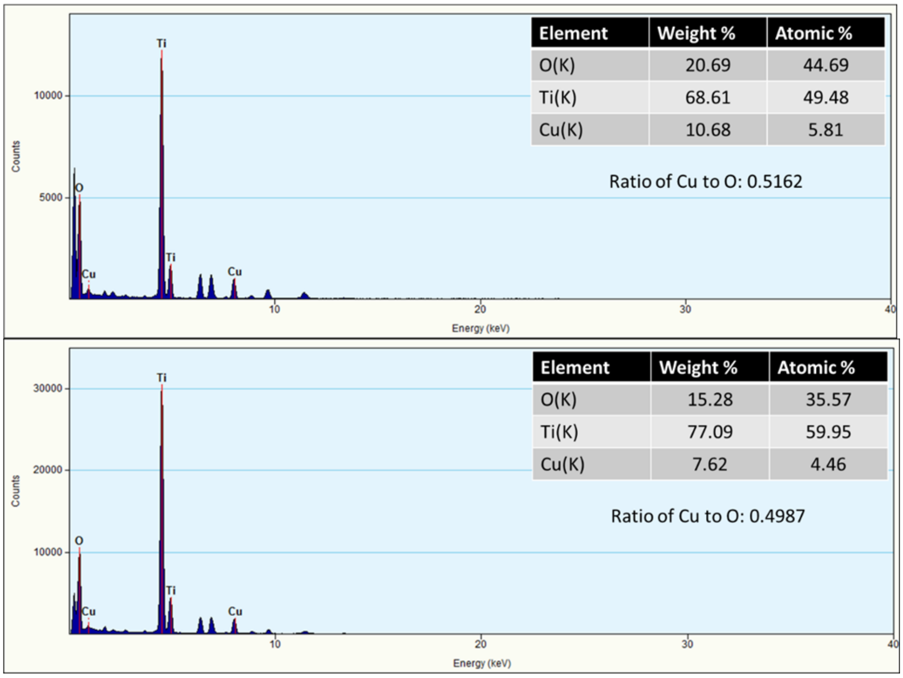

Element	Weight %	Atomic %
O(K)	20.69	44.69
Ti(K)	68.61	49.48
Cu(K)	10.68	5.81

Ratio of Cu to O: 0.5162

Element	Weight %	Atomic %
O(K)	15.28	35.57
Ti(K)	77.09	59.95
Cu(K)	7.62	4.46

Ratio of Cu to O: 0.4987

Figure 43. EDX spectra on the (10%wt) Cu_2O-TiO_2 composite material before and after the reaction.

References

[1] A.K.R. Police, S.V.P. Vattikuti, K.K. Mandari, M. Chennaiahgari, P.S. Phanikrishna, D.K. Valluri, C. Byon, Bismuth oxide cocatalyst and copper oxide sensitizer in Cu2O/TiO2/Bi2O3 ternary photocatalyst for efficient hydrogen production under solar light irradiation, Ceramics International. 44 (2018) 11783–11791. https://doi.org/10.1016/j.ceramint.2018.03.262.

[2] N. Abas, A. Kalair, N. Khan, Review of fossil fuels and future energy technologies, Futures. 69 (2015) 31–49. https://doi.org/10.1016/j.futures.2015.03.003.

[3] M. Wang, S. Shen, L. Li, Z. Tang, J. Yang, Effects of sacrificial reagents on photocatalytic hydrogen evolution over different photocatalysts, Journal of Materials Science. 52 (2017) 5155–5164. https://doi.org/10.1007/s10853-017-0752-z.

[4] P.A. Owusu, S. Asumadu-Sarkodie, A review of renewable energy sources, sustainability issues and climate change mitigation, Cogent Engineering. 3 (2016) 1–14. https://doi.org/10.1080/23311916.2016.1167990.

[5] K. Van Der Wiel, H.C. Bloomfield, R.W. Lee, L.P. Stoop, R. Blackport, J.A. Screen, F.M. Selten, The influence of weather regimes on European renewable energy production and demand, Environmental Research Letters. 14 (2019). https://doi.org/10.1088/1748-9326/ab38d3.

[6] L. Yao, W. Wang, L. Wang, Y. Liang, J. Fu, H. Shi, Chemical bath deposition synthesis of TiO2/Cu2O core/shell nanowire arrays with enhanced photoelectrochemical water splitting for H2 evolution and photostability, International Journal of Hydrogen Energy. 43 (2018) 15907–15917. https://doi.org/10.1016/j.ijhydene.2018.06.127.

[7] A. Inayat, M. Raza, District cooling system via renewable energy sources: A review, Renewable and Sustainable Energy Reviews. 107 (2019) 360–373. https://doi.org/10.1016/j.rser.2019.03.023.

[8] S.K. Kar, A. Sharma, B. Roy, Solar energy market developments in India, Renewable and Sustainable Energy Reviews. 62 (2016) 121–133. https://doi.org/10.1016/j.rser.2016.04.043.

[9] X. Li, B. Liu, Y. Chen, X. Fan, Y. Li, F. Zhang, G. Zhang, W. Peng, Decoration of Cu2O photocathode with protective TiO2 and active WS2 layers for enhanced photoelectrochemical hydrogen evolution, Nanotechnology. 29 (2018). https://doi.org/10.1088/1361-6528/aae569.

[10] T. Johannes, L. Jochen, Hydrogen and Fuel Cell. Technologies and Market Perspectives, Springer International Publishing, 2014. https://doi.org/10.1007/978-3-662-44972-1.

[11] S.K. Kar, Energy Sustainability Through Green Energy, n.d.

[12] A.M. Abdalla, S. Hossain, O.B. Nisfindy, A.T. Azad, M. Dawood, A.K. Azad, Hydrogen production, storage, transportation and key challenges with applications: A review, Energy Conversion and Management. 165 (2018) 602–627. https://doi.org/10.1016/j.enconman.2018.03.088.

[13] P. Nikolaidis, A. Poullikkas, A comparative overview of hydrogen production processes, Renewable and Sustainable Energy Reviews. 67 (2017) 597–611. https://doi.org/10.1016/j.rser.2016.09.044.

[14] I. Staffell, D. Scamman, V. Abad, P. Balcombe, P.E. Dodds, P. Ekins, K.R. Ward, Environmental Science The role of hydrogen and fuel cells in the global energy system, (2019) 463–491. https://doi.org/10.1039/c8ee01157e.

[15] I.V. Kanna, P. Paturu, I.V. Kanna, A study of hydrogen as an alternative fuel, 0750 (2018). https://doi.org/10.1080/01430750.2018.1484803.

[16] O. V. Marchenko, S. V. Solomin, The future energy: Hydrogen versus electricity, International Journal of Hydrogen Energy. 40 (2015) 3801–3805. https://doi.org/10.1016/j.ijhydene.2015.01.132.

[17] R.S. Ã, The hydrogen economy , fuel cells , and electric cars, 25 (2003) 455–476. https://doi.org/10.1016/j.techsoc.2003.09.024.

[18] C.M. Kalamaras, A.M. Efstathiou, Hydrogen Production Technologies: Current State and Future Developments, Conference Papers in Energy. 2013 (2013) 1–9. https://doi.org/10.1155/2013/690627.

[19] N. Muradov, Low to near-zero CO2 production of hydrogen from fossil fuels: Status and perspectives, International Journal of Hydrogen Energy. 42 (2017) 14058–14088. https://doi.org/10.1016/j.ijhydene.2017.04.101.

[20] D. Gardner, Hydrogen production from renewables, Renewable Energy Focus. 9 (2009) 34–37. https://doi.org/10.1016/s1755-0084(09)70036-5.

[21] M. Mohsin, A.K. Rasheed, R. Saidur, Economic viability and production capacity of wind generated renewable hydrogen, International Journal of Hydrogen Energy. 43 (2018) 2621–2630. https://doi.org/10.1016/j.ijhydene.2017.12.113.

[22] W. Nabgan, T.A. Tuan Abdullah, R. Mat, B. Nabgan, Y. Gambo, M. Ibrahim, A. Ahmad, A.A. Jalil, S. Triwahyono, I. Saeh, Renewable hydrogen production from bio-oil derivative via catalytic steam reforming: An overview, Renewable and Sustainable Energy Reviews. 79 (2017) 347–357. https://doi.org/10.1016/j.rser.2017.05.069.

[23] D. Jing, L. Guo, L. Zhao, X. Zhang, H. Liu, M. Li, S. Shen, G. Liu, X. Hu, X. Zhang, K. Zhang, L. Ma, P. Guo, Efficient solar hydrogen production by photocatalytic water splitting: From fundamental study to pilot demonstration, International Journal of Hydrogen Energy. 35 (2010) 7087–7097. https://doi.org/10.1016/j.ijhydene.2010.01.030.

[24] L. Clarizia, D. Russo, I. Di Somma, R. Andreozzi, R. Marotta, Hydrogen generation through solar photocatalytic processes: A review of the configuration and the properties of effective metal-based semiconductor nanomaterials, Energies. 10 (2017). https://doi.org/10.3390/en10101624.

[25] X. Chen, S. Shen, L. Guo, S.S. Mao, Semiconductor-based photocatalytic hydrogen generation, Chemical Reviews. 110 (2010) 6503–6570. https://doi.org/10.1021/cr1001645.

[26] G. Peng, M. Volokh, J. Tzadikov, J. Sun, M. Shalom, Carbon Nitride / Reduced Graphene Oxide Film with Enhanced Electron Diffusion Length : An Efficient Photo- Electrochemical Cell for Hydrogen Generation, 1800566 (2018) 1–7. https://doi.org/10.1002/aenm.201800566.

[27] S. Yun, N. Vlachopoulos, A. Qurashi, S. Ahmad, A. Hagfeldt, Dye sensitized photoelectrolysis cells, Chem Soc Rev. (2019) 3705–3722. https://doi.org/10.1039/c8cs00987b.

[28] P.K. Dubey, R. Kumar, R.S. Tiwari, O.N. Srivastava, A.C. Pandey, P. Singh, Surface modification of aligned TiO 2 nanotubes by Cu 2 O nanoparticles and their enhanced photo electrochemical properties and hydrogen generation application, International Journal of Hydrogen Energy. 43 (2018) 6867–6878. https://doi.org/10.1016/j.ijhydene.2018.02.127.

[29] H. Ahmad, S.K. Kamarudin, L.J. Minggu, M. Kassim, Hydrogen from photo-catalytic water splitting process: A review, Renewable and Sustainable Energy Reviews. 43 (2015) 599–610. https://doi.org/10.1016/j.rser.2014.10.101.

[30] K.C. Christoforidis, P. Fornasiero, Photocatalytic Hydrogen Production: A Rift into the Future Energy Supply, ChemCatChem. 9 (2017) 1523–1544. https://doi.org/10.1002/cctc.201601659.

[31] R. Lucchetti, L. Onotri, L. Clarizia, F. Di Natale, I. Di Somma, R. Andreozzi, R. Marotta, Removal of nitrate and simultaneous hydrogen generation through photocatalytic reforming of glycerol over “in situ” prepared zero-valent nano copper/P25, Applied Catalysis B: Environmental. 202 (2017) 539–549. https://doi.org/https://doi.org/10.1016/j.apcatb.2016.09.043.

[32] T. Miwa, S. Kaneco, H. Katsumata, T. Suzuki, K. Ohta, S. Chand Verma, K. Sugihara, Photocatalytic hydrogen production from aqueous methanol solution

with CuO/Al2O3/TiO2 nanocomposite, International Journal of Hydrogen Energy. 35 (2010) 6554–6560. https://doi.org/10.1016/j.ijhydene.2010.03.128.

[33] B. Rico-Oller, A. Boudjemaa, H. Bahruji, M. Kebir, S. Prashar, K. Bachari, M. Fajardo, S. Gómez-Ruiz, Photodegradation of organic pollutants in water and green hydrogen production via methanol photoreforming of doped titanium oxide nanoparticles, Science of the Total Environment. 563–564 (2016) 921–932. https://doi.org/10.1016/j.scitotenv.2015.10.101.

[34] T.D. Munusamy, S.Y. Chin, M. Tarek, M.M.R. Khan, Sustainable hydrogen production by CdO/exfoliated g-C3N4 via photoreforming of formaldehyde containing wastewater, International Journal of Hydrogen Energy. 46 (2021) 30988–30999. https://doi.org/10.1016/j.ijhydene.2021.01.176.

[35] Z. Wei, J. Liu, W. Shangguan, A review on photocatalysis in antibiotic wastewater: Pollutant degradation and hydrogen production, Chinese Journal of Catalysis. 41 (2020) 1440–1450. https://doi.org/10.1016/S1872-2067(19)63448-0.

[36] P. Chowdhury, G. Malekshoar, M.B. Ray, J. Zhu, A.K. Ray, Sacrificial hydrogen generation from formaldehyde with Pt/TiO2 photocatalyst in solar radiation, Industrial and Engineering Chemistry Research. 52 (2013) 5023–5029. https://doi.org/10.1021/ie3029976.

[37] S. Zhang, L. Wang, C. Liu, J. Luo, J. Crittenden, X. Liu, T. Cai, J. Yuan, Y. Pei, Y. Liu, Photocatalytic wastewater purification with simultaneous hydrogen production using MoS2 QD-decorated hierarchical assembly of ZnIn2S4 on reduced graphene oxide photocatalyst, Water Research. 121 (2017) 11–19. https://doi.org/10.1016/j.watres.2017.05.013.

[38] H.L. Chou, B.J. Hwang, C.L. Sun, Catalysis in Fuel Cells and Hydrogen Production, Elsevier B.V., 2013. https://doi.org/10.1016/B978-0-444-53880-2.00014-4.

[39] S.E. Braslavsky, Glossary of terms used in photochemistry 3rd edition: (IUPAC Recommendations 2006), Pure and Applied Chemistry. 79 (2007) 293–465. https://doi.org/10.1351/pac200779030293.

[40] S. Der Fachgruppe, Sondertagung der Fachgruppe, (1934) 223–224.

[41] A. Fujishima, K. Honda, Electrochemical photolysis of water at a semiconductor electrode., Nature. 238 (1972) 37–38. https://doi.org/10.1038/238037a0.

[42] N. Fajrina, M. Tahir, A critical review in strategies to improve photocatalytic water splitting towards hydrogen production, International Journal of Hydrogen Energy. 44 (2019) 540–577. https://doi.org/10.1016/j.ijhydene.2018.10.200.

[43] X. Chen, S. Shen, L. Guo, S.S. Mao, Semiconductor-based photocatalytic hydrogen generation, Chemical Reviews. 110 (2010) 6503–6570. https://doi.org/10.1021/cr1001645.

[44] E.A. Kozlova, V.N. Parmon, Heterogeneous semiconductor photocatalysts for hydrogen production from aqueous solutions of electron donors, Russian Chemical Reviews. 86 (2017) 870–906. https://doi.org/10.1070/rcr4739.

[45] A. Hakki, Y. AlSalka, C.B. Mendive, J. Ubogui, P.C. Dos Santos Claro, D. Bahnemann, Hydrogen production by heterogeneous photocatalysis, Elsevier, 2018. https://doi.org/10.1016/B978-0-12-409547-2.13795-3.

[46] H.J. Yoon, J. Hyun Yang, S.J. Park, C.K. Rhee, Y. Sohn, Photocatalytic CO2 reduction and hydrogen production over Pt/Zn-embedded β-Ga2O3 nanorods, Applied Surface Science. 536 (2021) 147753. https://doi.org/10.1016/j.apsusc.2020.147753.

[47] Z.C. Zhao, C.L. Yang, Q.T. Meng, M.S. Wang, X.G. Ma, Photocatalytic hydrogen production from water splitting with N-doped β-Ga2O3 and visible light, Spectrochimica Acta - Part A: Molecular and Biomolecular Spectroscopy. 211 (2019) 71–78. https://doi.org/10.1016/j.saa.2018.11.039.

[48] P. Mazierski, A. Mikolajczyk, B. Bajorowicz, A. Malankowska, A. Zaleska-Medynska, J. Nadolna, The role of lanthanides in TiO2-based photocatalysis: A review, Applied Catalysis B: Environmental. 233 (2018) 301–317. https://doi.org/10.1016/j.apcatb.2018.04.019.

[49] T. Khoa Le, D. Flahaut, H. Martinez, H.K. Hung Nguyen, T.K. Xuan Huynh, Study of the effects of surface modification by thermal shock method on photocatalytic activity of TiO2 P25, Applied Catalysis B: Environmental. 165 (2015) 260–268. https://doi.org/10.1016/j.apcatb.2014.10.024.

[50] A. Trenczek-Zajac, J. Banaś, K. Lwierczek, K. Zazakowny, M. Radecka, Photosensitization of TiO2 P25 with CdS Nanoparticles for Photocatalytic Applications, Archives of Metallurgy and Materials. 62 (2017) 841–849. https://doi.org/10.1515/amm-2017-0124.

[51] M. Humayun, F. Raziq, A. Khan, W. Luo, Modification strategies of TiO2 for potential applications in photocatalysis: A critical review, Green Chemistry Letters and Reviews. 11 (2018) 86–102. https://doi.org/10.1080/17518253.2018.1440324.

[52] G. Brauer, J. Kuriplach, C.C. Ling, A.B. Djurišić, Activities towards p-type doping of ZnO, Journal of Physics: Conference Series. 265 (2011). https://doi.org/10.1088/1742-6596/265/1/012002.

[53] C.B. Ong, L.Y. Ng, A.W. Mohammad, A review of ZnO nanoparticles as solar photocatalysts: Synthesis, mechanisms and applications, Renewable and Sustainable Energy Reviews. 81 (2018) 536–551. https://doi.org/10.1016/j.rser.2017.08.020.

[54] M. Pirhashemi, A. Habibi-Yangjeh, S. Rahim Pouran, Review on the criteria anticipated for the fabrication of highly efficient ZnO-based visible-light-driven photocatalysts, Journal of Industrial and Engineering Chemistry. 62 (2018) 1–25. https://doi.org/10.1016/j.jiec.2018.01.012.

[55] K. Qi, B. Cheng, J. Yu, W. Ho, Review on the improvement of the photocatalytic and antibacterial activities of ZnO, Journal of Alloys and Compounds. 727 (2017) 792–820. https://doi.org/10.1016/j.jallcom.2017.08.142.

[56] A.N. Kadam, T.G. Kim, D.S. Shin, K.M. Garadkar, J. Park, Morphological evolution of Cu doped ZnO for enhancement of photocatalytic activity, Journal of Alloys and Compounds. 710 (2017) 102–113. https://doi.org/10.1016/j.jallcom.2017.03.150.

[57] Z. Fan, J.G. Lu, Zinc oxide nanostructures: Synthesis and properties, Journal of Nanoscience and Nanotechnology. 5 (2005) 1561–1573. https://doi.org/10.1166/jnn.2005.182.

[58] M.A. Mohd Adnan, N.M. Julkapli, S.B. Abd Hamid, Review on ZnO hybrid photocatalyst: Impact on photocatalytic activities of water pollutant degradation, Reviews in Inorganic Chemistry. 36 (2016) 77–104. https://doi.org/10.1515/revic-2015-0015.

[59] A. Hernández-Ramírez, I. Medina-Ramírez, Photocatalytic Semiconductors Synthesis, Characterization, and Environmental Applications, Springer US, Mexico, 2015.

[60] A. Janotti, C.G. Van De Walle, Fundamentals of zinc oxide as a semiconductor, Reports on Progress in Physics. 72 (2009). https://doi.org/10.1088/0034-4885/72/12/126501.

[61] J. Yang, H. Yan, X. Wang, F. Wen, Z. Wang, D. Fan, J. Shi, C. Li, Roles of cocatalysts in Pt-PdS/CdS with exceptionally high quantum efficiency for photocatalytic hydrogen production, Journal of Catalysis. 290 (2012) 151–157. https://doi.org/10.1016/j.jcat.2012.03.008.

[62] R. bin Wei, Z.L. Huang, G.H. Gu, Z. Wang, L. Zeng, Y. Chen, Z.Q. Liu, Dual-cocatalysts decorated rimous CdS spheres advancing highly-efficient visible-light photocatalytic hydrogen production, Applied Catalysis B: Environmental. 231 (2018) 101–107. https://doi.org/10.1016/j.apcatb.2018.03.014.

[63] Y. Nakano, S. Saeki, T. Morikawa, Optical bandgap widening of p -type Cu2 O films by nitrogen doping, Applied Physics Letters. 94 (2009) 1–4. https://doi.org/10.1063/1.3072804.

[64] M.O. Segovia-Guzmán, M. Román-Aguirre, J.Y. Verde-Gomez, V.H. Collins-Martínez, G. Zaragoza-Galán, V.H. Ramos-Sánchez, Green Cu2O/TiO2 heterojunction for glycerol photoreforming, Catalysis Today. (2018). https://doi.org/10.1016/j.cattod.2018.05.031.

[65] E. Luévano-Hipólito, L.M. Torres-Martínez, D. Sánchez-Martínez, M.R. Alfaro Cruz, Cu2O precipitation-assisted with ultrasound and microwave radiation for photocatalytic hydrogen production, International Journal of Hydrogen Energy. 42 (2017) 12997–13010. https://doi.org/10.1016/j.ijhydene.2017.03.192.

[66] P.E. de Jongh, D. Vanmaekelbergh, J.J. Kelly, Cu2O: A catalyst for the photochemical decomposition of water?, Chemical Communications. (1999) 1069–1070. https://doi.org/10.1039/a901232j.

[67] J. Ma, K. Wang, L. Li, T. Zhang, Y. Kong, S. Komarneni, Visible-light photocatalytic decolorization of Orange II on Cu2O/ZnO nanocomposites, Ceramics International. 41 (2015) 2050–2056. https://doi.org/10.1016/j.ceramint.2014.09.137.

[68] F. Biccari, Defects and Doping in Cu2O, Solid State Communications. (2009) 262. https://doi.org/10.1016/0038-1098(70)90325-X.

[69] M.D. Susman, Y. Feldman, A. Vaskevich, I. Rubinstein, Chemical deposition of Cu2O nanocrystals with precise morphology control, ACS Nano. 8 (2014) 162–174. https://doi.org/10.1021/nn405891g.

[70] Z. Yang, C. Ma, W. Wang, M. Zhang, X. Hao, S. Chen, Fabrication of Cu2O-Ag nanocomposites with enhanced durability and bactericidal activity, Journal of Colloid and Interface Science. 557 (2019) 156–167. https://doi.org/10.1016/j.jcis.2019.09.015.

[71] T. Minami, Y. Nishi, T. Miyata, Cu2O-based solar cells using oxide semiconductors, Journal of Semiconductors. 37 (2016). https://doi.org/10.1088/1674-4926/37/1/014002.

[72] D.S. Zimbovskii, A.N. Baranov, Synthesis of Cu2O-Based Heterostructures and Their Photocatalytic Properties for Water Splitting, Inorganic Materials. 56 (2020) 366–373. https://doi.org/10.1134/S0020168520040159.

[73] L. Clarizia, G. Vitiello, D.K. Pallotti, B. Silvestri, M. Nadagouda, S. Lettieri, G. Luciani, R. Andreozzi, P. Maddalena, R. Marotta, Effect of surface properties of copper-modified commercial titanium dioxide photocatalysts on hydrogen production through photoreforming of alcohols, International Journal of Hydrogen Energy. 42 (2017) 28349–28362. https://doi.org/https://doi.org/10.1016/j.ijhydene.2017.09.093.

[74] G. Liu, Y. Sheng, J.W. Ager, M. Kraft, R. Xu, Research advances towards large-scale solar hydrogen production from water, EnergyChem. 1 (2019) 100014. https://doi.org/10.1016/j.enchem.2019.100014.

[75] J. Krýsa, G. Waldner, H. Měšťánková, J. Jirkovský, G. Grabner, Photocatalytic degradation of model organic pollutants on an immobilized particulate TiO2 layer. Roles of adsorption processes and mechanistic complexity, Applied Catalysis B: Environmental. 64 (2006) 290–301. https://doi.org/10.1016/j.apcatb.2005.11.007.

[76] Z.H.N. Al-Azri, W.T. Chen, A. Chan, V. Jovic, T. Ina, H. Idriss, G.I.N. Waterhouse, The roles of metal co-catalysts and reaction media in photocatalytic hydrogen production: Performance evaluation of M/TiO2 photocatalysts (M = Pd, Pt, Au) in different alcohol-water mixtures, Journal of Catalysis. 329 (2015) 355–367. https://doi.org/10.1016/j.jcat.2015.06.005.

[77] V. Kumaravel, S. Mathew, J. Bartlett, S.C. Pillai, Photocatalytic hydrogen production using metal doped TiO2: A review of recent advances, Applied

Catalysis B: Environmental. 244 (2019) 1021–1064. https://doi.org/10.1016/j.apcatb.2018.11.080.

[78] X. Wang, H. Dong, Z. Hu, Z. Qi, L. Li, Fabrication of a Cu2O/Au/TiO2composite film for efficient photocatalytic hydrogen production from aqueous solution of methanol and glucose, Materials Science and Engineering B: Solid-State Materials for Advanced Technology. 219 (2017) 10–19. https://doi.org/10.1016/j.mseb.2017.02.011.

[79] X. Zhang, T. Peng, S. Song, Recent advances in dye-sensitized semiconductor systems for photocatalytic hydrogen production, Journal of Materials Chemistry A. 4 (2016) 2365–2402. https://doi.org/10.1039/c5ta08939e.

[80] W. Jones, D.J. Martin, A. Caravaca, A.M. Beale, M. Bowker, T. Maschmeyer, G. Hartley, A. Masters, A comparison of photocatalytic reforming reactions of methanol and triethanolamine with Pd supported on titania and graphitic carbon nitride, Applied Catalysis B: Environmental. 240 (2019) 373–379. https://doi.org/10.1016/j.apcatb.2017.01.042.

[81] R. Singh, S. Dutta, A review on H2 production through photocatalytic reactions using TiO2/TiO2-assisted catalysts, Fuel. 220 (2018) 607–620. https://doi.org/10.1016/j.fuel.2018.02.068.

[82] A.A. Ismail, S.A. Al-sayari, D.W. Bahnemann, Photodeposition of precious metals onto mesoporous TiO 2 nanocrystals with enhanced their photocatalytic activity for methanol oxidation, Catalysis Today. 209 (2013) 2–7. https://doi.org/10.1016/j.cattod.2012.09.027.

[83] P.S. Basavarajappa, S.B. Patil, N. Ganganagappa, K.R. Reddy, A. v. Raghu, C.V. Reddy, Recent progress in metal-doped TiO2, non-metal doped/codoped TiO2 and TiO2 nanostructured hybrids for enhanced photocatalysis, International Journal of Hydrogen Energy. 45 (2020) 7764–7778. https://doi.org/10.1016/j.ijhydene.2019.07.241.

[84] L. Clarizia, D. Russo, I. di Somma, R. Andreozzi, R. Marotta, Metal-based semiconductor nanomaterials for photocatalysis, Elsevier Ltd., 2018. https://doi.org/10.1016/B978-0-08-101977-1.00010-7.

[85] A. Bazzo, A. Urakawa, Understanding synergetic effects of Zn and Rh-Cr promotion to wide-bandgap Ga, Ta and Ti oxides in photocatalytic water splitting, Catalysis Science and Technology. 6 (2016) 4243–4253. https://doi.org/10.1039/c5cy01681a.

[86] S. Sakthivel, S.U. Geissen, D.W. Bahnemann, V. Murugesan, A. Vogelpohl, Enhancement of photocatalytic activity by semiconductor heterojunctions: α-Fe2O3, WO3 and CdS deposited on ZnO, Journal of Photochemistry and Photobiology A: Chemistry. 148 (2002) 283–293. https://doi.org/10.1016/S1010-6030(02)00055-2.

[87] S.S. Jeong, A. Mittiga, E. Salza, A. Masci, S. Passerini, Electrodeposited ZnO/Cu2O heterojunction solar cells, Electrochimica Acta. 53 (2008) 2226–2231. https://doi.org/10.1016/j.electacta.2007.09.030.

[88] Y. Bessekhouad, D. Robert, J. v. Weber, Photocatalytic activity of Cu2O/TiO2, Bi 2O3/TiO2 and ZnMn2O 4/TiO2 heterojunctions, Catalysis Today. 101 (2005) 315–321. https://doi.org/10.1016/j.cattod.2005.03.038.

[89] P. Lv, L. Lin, W. Zheng, M. Zheng, F. Lai, Photosensitivity of ZnO/Cu2O thin film heterojunction, Optik. 124 (2013) 2654–2657. https://doi.org/10.1016/j.ijleo.2012.07.040.

[90] M. Reza Gholipour, C.T. Dinh, F. Béland, T.O. Do, Nanocomposite heterojunctions as sunlight-driven photocatalysts for hydrogen production from water splitting, Nanoscale. 7 (2015) 8187–8208. https://doi.org/10.1039/c4nr07224c.

[91] H. Wang, L. Zhang, Z. Chen, J. Hu, S. Li, Z. Wang, J. Liu, X. Wang, Semiconductor heterojunction photocatalysts: Design, construction, and photocatalytic

performances, Chemical Society Reviews. 43 (2014) 5234–5244. https://doi.org/10.1039/c4cs00126e.

[92] S.J.A. Moniz, S.A. Shevlin, D.J. Martin, Z.X. Guo, J. Tang, Visible-light driven heterojunction photocatalysts for water splitting-a critical review, Energy and Environmental Science. 8 (2015) 731–759. https://doi.org/10.1039/c4ee03271c.

[93] Y. Bessekhouad, D. Robert, J. v. Weber, Photocatalytic activity of Cu2O/TiO2, Bi 2O3/TiO2 and ZnMn2O 4/TiO2 heterojunctions, in: Catalysis Today, 2005. https://doi.org/10.1016/j.cattod.2005.03.038.

[94] M. Shabani, M. Haghighi, D. Kahforoushan, S. Heidari, Grain-like bismuth-rich bismuth/bismuth oxychlorides intra-heterojunction: Efficacious solar-light-driven photodegradation of fluoroquinolone antibiotics and 2-level factorial approach, Journal of the Taiwan Institute of Chemical Engineers. 96 (2019) 243–255. https://doi.org/10.1016/j.jtice.2018.11.018.

[95] R. Khan, R. Ahmad, P. Rai, L.W. Jang, J.H. Yun, Y.T. Yu, Y.B. Hahn, I.H. Lee, Glucose-assisted synthesis of Cu2O shuriken-like nanostructures and their application as nonenzymatic glucose biosensors, Sensors and Actuators, B: Chemical. 203 (2014) 471–476. https://doi.org/10.1016/j.snb.2014.06.128.

[96] J. Kou, C. Lu, W. Sun, L. Zhang, Z. Xu, Facile Fabrication of Cuprous Oxide-based Adsorbents for Deep Desulfurization, ACS Sustainable Chemistry and Engineering. 3 (2015) 3053–3061. https://doi.org/10.1021/acssuschemeng.5b01051.

[97] G. Singh, M. Kumar, K. Sharma, V. Bhalla, A supramolecular ensemble of a PBI derivative and Cu2O NPs: Potential photocatalysts for the Suzuki and Suzuki type coupling reactions, Green Chemistry. 18 (2016) 3278–3285. https://doi.org/10.1039/c5gc03012a.

[98] P. Li, W. Lv, S. Ai, Green and gentle synthesis of Cu2O nanoparticles using lignin as reducing and capping reagent with antibacterial properties, Journal of

Experimental Nanoscience. 11 (2016) 18–27. https://doi.org/10.1080/17458080.2015.1015462.

[99] G.H. J. Wang, Y. Hwee Ng, Y. Lim, Vegetable-extracted carbon dots and their nanocomposites for enhanced photocatalytic H2 production, RSC Advances. 4 (2014) 44117–44123. https://doi.org/10.1017/CBO9781107415324.004.

[100] M.J. Kolb, J. Wermink, F. Calle-Vallejo, L.B.F. Juurlink, M.T.M. Koper, Initial stages of water solvation of stepped platinum surfaces, Physical Chemistry Chemical Physics. 18 (2016) 3416–3422. https://doi.org/10.1039/c5cp04468e.

[101] M. Jing, P. Cui, K. Liu, Research status and development of Cu2O Thin Film film solar cells, in: Materials Science Forum, 2017: pp. 151–155. https://doi.org/10.4028/www.scientific.net/MSF.893.151.

[102] W. Niu, T. Moehl, W. Cui, R. Wick-Joliat, L. Zhu, S.D. Tilley, Extended Light Harvesting with Dual Cu2O-Based Photocathodes for High Efficiency Water Splitting, Advanced Energy Materials. 8 (2018) 1–8. https://doi.org/10.1002/aenm.201702323.

[103] B. Liu, Y. Wu, J. Zhang, X. Han, H. Shi, Visible-light-driven g-C 3 N 4 /Cu 2 O heterostructures with efficient photocatalytic activities for tetracycline degradation and microbial inactivation, Journal of Photochemistry and Photobiology A: Chemistry. 378 (2019) 1–8. https://doi.org/10.1016/j.jphotochem.2019.04.007.

[104] S. Wang, W. Wang, L. Yue, S. Cui, H. Wang, C. Wang, S. Chen, Hierarchical Cu2O nanowires covered by silver nanoparticles-doped carbon layer supported on Cu foam for rapid and efficient water disinfection with lower voltage, Chemical Engineering Journal. 382 (2020) 122855. https://doi.org/10.1016/j.cej.2019.122855.

[105] H. Manisha, P.D. Priya Swetha, Y.B. Shim, K.S. Prasad, Microwave Assisted Synthesis of Hybrid Cu2O Microcubes for Photocatalysis and Electrocatalysis,

Materials Today: Proceedings. 5 (2018) 16390–16393. https://doi.org/10.1016/j.matpr.2018.05.135.

[106] A. Rubino, P.G. Schiavi, P. Altimari, A. Latini, F. Pagnanelli, Ti/TiO2/Cu2O based electrodes as photocatalysts in PEC cells, Chemical Engineering Transactions. 73 (2019) 73–78. https://doi.org/10.3303/CET1973013.

[107] E. Luévano-Hipólito, L.M. Torres-Martínez, D. Sánchez-Martínez, M.R. Alfaro Cruz, Cu2O precipitation-assisted with ultrasound and microwave radiation for photocatalytic hydrogen production, International Journal of Hydrogen Energy. 42 (2017) 12997–13010. https://doi.org/10.1016/j.ijhydene.2017.03.192.

[108] Y.S. Cho, Y.D. Huh, Microwave assisted synthesis of Cu2O crystals with morphological evolution from octapod to octahedron, Bulletin of the Korean Chemical Society. 35 (2014) 309–312. https://doi.org/10.5012/bkcs.2014.35.1.309.

[109] S. Oros-Ruiz, R. Zanella, S.E. Collins, A. Hernández-Gordillo, R. Gómez, Photocatalytic hydrogen production by Au-MxOy (MAg, Cu, Ni) catalysts supported on TiO2, Catalysis Communications. (2014). https://doi.org/10.1016/j.catcom.2013.12.033.

[110] J. Fu, S. Cao, J. Yu, Dual Z-scheme charge transfer in TiO2–Ag–Cu2O composite for enhanced photocatalytic hydrogen generation, Journal of Materiomics. (2015). https://doi.org/10.1016/j.jmat.2015.02.002.

[111] L. Sinatra, A.P. Lagrow, W. Peng, A.R. Kirmani, A. Amassian, H. Idriss, O.M. Bakr, A Au/Cu2O-TiO2 system for photo-catalytic hydrogen production. A pn-junction effect or a simple case of in situ reduction?, Journal of Catalysis. (2015). https://doi.org/10.1016/j.jcat.2014.11.012.

[112] K. Lalitha, G. Sadanandam, V.D. Kumari, M. Subrahmanyam, B. Sreedhar, N.Y. Hebalkar, Highly stabilized and finely dispersed Cu2O/TiO2: A promising visible sensitive photocatalyst for continuous production of hydrogen from

glycerol:water mixtures, Journal of Physical Chemistry C. 114 (2010) 22181–22189. https://doi.org/10.1021/jp107405u.

[113] L. Li, L. Xu, W. Shi, J. Guan, Facile preparation and size-dependent photocatalytic activity of Cu 2O nanocrystals modified titania for hydrogen evolution, International Journal of Hydrogen Energy. 38 (2013) 816–822. https://doi.org/10.1016/j.ijhydene.2012.10.064.

[114] Z. Xi, C. Li, L. Zhang, M. Xing, J. Zhang, Synergistic effect of Cu2O/TiO2 heterostructure nanoparticle and its high H2 evolution activity, International Journal of Hydrogen Energy. 39 (2014) 6345–6353. https://doi.org/10.1016/j.ijhydene.2014.01.209.

[115] H. Xu, S. Ouyang, L. Liu, D. Wang, T. Kako, J. Ye, Porous-structured Cu2O/TiO2 nanojunction material toward efficient CO2 photoreduction, Nanotechnology. 25 (2014). https://doi.org/10.1088/0957-4484/25/16/165402.

[116] M. Wang, L. Sun, Z. Lin, J. Cai, K. Xie, C. Lin, P-n Heterojunction photoelectrodes composed of Cu2O-loaded TiO2 nanotube arrays with enhanced photoelectrochemical and photoelectrocatalytic activities, Energy and Environmental Science. 6 (2013) 1211–1220. https://doi.org/10.1039/c3ee24162a.

[117] L.W. Zheng Xing, Xu Zong, Jian Pan, On the engineering part of solar hydrogen production from water splitting: Photoreactor design, Chemical Engineering Science. (2013) 125–146. https://doi.org/10.1016/j.ces.2013.08.039.

[118] B. Long, H. Yang, M. Li, M.S. Balogun, W. Mai, G. Ouyang, Y. Tong, P. Tsiakaras, S. Song, Interface charges redistribution enhanced monolithic etched copper foam-based Cu 2 O layer/TiO 2 nanodots heterojunction with high hydrogen evolution electrocatalytic activity, Applied Catalysis B: Environmental. 243 (2019) 365–372. https://doi.org/10.1016/j.apcatb.2018.10.039.

[119] I. Tamiolakis, I.T. Papadas, K.C. Spyridopoulos, G.S. Armatas, Mesoporous assembled structures of Cu2O and TiO2 nanoparticles for highly efficient

photocatalytic hydrogen generation from water, RSC Advances. 6 (2016) 54848–54855. https://doi.org/10.1039/c6ra08546f.

[120] W.Y. Cheng, T.H. Yu, K.J. Chao, S.Y. Lu, Cu2O-decorated mesoporous TiO2 beads as a highly efficient photocatalyst for hydrogen production, ChemCatChem. 6 (2014) 293–300. https://doi.org/10.1002/cctc.201300681.

[121] W. Zhen, W. Jiao, Y. Wu, H. Jing, G. Lu, The role of a metallic copper interlayer during visible photocatalytic hydrogen generation over a Cu/Cu2O/Cu/TiO2 catalyst, Catalysis Science and Technology. 7 (2017) 5028–5037. https://doi.org/10.1039/c7cy01432e.

[122] W. Zhu, B. Chong, K. Qin, L. Guan, X. Hou, G.Z. Chen, Cuprous oxide/titanium dioxide nanotube-array with coaxial heterogeneous structure synthesized by multiple-cycle chemical adsorption plus reduction method, RSC Advances. 6 (2016) 59160–59168. https://doi.org/10.1039/c6ra06893f.

[123] L. Le, Y. Wu, Z. Zhou, H. Wang, R. Xiong, J. Shi, Cu2O clusters decorated on flower-like TiO2 nanorod array film for enhanced hydrogen production under solar light irradiation, Journal of Photochemistry and Photobiology A: Chemistry. 351 (2018) 78–86. https://doi.org/10.1016/j.jphotochem.2017.08.073.

[124] W. Niu, T. Moehl, W. Cui, R. Wick-Joliat, L. Zhu, S.D. Tilley, Extended Light Harvesting with Dual Cu2O-Based Photocathodes for High Efficiency Water Splitting, Advanced Energy Materials. 8 (2018) 1–8. https://doi.org/10.1002/aenm.201702323.

[125] S. Zhang, B. Peng, S. Yang, Y. Fang, F. Peng, The influence of the electrodeposition potential on the morphology of Cu2O/TiO2 nanotube arrays and their visible-light-driven photocatalytic activity for hydrogen evolution, International Journal of Hydrogen Energy. 38 (2013) 13866–13871. https://doi.org/10.1016/j.ijhydene.2013.08.081.

[126] T.N.Q. Trang, L.T.N. Tu, T. v. Man, M. Mathesh, N.D. Nam, V.T.H. Thu, A high-efficiency photoelectrochemistry of Cu2O/TiO2 nanotubes based composite for hydrogen evolution under sunlight, Composites Part B: Engineering. 174 (2019). https://doi.org/10.1016/j.compositesb.2019.106969.

[127] Y. Liu, Z. Ye, D. Li, M. Wang, Y. Zhang, W. Huang, Tuning CuO x -TiO 2 interaction and photocatalytic hydrogen production of CuO x /TiO 2 photocatalysts via TiO 2 morphology engineering, Applied Surface Science. 473 (2019) 500–510. https://doi.org/10.1016/j.apsusc.2018.12.177.

[128] P.A. Bharad, A. v. Nikam, F. Thomas, C.S. Gopinath, CuOx-TiO2 Composites: Electronically Integrated Nanocomposites for Solar Hydrogen Generation, ChemistrySelect. 3 (2018) 12022–12030. https://doi.org/10.1002/slct.201802047.

[129] Y. Liu, Z. Wang, W. Huang, Influences of TiO 2 phase structures on the structures and photocatalytic hydrogen production of CuO x /TiO 2 photocatalysts, Applied Surface Science. 389 (2016) 760–767. https://doi.org/10.1016/j.apsusc.2016.07.173.

[130] D. Praveen Kumar, N. Lakshmana Reddy, B. Srinivas, V. Durgakumari, V. Roddatis, O. Bondarchuk, M. Karthik, Y. Ikuma, M. v. Shankar, Stable and active CuxO/TiO2 nanostructured catalyst for proficient hydrogen production under solar light irradiation, Solar Energy Materials and Solar Cells. 146 (2016) 63–71. https://doi.org/10.1016/j.solmat.2015.11.030.

[131] P.K. Dubey, R. Kumar, R.S. Tiwari, O.N. Srivastava, A.C. Pandey, P. Singh, Surface modification of aligned TiO 2 nanotubes by Cu 2 O nanoparticles and their enhanced photo electrochemical properties and hydrogen generation application, International Journal of Hydrogen Energy. 43 (2018) 6867–6878. https://doi.org/10.1016/j.ijhydene.2018.02.127.

[132] L. Clarizia, G. Vitiello, G. Luciani, I. Di Somma, R. Andreozzi, R. Marotta, In situ photodeposited nanoCu on TiO2 as a catalyst for hydrogen production under

UV/visible radiation, Applied Catalysis A: General. 518 (2016) 142–149. https://doi.org/10.1016/j.apcata.2015.07.044.

[133] C. Ingunta, R., Piazza, S., Sunseri, Novel procedure for the template synthesis of metal nanostructures., Electrochem. Com-Mun. (2008) 506–509.

[134] W. Zhen, W. Jiao, Y. Wu, H. Jing, G. Lu, The role of a metallic copper interlayer during visible photocatalytic hydrogen generation over a Cu/Cu2O/Cu/TiO2 catalyst, Catalysis Science and Technology. 7 (2017) 5028–5037. https://doi.org/10.1039/c7cy01432e.

[135] L. Pan, J.H. Kim, M.T. Mayer, M.K. Son, A. Ummadisingu, J.S. Lee, A. Hagfeldt, J. Luo, M. Grätzel, Boosting the performance of Cu2O photocathodes for unassisted solar water splitting devices, Nature Catalysis. 1 (2018) 412–420. https://doi.org/10.1038/s41929-018-0077-6.

[136] M. Jung, J.N. Hart, J. Scott, Y.H. Ng, Y. Jiang, R. Amal, Exploring Cu oxidation state on TiO2 and its transformation during photocatalytic hydrogen evolution, Applied Catalysis A: General. 521 (2016) 190–201. https://doi.org/10.1016/j.apcata.2015.11.013.

[137] K.L. Chang, Q. Sun, Y.P. Peng, S.W. Lai, M. Sung, C.Y. Huang, H.W. Kuo, J. Sun, Y.C. Lin, Cu2O loaded titanate nanotube arrays for simultaneously photoelectrochemical ibuprofen oxidation and hydrogen generation, Chemosphere. 150 (2016) 605–614. https://doi.org/10.1016/j.chemosphere.2016.02.016.

[138] Q. Hu, J. Huang, G. Li, J. Chen, Z. Zhang, Z. Deng, Y. Jiang, W. Guo, Y. Cao, Effective water splitting using CuO x /TiO 2 composite films: Role of Cu species and content in hydrogen generation, Applied Surface Science. 369 (2016) 201–206. https://doi.org/10.1016/j.apsusc.2016.01.281.

[139] W. Yuan, J. Yuan, J. Xie, C.M. Li, Polymer-Mediated Self-Assembly of TiO2@Cu2O Core-Shell Nanowire Array for Highly Efficient

Photoelectrochemical Water Oxidation, ACS Applied Materials and Interfaces. 8 (2016) 6082–6092. https://doi.org/10.1021/acsami.6b00030.

[140] M. Nishikawa, M. Fukuda, Y. Nakabayashi, N. Saito, N. Ogawa, T. Nakajima, K. Shinoda, T. Tsuchiya, Y. Nosaka, A method to give chemically stabilities of photoelectrodes for water splitting: Compositing of a highly crystalized TiO 2 layer on a chemically unstable Cu 2 O photocathode using laser-induced crystallization process, Applied Surface Science. 363 (2016) 173–180. https://doi.org/10.1016/j.apsusc.2015.12.002.

[141] M. Kilo, C. Schild, A. Wokaun, A. Baiker, Surface oxidic phases of binary and ternary zirconia-supported metal catalysts investigated by Raman spectroscopy, Journal of the Chemical Society, Faraday Transactions. 88 (1992) 1453–1457. https://doi.org/10.1039/FT9928801453.

[142] G. Niaura, Surface-enhanced Raman spectroscopic observation of two kinds of adsorbed OH− ions at copper electrode, Electrochimica Acta. 45 (2000) 3507–3519.

[143] A. Compaan and H. Z. Cummins, Raman Scattering, Luminescence, and Exciton-Phonon Coupling in Cu2O, PHYSICAL REVIEW B. 6 (1972) 4753.

[144] D.Z.J. and X.Q. J. F. Xu, W. Ji, Z. X. Shen, S. H. Tang, X. R. Ye, Preparation and Characterization of CuO Nanocrystals, Journal of Solid State Chemistry. 147 (1999) 516–519. https://doi.org/10.1006/jssc.1999.8409.

[145] M.J.Weaver.J.W. Ho Yeung H. Chan, Christos G. Takoudis, Electrochemical Control of Gas-Phase Oxidation and Reduction of Copper as Probed by Surface-Enhanced Raman Spectroscopy, Electrochemical and Solid State Letters. 2 (1999) 189.

[146] R.H. Muller, An In Situ Roman Spectroscopy Study of the Anodic Oxidation of Copper in Alkaline Media, Journal of the Electrochemical Society. 139 (1992) 426–434. https://doi.org/10.1149/1.2069234.

[147] J.C. Hamilton, J.C. Farmer, R.J. Anderson, In Situ Raman Spectroscopy of Anodic Films Formed on Copper and Silver in Sodium Hydroxide Solution, Journal of The Electrochemical Society . 133 (1986) 739–745. https://doi.org/10.1149/1.2108666.

[148] G. Vitiello, L. Clarizia, W. Abdelraheem, S. Esposito, B. Bonelli, N. Ditaranto, A. Vergara, M. Nadagouda, D.D. Dionysiou, R. Andreozzi, G. Luciani, R. Marotta, Near UV-Irradiation of CuOx-Impregnated TiO2 Providing Active Species for H2 Production Through Methanol Photoreforming, ChemCatChem. 11 (2019) 4314–4326. https://doi.org/10.1002/cctc.201900818.

[149] Z. Li, J. Liu, D. Wang, Y. Gao, J. Shen, Cu2O/Cu/TiO2 nanotube Ohmic heterojunction arrays with enhanced photocatalytic hydrogen production activity, International Journal of Hydrogen Energy. (2012). https://doi.org/10.1016/j.ijhydene.2012.01.075.

[150] Z. Li, J. Liu, D. Wang, Y. Gao, J. Shen, Cu 2 O / Cu / TiO 2 nanotube Ohmic heterojunction arrays with enhanced photocatalytic hydrogen production activity, International Journal of Hydrogen Energy. 37 (2012) 6431–6437. https://doi.org/10.1016/j.ijhydene.2012.01.075.

[151] B.J. and J.C. T. Oku, R. Motoyoshi, K. Fujimoto, T. Akiyama, Structures and photovoltaic properties of copper oxides/fullerene solar cells, Journal of Physics Chemistry of Solids. 72 (2011) 1206–1211.

[152] T. Zhou, Z. Zang, J. Wei, J. Zheng, J. Hao, F. Ling, Efficient charge carrier separation and excellent visible light photoresponse in Cu 2 O nanowires, 50 (2018) 118–125. https://doi.org/10.1016/j.nanoen.2018.05.028.

[153] L. Yan, F. Yang, C.Y. Tao, X. Luo, L. Zhang, Highly efficient and stable Cu2O–TiO2 intermediate photocatalytic water splitting, Ceramics International. 46 (2020) 9455–9463. https://doi.org/10.1016/j.ceramint.2019.12.206.

[154] J.-G. Yu, H.-G. Yu, B. Cheng, X.-J. Zhao, J.C. Yu, W.-K. Ho, The Effect of Calcination Temperature on the Surface Microstructure and Photocatalytic Activity of TiO2

Thin Films Prepared by Liquid Phase Deposition, The Journal of Physical Chemistry B. 107 (2003) 13871–13879. https://doi.org/10.1021/jp036158y.

[155] Z.L. Lei Huang, Feng Peng, Hongjuan Wang, Hao Yu, Preparation and characterization of Cu2O/TiO2 nano–nano heterostructure photocatalysts, Catalysis Communications. 10 (2009) 1839–1843.

[156] C. Das, B. Ananthoju, A.K. Dhara, M. Aslam, S.K. Sarkar, K.R. Balasubramaniam, Electron-Selective TiO2 /CVD-Graphene Layers for Photocorrosion Inhibition in Cu2O Photocathodes, Advanced Materials Interfaces. 4 (2017) 1–10. https://doi.org/10.1002/admi.201700271.

[157] J. Wang, Z. Chen, G. Zhai, Y. Men, Boosting photocatalytic activity of WO 3 nanorods with tailored surface oxygen vacancies for selective alcohol oxidations, Applied Surface Science. 462 (2018) 760–771. https://doi.org/10.1016/j.apsusc.2018.08.181.

[158] W. Zhen, W. Jiao, Y. Wu, H. Jing, G. Lu, The role of a metallic copper interlayer during visible photocatalytic hydrogen generation over a Cu/Cu2O/Cu/TiO2 catalyst, Catalysis Science and Technology. 7 (2017) 5028–5037. https://doi.org/10.1039/c7cy01432e.

[159] J. Choi, J.T. Song, H.S. Jang, M.J. Choi, D.M. Sim, S. Yim, H. Lim, Y.S. Jung, J. Oh, Interfacial band-edge engineered TiO2 protection layer on Cu2O photocathodes for efficient water reduction reaction, Electronic Materials Letters. 13 (2017) 57–65. https://doi.org/10.1007/s13391-017-6316-1.

[160] I. Majeed, M.A. Nadeem, A. Badshah, F.K. Kanodarwala, H. Ali, M.A. Khan, J.A. Stride, M.A. Nadeem, Titania supported MOF-199 derived Cu-Cu2O nanoparticles: Highly efficient non-noble metal photocatalysts for hydrogen production from alcohol-water mixtures, Catalysis Science and Technology. 7 (2017) 677–686. https://doi.org/10.1039/c6cy02328b.

[161] R. Ahmad Rather, A Cu+1/Cu0-TiO2 mesoporous nanocomposite exhibits improved H2 production from H2O under direct solar irradiation, Journal of Catalysis. 346 (2017) 1–9. https://doi.org/10.1016/j.jcat.2016.11.021.

[162] L. Clarizia, D. Spasiano, I. Di Somma, R. Marotta, R. Andreozzi, D.D. Dionysiou, Copper modified-TiO2 catalysts for hydrogen generation through photoreforming of organics. A short review, International Journal of Hydrogen Energy. 39 (2014) 16812–16831. https://doi.org/10.1016/j.ijhydene.2014.08.037.

[163] G. Li, J. Huang, J. Chen, Z. Deng, Q. Huang, Z. Liu, W. Guo, R. Cao, Highly Active Photocatalyst of Cu 2 O/TiO 2 Octahedron for Hydrogen Generation, ACS Omega. 4 (2019) 3392–3397. https://doi.org/10.1021/acsomega.8b03404.

[164] Z. Hu, X. Wang, H. Dong, S. Li, X. Li, L. Li, Efficient photocatalytic degradation of tetrabromodiphenyl ethers and simultaneous hydrogen production by TiO2-Cu2O composite films in N2atmosphere: Influencing factors, kinetics and mechanism, Journal of Hazardous Materials. 340 (2017) 1–15. https://doi.org/10.1016/j.jhazmat.2017.07.009.

[165] Q. Hu, J. Huang, G. Li, Y. Jiang, H. Lan, W. Guo, Y. Cao, Origin of the improved photocatalytic activity of Cu incorporated TiO 2 for hydrogen generation from water, Applied Surface Science. 382 (2016) 170–177. https://doi.org/10.1016/j.apsusc.2016.04.126.

[166] B. Han, Y.H. Hu, Highly Efficient Temperature-Induced Visible Light Photocatalytic Hydrogen Production from Water, Journal of Physical Chemistry C. 119 (2015) 18927–18934. https://doi.org/10.1021/acs.jpcc.5b04894.

[167] Y. Li, B. Wang, S. Liu, X. Duan, Z. Hu, Synthesis and characterization of Cu 2 O/TiO 2 photocatalysts for H 2 evolution from aqueous solution with different scavengers, Applied Surface Science. 324 (2015) 736–744. https://doi.org/10.1016/j.apsusc.2014.11.027.

[168] Y.H. Zhang, Y.L. Li, B.B. Jiu, F.L. Gong, J.L. Chen, S.M. Fang, H.L. Zhang, Highly enhanced photocatalytic H2 evolution of Cu2O microcube by coupling with TiO2 nanoparticles, Nanotechnology. 30 (2019). https://doi.org/10.1088/1361-6528/aafccb.

[169] C. Peng, W. Xu, P. Wei, M.C. Liu, L. Guo, P. Wu, K. Zhang, Y. Cao, H. Wang, H. Yu, F. Peng, X. Yan, Manipulating photocatalytic pathway and activity of ternary Cu2O/(001)TiO2@Ti3C2Tx catalysts for H2 evolution: Effect of surface coverage, International Journal of Hydrogen Energy. 44 (2019) 29975–29985. https://doi.org/10.1016/j.ijhydene.2019.09.190.

[170] T. Wei, Y.N. Zhu, X. An, L.M. Liu, X. Cao, H. Liu, J. Qu, Defect Modulation of Z-Scheme TiO2/Cu2O Photocatalysts for Durable Water Splitting, ACS Catalysis. 9 (2019) 8346–8354. https://doi.org/10.1021/acscatal.9b01786.

[171] G. Li, J. Huang, Z. Deng, J. Chen, Q. Huang, Z. Liu, W. Guo, R. Cao, Highly Active Photocatalyst of CuOx Modified TiO2 Arrays for Hydrogen Generation, Crystal Growth and Design. 19 (2019) 5784–5790. https://doi.org/10.1021/acs.cgd.9b00797.

[172] J.M. Kum, Y.J. Park, H.J. Kim, S.O. Cho, Plasmon-enhanced photocatalytic hydrogen production over visible-light responsive Cu/TiO2, Nanotechnology. 26 (2015). https://doi.org/10.1088/0957-4484/26/12/125402.

[173] D. Praveen Kumar, N. Lakshmana Reddy, M. Mamatha Kumari, B. Srinivas, V. Durga Kumari, B. Sreedhar, V. Roddatis, O. Bondarchuk, M. Karthik, B. Neppolian, M. V. Shankar, Cu2O-sensitized TiO2 nanorods with nanocavities for highly efficient photocatalytic hydrogen production under solar irradiation, Solar Energy Materials and Solar Cells. 136 (2015) 157–166. https://doi.org/10.1016/j.solmat.2015.01.009.

[174] H. Dotan, N. Mathews, T. Hisatomi, M. Grätzel, A. Rothschild, On the Solar to Hydrogen Conversion Efficiency of Photoelectrodes for Water Splitting, The

Journal of Physical Chemistry Letters. 5 (2014) 3330–3334. https://doi.org/10.1021/jz501716g.

[175] M.G. Adriana Paracchino, Nripan Mathews, Takashi Hisatomi, Morgan Stefik, S. David Tilley, Ultrathin films on copper(i) oxidewater splitting photocathodes: a study on performance and stability, Energy and Environmental Science. 5 (2012) 8673–8681.

[176] M.G. and S.D.T. J. Azevedo, L. Steier, P. Dias, M. Stefik, C. T. Sousa, J. P. Araújo, A. Mendes, On the stability enhancement of cuprous oxide water splitting photocathodes by low temperature steam annealing, Energy and Environmental Science. 7 (2014) 4044–4052.

[177] P. Dai, W. Li, J. Xie, Y. He, J. Thorne, G. McMahon, J. Zhan, D. Wang, Forming Buried Junctions to Enhance the Photovoltage Generated by Cuprous Oxide in Aqueous Solutions, Angewandte Chemie International Edition. 53 (2014) 13493–13497. https://doi.org/10.1002/anie.201408375.

[178] C. Li, T. Hisatomi, O. Watanabe, M. Nakabayashi, Positive onset potential and stability of Cu 2 O-based photocathodes in water splitting by atomic layer deposition of a Ga 2 O 3 buffer layer †, Environmental Science. (2015) 1493–1500. https://doi.org/10.1039/c5ee00250h.

[179] J. Luo, L. Steier, M.-K. Son, M. Schreier, M.T. Mayer, M. Grätzel, Cu2O Nanowire Photocathodes for Efficient and Durable Solar Water Splitting, Nano Letters. 16 (2016) 1848–1857. https://doi.org/10.1021/acs.nanolett.5b04929.

[180] C. Deng, R. Hong, M. Jing, J. Shi, T. Yan, C. Tao, D. Zhang, Photocatalytic performance of TiO2 thin film decorated with Cu2O nanoparticles by laser ablation, Optical Materials. 94 (2019) 130–137. https://doi.org/10.1016/j.optmat.2019.05.030.

[181] M. Hinojosa-Reyes, R. Camposeco-Solís, R. Zanella, V. Rodríguez González, Hydrogen production by tailoring the brookite and Cu2O ratio of sol-gel Cu-TiO2

photocatalysts, Chemosphere. 184 (2017) 992–1002. https://doi.org/10.1016/j.chemosphere.2017.06.066.

[182] K. Zhao, S. Zhao, J. Qi, H. Yin, C. Gao, A.M. Khattak, Y. Wu, A. Iqbal, L. Wu, Y. Gao, R. Yu, Z. Tang, Cu2O clusters grown on TiO2 nanoplates as efficient photocatalysts for hydrogen generation, Inorg. Chem. Front. 3 (2016) 488–493. https://doi.org/10.1039/C5QI00284B.

[183] H. Gao, J. Zhang, R. Wang, M. Wang, Highly efficient hydrogen production and formaldehyde degradation by Cu2O microcrystals, Applied Catalysis B: Environmental. 172–173 (2015) 1–6. https://doi.org/10.1016/j.apcatb.2015.02.004.

[184] L. Sang, J. Zhang, Y. Zhang, Y. Zhao, J. Lin, Preparation of Cu 2 O / TiO 2 nanotube arrays and their photoelectrochemical properties as hydrogen-evolving photoanode, 9560 (2015) 1–9. https://doi.org/10.1117/12.2187908.

[185] Y. Li, B. Wang, S. Liu, X. Duan, Z. Hu, Synthesis and characterization of Cu 2 O/TiO 2 photocatalysts for H 2 evolution from aqueous solution with different scavengers, Applied Surface Science. 324 (2015) 736–744. https://doi.org/10.1016/j.apsusc.2014.11.027.

[186] A. Devadoss, P. Sudhagar, C. Ravidhas, R. Hishinuma, C. Terashima, K. Nakata, T. Kondo, I. Shitanda, M. Yuasa, A. Fujishima, Simultaneous glucose sensing and biohydrogen evolution from direct photoelectrocatalytic glucose oxidation on robust Cu2O-TiO2 electrodes, Physical Chemistry Chemical Physics. 16 (2014) 21237–21242. https://doi.org/10.1039/c4cp03262d.

[187] L. Zhu, Z. Junying, Z. Chen, K. Liu, H. Gao, Effect of Cu2O Morphology on Photocatalytic Hydrogen Generation and Chemical Stability of TiO2/Cu2O Composite, Journal of Nanoscience and Nanotechnology. 13 (2013) 5104–5108. https://doi.org/10.1166/jnn.2013.7591.

[188] L.K. Tsui, G. Zangari, The influence of morphology of electrodeposited Cu2O and Fe 2O3 on the conversion efficiency of TiO2 nanotube photoelectrochemical

solar cells, Electrochimica Acta. 100 (2013) 220–225. https://doi.org/10.1016/j.electacta.2012.07.058.

[189] L. Luo, T. Zhang, X. Zhang, Y. Rongping, L. Yanjun, Z. Bing, X. Xu, Enhanced Hydrogen Production from Ethanol Photoreforming by Site-Specific Deposition of Au on Cu2O/TiO2 p-n Junction, Catalysts. (2020).

[190] Y. Wang, S. Cao, Y. Huan, T. Nie, Z. Ji, Z. Bai, X. Cheng, J. Xi, X. Yan, The effect of composite catalyst on Cu2O/TiO2 heterojunction photocathodes for efficient water splitting, Applied Surface Science. 526 (2020). https://doi.org/10.1016/j.apsusc.2020.146700.

[191] J.D. Wright, N.A.J.M. Sommerdijk, Sol-gel materials: chemistry and applications, Choice Reviews Online. 38 (2001) 38-6197-38–6197. https://doi.org/10.5860/choice.38-6197.

[192] N. Liu, X. Chen, J. Zhang, J.W. Schwank, A review on TiO2-based nanotubes synthesized via hydrothermal method: Formation mechanism, structure modification, and photocatalytic applications, Catalysis Today. 225 (2014) 34–51. https://doi.org/10.1016/j.cattod.2013.10.090.

[193] A. Kornas, J.E. Olszówka, P. Klein, V. Pashkova, Milling activation for the solvent-free synthesis of zeolites. A practical guide, Catalysts. 11 (2021) 1–25. https://doi.org/10.3390/catal11020246.

[194] D.S. Su, Ball-milling as an effective method for preparation and activation of catalysts *, 74 (n.d.).

[195] J. Zhou, M. Zhang, Y. Zhu, Photocatalytic enhancement of hybrid C3N4/TiO2 prepared via ball milling method, Physical Chemistry Chemical Physics. 17 (2015) 3647–3652. https://doi.org/10.1039/c4cp05173d.

[196] Q. Chen, H. Hou, D. Zhang, S. Hu, T. Min, B. Liu, C. Yang, W. Pu, J. Hu, J. Yang, Enhanced visible-light driven photocatalytic activity of hybrid ZnO/g-C3N4 by high performance ball milling, Journal of Photochemistry and Photobiology A:

Chemistry. 350 (2018) 1–9. https://doi.org/10.1016/j.jphotochem.2017.09.015.

[197] S. Suwanboon, P. Amornpitoksuk, A. Sukolrat, N. Muensit, Optical and photocatalytic properties of La-doped ZnO nanoparticles prepared via precipitation and mechanical milling method, Ceramics International. 39 (2013) 2811–2819. https://doi.org/10.1016/j.ceramint.2012.09.050.

[198] H. Schreyer, R. Eckert, S. Immohr, J. de Bellis, M. Felderhoff, F. Schüth, Milling Down to Nanometers: A General Process for the Direct Dry Synthesis of Supported Metal Catalysts, Angewandte Chemie - International Edition. 58 (2019) 11262–11265. https://doi.org/10.1002/anie.201903545.

[199] M. Ghaffari, P.Y. Tan, M.E. Oruc, O.K. Tan, M.S. Tse, M. Shannon, Effect of ball milling on the characteristics of nano structure SrFeO 3 powder for photocatalytic degradation of methylene blue under visible light irradiation and its reaction kinetics, Catalysis Today. 161 (2011) 70–77. https://doi.org/10.1016/j.cattod.2010.11.031.

[200] S. Bazazi, N. Arsalani, A. Khataee, A.G. Tabrizi, Comparison of ball milling-hydrothermal and hydrothermal methods for synthesis of ZnO nanostructures and evaluation of their photocatalytic performance, Journal of Industrial and Engineering Chemistry. 62 (2018) 265–272. https://doi.org/10.1016/j.jiec.2018.01.004.

[201] S. Sivasankaran, K. Sivaprasad, R. Narayanasamy, V.K. Iyer, Synthesis, structure and sinterability of 6061 AA100-x-x wt.% TiO2 composites prepared by high-energy ball milling, Journal of Alloys and Compounds. 491 (2010) 712–721. https://doi.org/10.1016/j.jallcom.2009.11.051.

[202] I.N. Reddy, C.V. Reddy, M. Sreedhar, J. Shim, M. Cho, D. Kim, Effect of ball milling on optical properties and visible photocatalytic activity of Fe doped ZnO nanoparticles, Materials Science and Engineering B: Solid-State Materials for

Advanced Technology. 240 (2019) 33–40. https://doi.org/10.1016/j.mseb.2019.01.002.

[203] J.O. Carneiro, S. Azevedo, F. Fernandes, E. Freitas, M. Pereira, C.J. Tavares, S. Lanceros-Méndez, V. Teixeira, Synthesis of iron-doped TiO2 nanoparticles by ball-milling process: The influence of process parameters on the structural, optical, magnetic, and photocatalytic properties, Journal of Materials Science. 49 (2014) 7476–7488. https://doi.org/10.1007/s10853-014-8453-3.

[204] C. Shifu, C. Lei, G. Shen, C. Gengyu, The preparation of coupled SnO2/TiO2 photocatalyst by ball milling, Materials Chemistry and Physics. 98 (2006) 116–120. https://doi.org/10.1016/j.matchemphys.2005.08.073.

[205] C. Shifu, C. Lei, G. Shen, C. Gengyu, The preparation of coupled WO3/TiO2 photocatalyst by ball milling, Powder Technology. 160 (2005) 198–202. https://doi.org/10.1016/j.powtec.2005.08.012.

[206] S. Chen, S. Zhang, W. Zhao, W. Liu, Study on the photocatalytic activity of TiN/TiO2 nanoparticle formed by ball milling, Journal of Nanoparticle Research. 11 (2009) 931–938. https://doi.org/10.1007/s11051-008-9475-z.

[207] Y.I. Choi, H.J. Jung, W.G. Shin, Y. Sohn, Band gap-engineered ZnO and Ag/ZnO by ball-milling method and their photocatalytic and Fenton-like photocatalytic activities, Applied Surface Science. 356 (2015) 615–625. https://doi.org/10.1016/j.apsusc.2015.08.118.

[208] H. Lv, X. Zhao, H. Niu, S. He, Z. Tang, F. Wu, J.P. Giesy, Ball milling synthesis of covalent organic framework as a highly active photocatalyst for degradation of organic contaminants, Journal of Hazardous Materials. 369 (2019) 494–502. https://doi.org/10.1016/j.jhazmat.2019.02.046.

[209] D. Wu, C. Li, D. Zhang, L. Wang, X. Zhang, Z. Shi, Q. Lin, Enhanced photocatalytic activity of Gd3+ doped TiO2 and Gd2O3 modified TiO2 prepared via ball milling method, Journal of Rare Earths. 37 (2019) 845–852. https://doi.org/10.1016/j.jre.2018.10.011.

[210] G. Chen, D. Li, F. Li, Y. Fan, H. Zhao, Y. Luo, R. Yu, Q. Meng, Ball-milling combined calcination synthesis of MoS 2/CdS photocatalysts for high photocatalytic H 2 evolution activity under visible light irradiation, Applied Catalysis A: General. 443–444 (2012) 138–144. https://doi.org/10.1016/j.apcata.2012.07.033.

[211] C. Shifu, Z. Sujuan, L. Wei, Z. Wei, Study on the photocatalytic activity of p-n junction photocatalyst Cu 2O/TiO 2, Journal of Nanoscience and Nanotechnology. 9 (2009) 4397–4403. https://doi.org/10.1166/jnn.2009.M67.

[212] M. Muscetta, L. Clarizia, C. Garlisi, G. Palmisano, R. Marotta, R. Andreozzi, F. Ii, I. Chimica, P. Industriale, Hydrogen production upon UV-light irradiation of Cu / TiO 2 photocatalyst in the presence of alkanol- amines, International Journal of Hydrogen Energy. (2020). https://doi.org/10.1016/j.ijhydene.2020.07.002.

[213] X. CHEN, G. LIU, G. ZHANG, H. WAN, W. ZHA, Preparation of Copper Oxide/TiO2 Composite Films by Mechanical Ball Milling and Investigated Photocatalytic Activity, Materials Science. XX (2021). https://doi.org/10.5755/j02.ms.24735.

[214] P. Basnet, E. Anderson, Y. Zhao, Hybrid Cu x O–TiO 2 Nanopowders Prepared by Ball Milling for Solar Energy Conversion and Visible-Light-Induced Wastewater Treatment , ACS Applied Nano Materials. 2 (2019) 2446–2455. https://doi.org/10.1021/acsanm.9b00325.

[215] R.G. Zepp, M.M. Gumz, W.L. Miller, H. Gao, Photoreaction of valerophenone in aqueous solution, Journal of Physical Chemistry A. 102 (1998) 5716–5723. https://doi.org/10.1021/jp981130l.

[216] H.J. Kuhn, S.E. Braslavsky, R. Schmidt, Chemical actinometry (IUPAC technical report), Pure and Applied Chemistry. 76 (2004) 2105–2146. https://doi.org/10.1351/pac200476122105.

[217] P. Cheng, W. Li, T. Zhou, Y. Jin, M. Gu, Physical and photocatalytic properties of zinc ferrite doped titania under visible light irradiation, Journal of Photochemistry and Photobiology A: Chemistry. 168 (2004) 97–101. https://doi.org/10.1016/j.jphotochem.2004.05.018.

[218] M. Bellardita, C. Garlisi, L.Y. Ozer, A.M. Venezia, J. Sá, F. Mamedov, L. Palmisano, G. Palmisano, Highly stable defective TiO2-x with tuned exposed facets induced by fluorine: Impact of surface and bulk properties on selective UV/visible alcohol photo-oxidation, Applied Surface Science. 510 (2020). https://doi.org/10.1016/j.apsusc.2020.145419.

[219] A. Paracchino, V. Laporte, K. Sivula, M. Grätzel, E. Thimsen, Highly active oxide photocathode for photoelectrochemical water reduction, Nature Materials. 10 (2011) 456–461. https://doi.org/10.1038/nmat3017.

[220] Y. Tachibana, R. Muramoto, Photoelectrochemistry of p-type Cu 2 O semiconductor, 32 (2006) 575–583.

[221] M. Hara, Cu2O as a photocatalyst for overall water splitting under visible light irradiation, Chemical Communications. 2 (1998) 357–358. https://doi.org/10.1039/a707440i.

[222] National Center for Biotechnology Information (2020). PubChem Compound Summary for CID 887, Methanol., PubChem. (n.d.). https://pubchem.ncbi.nlm.nih.gov/compound/Methanol.

[223] R. Gottipati, S. Mishra, Process optimization of adsorption of Cr(VI) on activated carbons prepared from plant precursors by a two-level full factorial design, Chemical Engineering Journal. 160 (2010) 99–107. https://doi.org/10.1016/j.cej.2010.03.015.

[224] M. Muscetta, R. Andreozzi, L. Clarizia, I. di Somma, R. Marotta, Hydrogen production through photoreforming processes over Cu2O/TiO2 composite materials: A mini-review, International Journal of Hydrogen Energy. (2020). https://doi.org/10.1016/j.ijhydene.2020.07.225.

[225] J. Antony, A Systematic Methodology for Design of Experiments, Second Edi, Elsevier Ltd, 2014. https://doi.org/10.1016/b978-0-08-099417-8.00004-3.

[226] H. Eskandarloo, A. Badiei, M.A. Behnajady, G. Mohammadi Ziarani, Photo and Chemical Reduction of Copper onto Anatase-Type TiO2 Nanoparticles with Enhanced Surface Hydroxyl Groups as Efficient Visible Light Photocatalysts, Photochemistry and Photobiology. 91 (2015) 797–806. https://doi.org/10.1111/php.12455.

[227] Z. Xi, C. Li, L. Zhang, M. Xing, J. Zhang, Synergistic effect of Cu2O/TiO2 heterostructure nanoparticle and its high H2 evolution activity, International Journal of Hydrogen Energy. 39 (2014) 6345–6353. https://doi.org/10.1016/j.ijhydene.2014.01.209.

[228] G. Chen, D. Li, F. Li, Y. Fan, H. Zhao, Y. Luo, R. Yu, Q. Meng, Ball-milling combined calcination synthesis of MoS 2/CdS photocatalysts for high photocatalytic H 2 evolution activity under visible light irradiation, Applied Catalysis A: General. 443–444 (2012) 138–144. https://doi.org/10.1016/j.apcata.2012.07.033.

[229] A.M. Luís, M.C. Neves, M.H. Mendonça, O.C. Monteiro, Influence of calcination parameters on the TiO2 photocatalytic properties, Materials Chemistry and Physics. 125 (2011) 20–25. https://doi.org/10.1016/j.matchemphys.2010.08.019.

[230] A. Sangeetha, S. Jaya Seeli, K.P. Bhuvana, M.A. Kader, S.K. Nayak, Correlation between calcination temperature and optical parameter of zinc oxide (ZnO) nanoparticles, Journal of Sol-Gel Science and Technology. 91 (2019) 261–272. https://doi.org/10.1007/s10971-019-05000-8.

[231] N. Fajrina, M. Tahir, A critical review in strategies to improve photocatalytic water splitting towards hydrogen production, International Journal of Hydrogen Energy. 44 (2019) 540–577. https://doi.org/10.1016/j.ijhydene.2018.10.200.

[232] L. Huaxu, W. Fuqiang, C. Ziming, H. Shengpeng, X. Bing, G. Xiangtao, L. bo, T. Jianyu, L. Xiangzheng, C. Ruiyang, L. Wen, L. Linhua, Analyzing the effects of reaction temperature on photo-thermo chemical synergetic catalytic water splitting under full-spectrum solar irradiation: An experimental and

thermodynamic investigation, International Journal of Hydrogen Energy. 42 (2017) 12133–12142. https://doi.org/10.1016/j.ijhydene.2017.03.194.

[233] Z. Zhang, P.A. Maggard, Investigation of photocatalytically-active hydrated forms of amorphous titania, TiO2·nH2O, Journal of Photochemistry and Photobiology A: Chemistry. 186 (2007) 8–13. https://doi.org/10.1016/j.jphotochem.2006.07.004.

[234] L. Clarizia, Hydrogen production through photoreforming of oxygenated organic substrates over Cu/TiO2 catalysts, (2017) 1–154. https://pdfs.semanticscholar.org/1321/7a7fd331cd35341d871297348bb274692617.pdf?_ga=2.232541020.232120235.1565266071-86349393.1556861591.

[235] A. Ravindran, K.M. Ragsdell, G. v. Reklaitis, Engineering Optimization: Methods and Applications: Second Edition, 2007. https://doi.org/10.1002/9780470117811.

[236] L. Clarizia, I. di Somma, L. Onotri, R. Andreozzi, R. Marotta, Kinetic modeling of hydrogen generation over nano-Cu(s)/TiO2 catalyst through photoreforming of alcohols, Catalysis Today. 281 (2017) 117–123. https://doi.org/10.1016/j.cattod.2016.05.053.